EPFL

Thèse n° 7344

Inkjet printing of soft machines

Présentée le 9 janvier 2020

à la Faculté des sciences et techniques de l'ingénieur
Laboratoire des microsystèmes pour les technologies spatiales
Programme doctoral en microsystèmes et microélectronique

pour l'obtention du grade de Docteur ès Sciences

par

Samuel SCHLATTER

Acceptée sur proposition du jury

Prof. Y. Bellouard, président du jury
Prof. H. Shea, Dr S. Rosset, directeurs de thèse
Prof. R. Vertechy, rapporteur
Prof. S. Seelecke, rapporteur
Prof. V. Subramanian, rapporteur

École
polytechnique
fédérale
de Lausanne

2020

To my granddad. He would have been proud to see me finish my PhD.

Acknowledgements

Foremost, I would like to thank my supervisor Prof. Herbert Shea and my co-supervisor Dr. Samuel Rosset for their continued support, patience, and input to this thesis. I am very grateful to have such dedicated and knowledgeable supervisors.

I would also like to thank the remainder of my thesis committee: Prof. Vivek, Subramanian, Prof. Rocco Vertechy, Prof. Stefan Seelecke, Prof. Yves Bellouard. Thank you for generously offering your time and input towards this thesis.

A special thank you to Dr. Peter Van der Wal for your help on chemistry matters.

I am grateful to have been part of the MICACT program. Giving me the possibility to travel and meet fellow researchers across Europe.

A special thank you to Edwin Jager for hosting me in Sweden. Working with you and your team was a pleasure.

I thank my colleagues in the soft transducer group (LMTS). Past and present. What a great team.

Myriam Poliero you are the best secretary and friend a student can have.

Janina Löffler, thank you for being the fun loving person you are. It's been a pleasure living with you.

My friends who have made Neuchâtel home.

And of course my family. For the never ending love and support.

Neuchâtel, December 19, 2019 S. S.

Abstract

Soft machines and soft robots are an area of intense research because soft systems are safer to interact with, are better at handling fragile objects, can produce complex shapes with fewer transducers, are robust, and are ideal for wearable applications. However soft robots and soft machines are far from replicating the number degrees of freedom and the dexterity found in nature. Most soft machines are fabricated from silicone, use external pneumatic actuation, and lack sensing. To move towards soft machines with more degrees of freedom and higher dexterity new fabrication techniques are required. In this work ink-jet printing is used to fabricate soft machines with integrated dielectric elastomer (DE) and hydraulically amplified self-healing electrostatic (HASEL) transducers. Two demonstrators are presented to show how printed silicone, printed electrodes, and printed channels can be combined into a multi-layer multi-transducer soft peristaltic pump. The peristaltic pump shows how inkjet printed channels and transducers can be combined to control the flow of liquids. A method of motion for soft robots is also presented. The slug drive is a soft robotic drive train consisting 28 densely packed HASEL actuators. By producing a wave of contraction the slug drive is able to inch forwards in a way similar to invertebrate animals. The demonstrators show how ink-jet printing can be used to rapidly prototype soft machines with neatly and densely integrated soft transducers.

Contents

1 Introduction

1.1 Motivation

> A soft machine is a stretchable device consisting of mechanical components and electrical transducers which work in unison to automatically perform a task.

To better understand what a soft machine is we must first understand what a machine is. A machine may be purely mechanical, or may it may include electrical components to automate a task. Modern machines are generally a combination of both, and through electrical control are becoming increasingly automated. Consider the development of the washing machine. Most early washing machines consisted of a drum which could be rotated with a crank. Some deluxe models even included a pair of rollers to squeeze the clothes dry. However the mechanical motion was applied by the user. Modern washing machines have many similarities to their predecessors but they require much less input. Dirty clothes are tossed in, a button is pushed, and clean clothes come out. The complete process is automated. Valves are opened to let water in, sensors measure the soil level, a custom program is applied, the clothes are spun dry, and the user is alerted when the cycle has finished. This level of automation is possible due to the integration of logic, sensors, and actuators in modern machines.

Soft machines serve the same purpose, the only difference is that they are soft. By soft we are referring to the mechanical properties of the machine. In engineering terms it is how easily the machine deforms by stretching (elasticity). Stretchability is an intrinsic material property which does not depend on the size or shape of the material. This property is represented by the Young's modulus which is a ratio between stress (force per unit area) and strain (deformation). A material which deforms readily has a low Young's modulus. This includes biological tissue, gels, and elastomers (Rus and Tolley, 2015; Majidi, 2014) . These materials typically have moduli lower than 10 MPa. To be explicit the word soft in this thesis refers to machines made from stretchable materials.

But why should machines be soft? Consider a robotic arm which is used on a fruit sorting line. Although robots are learning fast there are still certain activities which humans are better at performing than their metal counterparts. Humans and robots will therefore have to work side by side in the foreseeable future. Since traditional robots are fast, hard, and strong they could potentially be lethal to humans if they were to strike one. Generally robots are placed in an enclosure to prevent such a scenario from ever taking place. However a robot which can be placed in the same working environment as a human would be much more versatile. To achieve this robots and machines have to become more like us - soft. Soft robots are less likely to be a threat to humans. In addition a soft robot would be less likely to damage itself. Although robots are preprogrammed to avoid striking objects in its vicinity it is not able to predict what items are placed around it. In such a scenario it may strike solid object at full speed and almost certainly damage itself. A big benefit of soft machines is that they are more resilient to damage because they deform and absorb energy on impact. Finally a robotic arm with a metal gripper is unlikely to have the dexterity to handle soft fruit. Computing the correct pressure required to grasp a piece of fruit is difficult. The pressure must be regulated to grasp the fruit but not so much as to crush it. Soft grippers are compliant and can deform to take on the shape of the fruit. The ability of soft robots to take on complex shapes and adapt to objects of different stiffnesses makes them extremely attractive for applications where dexterity is required.

Today's soft grippers can pick many different types of objects but cannot manipulate an objects like we do. The most common type of soft gripper are fluidic type of grippers with inflatable chambers (Figure 1.1). The fingers of the robotic grippers are built with asymmetry so that the fingers bend when the chambers are inflated. Grippers based on this technology are already being used in industry to move fragile and challenging to grasp materials such as dough, meat and bags containing air (mGrip, Soft Robotics Inc.). These type of grippers are also being explored in literature to grasp unusual objects such as jellyfish (Sinatra et al., 2019) and filled cupcake containers(Wang et al., 2017). The grippers are good at grasping objects on a conveyor belt when the location,type, and weight of object is known. However the grippers do not know if an object has been grasped, in what orientation it is in the gripper, and the gripper is not able to manipulate the object to improve the grip on the object. The grippers shown in figure 1.1 only have basic open and close control. Our hands are far more sophisticated than this and are able to sense the object and reorientate it without looking at the hands. The human hand is able to achieve such feats because the skin is covered with thousands of receptors and the hand consists of many bones and muscles giving it many degrees of freedom.

Humans and animals achieve a high level of control by having many muscles and receptors in a feedback loop to carefully control the position, speed, and force they use to interact with their environments. Recent efforts in soft robotics are trying to do the same. By increasing the transducer count in soft robotics it is possible to achieve higher degrees of freedom and higher dexterity. A technique called embedded 3D (EMB3D)

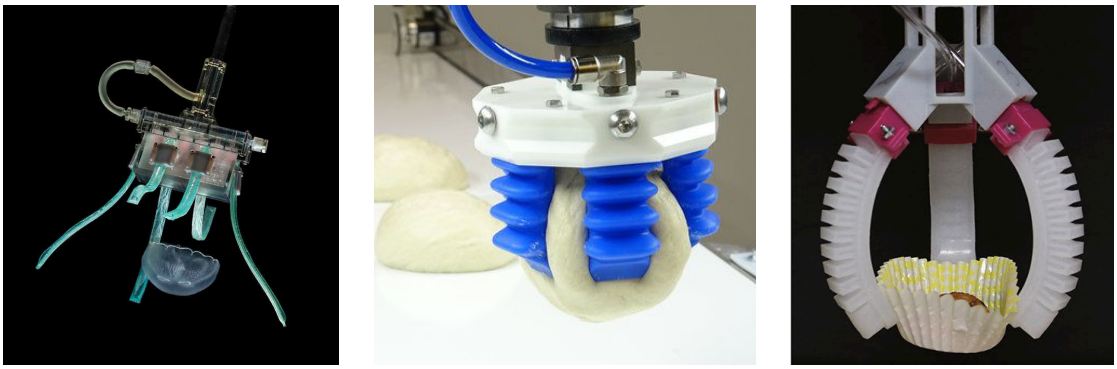

(a) (b) (c)

Figure 1.1 – Soft pneumatic grippers picking up fragile and difficult to handle objects (a) An ultragentle soft robotic gripper capable of grasping delicate marine life specimens including brittle animals (e.g., corals) and echinoderms (e.g., sea cucumbers) and jellyfish (Sinatra et al., 2019) (b) An MGRIP end-effector from Soft Robotics Inc. handling dough balls. The soft gripper can precisely place dough balls on a production line without leaving markings on the dough (From https://www.softroboticsinc.com/bakery-case-study retrieved 15.10.2019) (c) A pneumatic soft gripper lifting a cupcake liner filled with a 23 g of salmon. The gripper is able to lift the cupcake liner without crushing it (Wang et al., 2017)

printing was used to fabricate a pneumatic based soft gripper consisting of three smart fingers called Somato-Sensitive Actuators or SSAs (Truby et al., 2018). The SSAs use a similar method for actuation as the grippers shown in figure 1.1 and have been given the ability to feel by integrating a network of resistive strain sensors. The SSA is able to sense its own shape and curvature and is able to detect when an object is present in the gripper. The SSA was made by filling a mould with viscous silicone and a direct ink write printer was used to inject iono-gel based conductors. The SSA shows how digital fabrication can be utilised to produce soft robots with the ability to feel just like the human hand.

The fabrication process of EMB3D printing is able to rapidly produce large 3D shapes with integrated transducers, however there are some clear limitations to this fabrication technique. Firstly, the actuation mechanism is not integrated into the structure itself. An external compressor and flow controller is required to actuate the device. This is a problem when an SSA with more degrees of freedom is required. More degrees of freedom require more individually controlled actuators (chambers). More chambers require more connections making it difficult to neatly integrate everything into the SSA. This is a problem with all soft machines which do not have integrated transducers. Secondly, it is difficult to interpret the output of resistive strain sensors because they are dependent on many variables (Frutiger et al., 2015; Atalay, 2018). The output of resistive sensors may be strongly dependent on the rate of deformation (Shintake et al., 2018), humidity (Cochrane, 2007), and temperature (Bessonov et al., 2014). This was also observed in the SSA. The supplementary information reveals that the sensors are highly

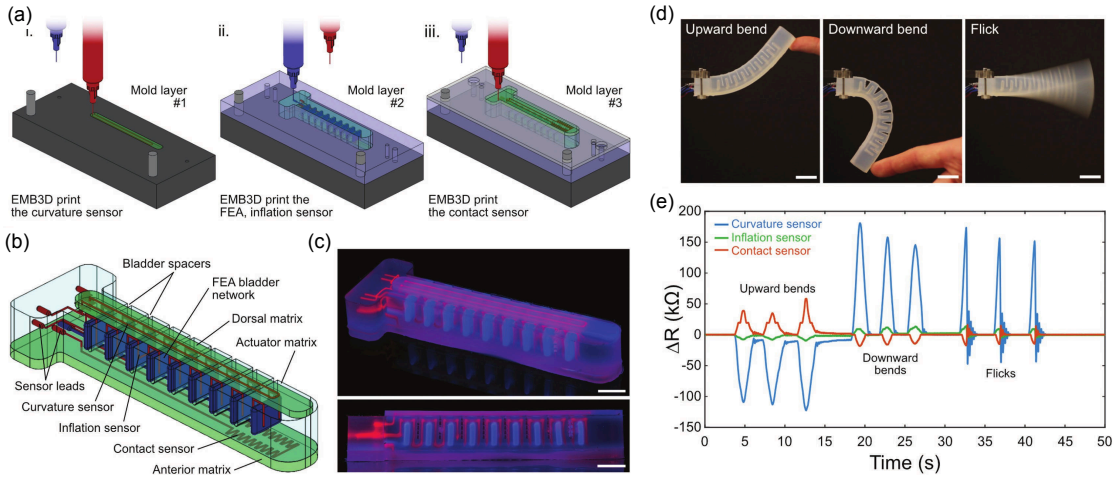

Figure 1.2 – A single finger, or soft somatosensitive actuator (SSA), of a smart gripper with integrated sensors (modified from Truby et al., 2018. (a.i) A thick base block with a recessed area is filled with uncured PDMS and an ionogel curvature sensor is injected (a.ii) A second mould layer is attached and filled with uncured PDMS. The chambers are formed by injecting a fugitive material and an inflation sensor is patterned around these by injecting an ionogel (a.iii) A third mould is attached and filled with uncured PDMS. An ionogel contact sensor is patterned inside this layer (b) A 3D diagram showing the layout of chambers and sensors (c) black light exposure photographs of SSA with fugitive chambers filled with blue fluorescent dye and the sensor network filled with red fluorescent dye. Scale bars are 10 mm (d) Photographs of an un-inflated SSA being bent upwards, downwards, and flicked (e) the resistance change of the curvature, inflation, and contact sensor when the three actions are repeated three times. Scale bars are 20 mm.

dependent on humidity. The sensors reading drifts between 40% in low humidity and 80% in high humidity in just one day. The resistance of the SSA sensors were shown to also be dependent on temperature. The sensors decrease in resistance by 225 kΩ when the temperature is increased from 0° C to 100° C. The resistance change is comparable to the output of the contact sensors of the SSA (approximately 400 kΩ). It is therefore hard to determine whether the change in resistance is due to deformation, humidity or temperature. A better way to measure strain is with a capacitive sensing (Litteken, 2017). Capacitive sensing is based on geometric changes and is less dependent on humidity, temperature, cycle number, and rate.

The limitations of the EMB3D process can be overcome by choosing a more suitable transducer and printing technology. A recent review ((Rich et al., 2018)) lists the main transducer technologies which may be integrated into soft robots to make untethered devices (Figure 1.3). The review included pneumatic actuators, liquid-crystal elastomer actuators (LCE), bio-hybrid actuators, shape memory alloys (SMA), ionic polymer-metal composites (IPMC), and dielectric elastomer (DE) actuators. The problem with pneumatic actuators and LCEs is that the external hardware to control them is difficult

to miniaturise. SMA being electro-thermal actuators are not intrinsically soft and are not well suited for high frequency applications. Bio-hybrid actuators are based on living cells. A lot of work needs to be done before they can be used outside of the Petri dish. The main limitation of IPMCs is the mode of actuation. IPMCs are typically used in bending mode. Overall the most attractive technology for integrating into soft structures are DE actuators. DE actuators are compliant capacitors which deform when a high voltage (100 V/µm) is applied (Figure 1.4). DEA are made of intrinsically soft materials, are electrically controlled, are fast, and have suitable levels of strain.

Actuation method	Strain (%)	Work density (kJ m^{-3})	Modulus (MPa)	Power density (kW m^{-3})	Strain rate (% s^{-1})	Frequency (Hz)	Auxiliary equipment	Deformation type
Skeletal muscle	20–40	8–40	10–60	50–300	10–50	1–10	Body metabolism	Contraction
Pneumatic actuator	10–40	1–200	0.1–100	10–1,000	10–70	1–5	Pneumatic pump, valves	Contraction, bending, expansion
Liquid-crystal elastomer	10–50	1–50	**0.1–3**	0.01–10	1–10	0.001–1	Light or heat source	Contraction, bending
Bio-hybrid actuator	10–25	0.1–10	**0.01–1**	1–10	10–100	1–5	Biocompatible medium	Contraction
Shape-memory alloy	4–8	**10^4–10^5**	28–75 × 10^3	**10^3–10^5**	10–50	0.5–5	Power supply	Contraction, bending
Ionic polymer–metal composite	0.5–10	1–10	25–2,500	0.01–1	1–3	0.1–2	Power supply	Bending
Dielectric elastomer acutator	**1–1,000**	100–500	**0.1–3**	**10^3–10^5**	**10^2–10^5**	**1–100**	Power supply	Bending, expansion

Bold denotes better performance. Bulky and more complex auxiliary equipment presents a significant challenge to untethered implementation.

Figure 1.3 – Performance of soft transducers for untethered soft robots (Reproduced from Rich2018). Bold denotes better performance. The auxillary equipment is also listed. Electrical control is the preferred energy supply because it is compatible with standard electronics.

Recently a variation on the traditional DE actuator has been introduced. Hydraulically Amplified Self-Healing Electrostatic (HASEL) actuators (Acome et al., 2018a). The transduction mechanism of HASEL actuators is very similar to DE actuators (Figure 1.4). The only difference being an additional layer of liquid between the electrodes. Introducing a dielectric liquid into a DE actuator has several advantages. The liquid reduces the stiffness of the actuator thus improving actuation performance. The liquid gives the actuator the ability to heal (more on this in the background section 2.2). In addition HASEL transducers do not have to be manufactured from stretchable materials which increases the number of materials which HASEL devices can be fabricated from. In this thesis one technology is not chosen over the other. Instead the strengths of both electrostatic transducers are harnessed. For example sensing could be accomplished with a capacitive DE sensor and actuation could achieved using a HASEL actuator.

A more suitable way to fabricate soft machines is to use a digital additive manufacturing approach. Additive manufacturing is the process of adding material layer by layer to produce 2.5D or 3D structures (Ngo et al., 2018). Soft machines like the SSA developed by Truby et al. (2018) are complex 3D structures consisting of multiple materials. Additive manufacturing enables the fabrication of complex soft machines. Using additive manufacturing does not require moulds or masks. Making it easier to modify the design. In addition multiple variations of the same design may be printed simultaneously. This

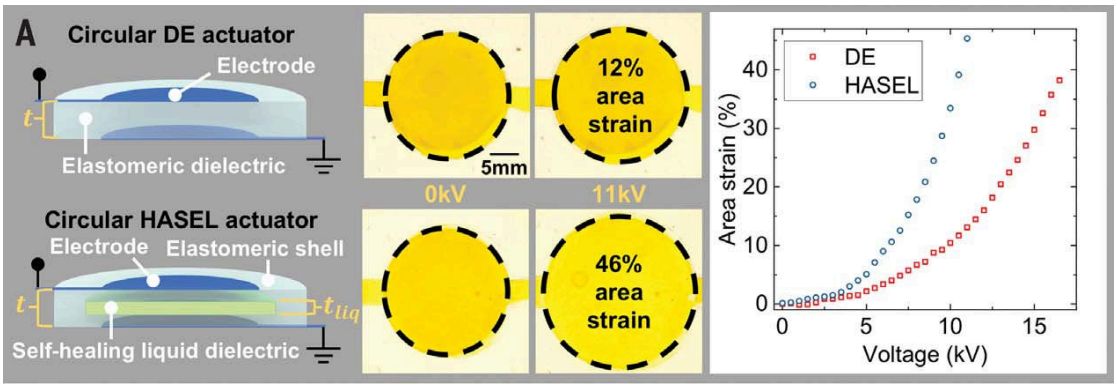

Figure 1.4 – Comparison of DE and HASEL actuators (left) The cross section of DE actuator and a donut-like HASEL actuator (middle and right) A comparison of the actuation performance of a DE and a HASEL actuator. The HASEL actuator is softer due to the dielectric liquid and produces more strain at a given voltage. The actuators compared had the same total dielectric thickness and both were fabricated from the same elastomer (Ecoflex 00-30, Smooth-on). Figure modified from Acome et al. (2018a)

makes it easy to rapidly prototype and test different designs. The cost is also lower when producing small production runs because there are no tooling costs. Making it perfect for small custom print jobs. Furthermore additive manufacturing is digitally controlled. The automation ensures that each part produced has similar properties.

There are a number of additive manufacturing approaches but not all are suitable for printing soft machines. Electrostatic transducers are layered structures with thin alternating layers of compliant electrodes and insulating elastomer layers. The additive manufacturing process must be able to print thin layers (10-20 µm) and alternate multiple materials. Most additive manufacturing can be grouped into the following categories: vat vat photopolymerization (SLA, DLP), powder bed fusion (SLS, MJF), material extrusion (FDM, DIW), material jetting (IJP AJP) (Bikas et al., 2019). Of these vat polymerisation and powder bed fusion are not suitable for multi-material printing. Material extrusion systems are not able to produce layers thin enough. At present only material jetting is able to produce thin layers of alternating materials. There are three material jetting processes: inkjet printing, aerosol-jet printing and electro-hydrodynamic jet printing (Figure 1.5). Of the three ink-jet printing is the most suitable because it is a good compromise between resolution and speed (Shin et al., 2015) and has been used to print compliant electrodes and elastomers (See below).

Since HASEL transducers are relatively new there has only been a single publication on printing these devices (Manion et al., 2018). The shell of a donut-like HASEL actuator was printed with a commercial printer,Stratasys Objet500 Connex3, and the materials Agilus clear and Tangoblack-plus. Multi-wall carbon nano tube (MWCNT) electrodes were manually applied. The authors claim that the printed actuator performed better than the actuators presented by Acome et al. (2018a).

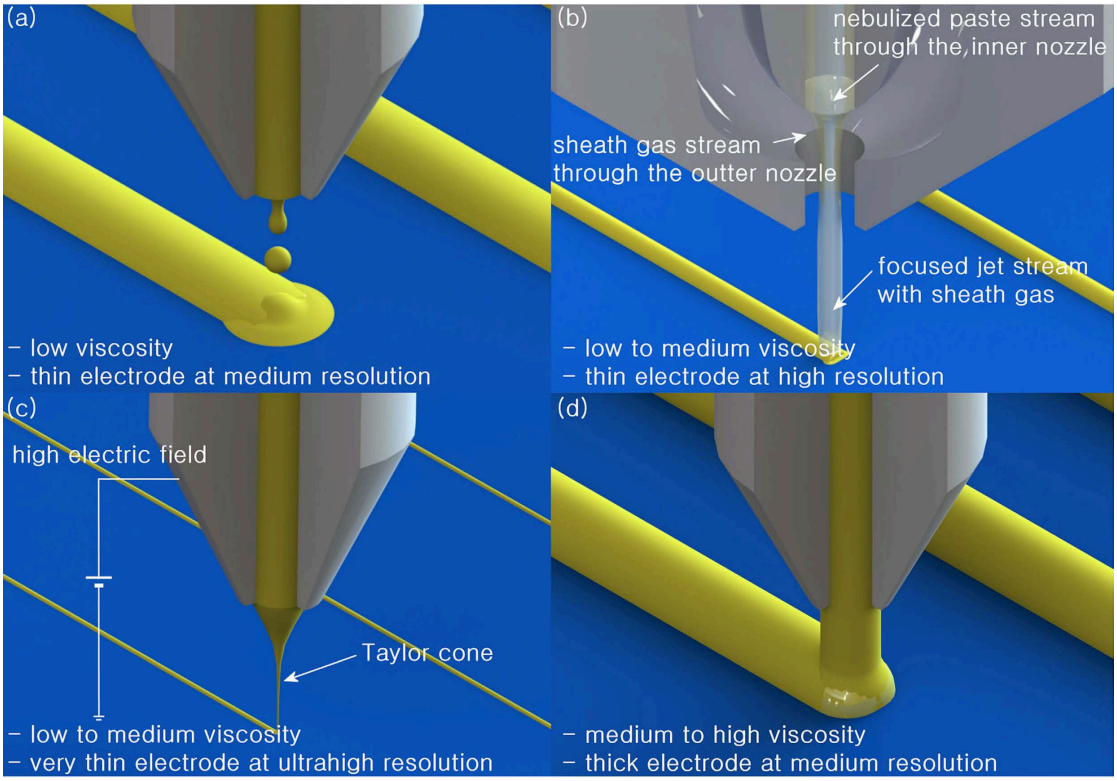

Figure 1.5 – Comparison of various non-contact printing techniques (a) inkjet printing (b) aerosol jet printing (c) electrohydrodynamic jet printing (d) direct ink writing (DIW). The ink requirements and printing resolution is qualitatively compared (Shin2015)

More work has been conducted on printing DE actuators. Ink-jet printing has been used to pattern compliant electrodes on to pre-fabricated silicone membranes (Baechler et al., 2016). A dilute dispersion of MWCNT's (AQUACYL™ AQ0302, Nanocyl SA.) was produced by adding iso-propyl alcohol along with some additives to improve the rheology of the ink. The MWCNT electrode had a conductivity of less than 10 $k\Omega\,\square^{-1}$ at rest and increased by a factor of 10 at 10% strain. The printed printed electrodes are extremely thin 10 nm per printing pass. However the electrode is relatively stiff and cracks when stretched. No tests were conducted how this may affect the cyclic properties of the electrode.

The dielectric membranes of DE actuators have also been printed. One of the first attempts was using a commercially available 3D printer (Rossiter et al., 2009). The printer, Eden 350V by Objet Geometries, uses an ink-jet nozzle to pattern a photo-curable acrylic based polymer layer by layer. Because the printer is ink-jet based printer it was possible to print relatively uniform dielectric layers with a thickness of 90 µm in three passes. An actuator was fabricated by brushing on a silver grease electrodes. Actuation was observed, but the actuator exhibited strong hysteresis due to the visco-elastic nature of the dielectric material. In addition actuation diminished with repeated

voltage stimulation. Both of these behaviours are undesirable in DE actuators.

Fluid deposition modelling (FDM) printing of thermoplastic polyurethanes (TPUs) has also been used to print dielectric membranes for DE actuators (Gonzalez et al., 2019). A commercially available TPU, Diabase X60 Ultra Flexible Filament, was used to produce dielectric membranes from 0.2 mm to 1 mm thick. Different printing paths where explored to determine the effect this has on the uniformity of the membranes. The samples with the concentric circles had a maximum height variation of 16 µm and the parallel lines had a height variation of 56 µm. The printed membranes were shown to have a stiffness between 3MPa and 8 MPa. The breakdown strength of the polymer was relatively low between 5 V/µm to 30 V/µm. The actuators which were prepared with these dielectric materials produced area strains lower than 5%.

Digital printing has also been used to print complete DE transducers - alternating layers of electrode and dielectric materials. Aerosol jet printing (AJP) was used to pattern reduced graphene oxide (rGO) electrodes with a thermally cured two part silicone (Reitelshöfer et al., 2016). Actuators with a dielectric thickness of approximately 60 µm and electrodes with a sheet resistance of 4 $k\Omega\,\square^{-1}$ were fabricated. According to the paper, the devices actuated but no evidence was given to support this.

Direct ink write (DIW) printing has also been used to print complete DE actuators. A cantilever bending actuator was fabricated by printing a DE actuator on a flexible base layer. When the DEA actuates it caused the structure to bend. The structure was fabricated with UV curable ionic hydro-gel electrodes and a UV curable silicone based dielectric layer. The thicknesses of the base layer, hydro-gel electrodes, and dielectric layer were 300 µm, 380 µm, and 500 µm respectively. The 30 mm long cantilever actuator was shown to deflect by about 10 mm. To date many different materials and printing processes have been used pattern the electrode, dielectric material or both. However there appears to be a barrier to using these new fabrication techniques to build more complex devices.

Despite the growing interest in printing DE actuators, few have explored the potential of printing complex devices. This may be due to the following reasons. First the materials required to print electrostatic transducer are not commercially available. This presents a large obstacle to producing devices. Before any device can be fabricated the materials must be formulated and characterised. Second, the printing technique must be carefully selected to produce printed layers with the right electro-mechanical properties. Many of the studies have used commercially available equipment and materials to print dielectric layers. Either the layer thickness and uniformity was not suitable or the material properties were less than satisfactory. Third, the materials used for fabricating electrostatic transducers are difficult to stack. When the materials are stacked the vastly different surface properties of the dielectric and electrode materials may result in poor dielectric layers which lead to unreliable devices. Finally, there

are many practical reasons why one may opt to use standard fabrication techniques. Additive manufacturing techniques often take longer to produce a single device when set-up and cleaning are taken into account. And the equipment may not be available due to cost limitations.

To date ink-jet printing has only been used to print simple characterisation devices. Most of the literature reports on printing electrodes or dielectric materials. Only two studies looked at printing complete DE actuators. The studies of completely printed DEs show some of the challenges when layering different materials. However the devices are simple planar actuators or bending actuators. The devices do not take advantage of digital fabrication. Ink-jet printers are able to produce high resolution multi-layer prints. In this thesis the ability to print complex structures consisting of densely integrated transducers will be explored. Making use of the high resolution printing to print many actuators side by side and making use of the ability to create multi layer structures to make complex networks of conductors and channels. In order to do this the challenges of producing the materials and combining them into a multi-layer and multi-material structures will have to be addressed.

1.2 Research objectives and scope

The objective of this thesis is to use digital fabrication, ink-jet printing, to integrate many electrostatic transducers into a soft machine. The focus is on the process of formulating the materials, characterising the electro-mechanical properties, and developing new processes for layering them. In addition, two devices are manufactured to demonstrate the benefits of ink-jet printing complex soft machines. The specific objectives are listed below:

Formulate, print, and characterise an electrode material. The equivalent resistance (resistance of traces and electrode combined) must be less than 10 MΩ to ensure the electrostatic actuators can operate at high frequencies. The thickness of the electrodes should be significantly thinner than the dielectric layer (<10%). The thickness of DE electrodes should be minimised to reduce their impact on actuation. The electrodes must be able to withstand the strain generated by electrostatic transducers and strains induced by bending (~ 10% strain). The electrode must be pattern-able on printed silicone membranes.

Formulate, print, and characterise a sacrificial material to form channels. Channels are required for HASEL transducers. The material must be printable on silicone and should be readily soluble at room temperature in solvents which are compatible with silicone.

Formulate, print, and characterise a silicone based dielectric material. The printed di-

electric layers must be thin <50 µm, uniform (<5% variation in surface height) and the breakdown strength should be maintained despite processing the material differently. The dielectric membranes must be pattern-able on the printed electrode and sacrificial materials.

Fabricate demonstration devices to explore the benefits of printing soft machines. The demonstration devices must consist of multiple actuators. The actuators must in the millimeter scale to enable dense integration of actuators. The means to interconnect multiple actuators will also have to be explored.

Given that the materials required for printed electrostatic transducers are not commercially available and no processes exist for printing these materials, a large portion of the study is dedicated to the formulation and characterisation of these materials. The examples of soft machines presented in the introduction were included to illustrate distant goals of this thesis. Large three dimensional structures such as the SSA gripper will not be realised. Instead 2.5D devices are fabricated which consist of 10 printed layers or less. Novel methods are explored to produce 3D structures by printing channels and chambers which can be inflated. In addition the demonstration devices will only be composed of actuators. In the introduction many references were made to integrated transducers, implying that sensors will also be integrated. Sensor development requires many iterations of sensor design, testing and calibration which does not contribute to the overall goals of this thesis.

1.3 Overview of thesis and contribution

The thesis consists of three parts. The introductory chapters cover the fundamentals of electrostatic transducers and ink-jet printing. Special attention is given to the materials and processes used to fabricate them. The novel contribution of this thesis can be found in the two major parts of the thesis. Part one is concerned with the formulation of ink-jet printable materials, the processes used to print them, and the characterisation of these materials. In the second part the materials from part one are printed into multi-layer soft machines. Two soft machines are demonstrated. The first is a soft peristaltic pump showing how integrated transducers can be used to manipulate fluids. The second is a soft robot inspired by the locomotion of invertebrate animals. An overview of the thesis is given below.

Introductory chapters

2. Fundamentals of electrostatic transducers and inkjet printing gives a basic introduction to DE and HASEL transducers.The sections cover the basic actuation principle, give some application examples, fabrication methods, and highlight some of the limitations these fabrication methods pose on the devices. In addition

the basics of piezoelectric inkjet printing is covered.

Part I: Formulation and characterisation of inkjet printed materials

3. Carbon black binder-less electrodes presents a method to print thin stretchable electrodes based on carbon black and a non polar solvent. Using a non-polar solvent makes it possible to print this electrode onto silicone surfaces without any surface treatment or modification of the silicone membranes. The electrode does not contain a binder and is therefore highly conductive and dries in a matter of seconds. The shape and resistance of the electrode is characterised for electrodes at different printing temperatures. Showing how the resolution of printed traces depends greatly on printing temperature. The electrodes are also tested in-situ to determine the performance of the electrodes when stretched over many cycles in a realistic high voltage and biaxial stretch scenario. The same tests are also used to show that thick electrodes degrade more rapidly than thin electrodes.

4. Sacrificial channels shows how an alcohol soluble polymer can be ink-jet printed to produce channels in soft silicone devices. The poor adhesion between silicone and other polymers is exploited to make channels which can be rapidly opened at a rate of millimetres per second. The sacrificial material contains a high volatility and low surface tension solvent making it possible to print sacrificial materials directly on to silicone without any surface treatment. Sacrificial channels as narrow as 150 µm can be printed with the equipment and methods used in this work.

5. Silicone dielectric layers were printed by combining a two part thermal cure silicone with a low viscosity solvent. The low viscosity mixture can be printed on virtually any material to produce thin dielectric layers. In addition a printing strategy was developed to print thicker membranes which are resilient to material contrasts. The uniformity of the printed layers is characterised in the vicinity of sacrificial channels and around printed holes (electrical vias). The breakdown strength of the printed membranes was also characterised.

Part 2: Printed soft machines to demonstrate benefits of printing

6. Ink-jet printed soft peristaltic pump demonstrates how soft transducers can be integrated directly into a fluidic system to control the flow of liquids. Integrating soft transducers hopes to reduce the amount of external equipment required for fluidic systems thus reducing the cost and increasing the portability of such systems. The process presented shows how to make a completely soft multilayer structure with overlapping channels to pump water and other biological fluids. The fluidic pump is electrically controlled meaning that readily available compact electronics can be used to control the device. A novel electrode layout is presented showing how HASEL actuators can be made to push liquids along channels. Since the HASEL actuators must be closely spaced to pump fluids effectively the pump also

highlights how printing silicone can be used to encapsulate high voltage electrodes to create soft machines with more dense integration of transducers. A reliable process for making fluid connections to soft machines is also presented.

7. **Ink-jet printed soft slug-drive** is a completely soft linear motor intended for soft robots. The slug drive is a concept which shows how small repetitive deformations of HASEL transducers can be combined to to displace a soft robot. The method of motion is similar to the motion of invertebrate animals such as worms, snails and slugs. The slug drive shows how many HASEL actuators are integrated into a soft structure to produce the propagating wave of compression to move a soft robot. The slug drive uses an air cushion, akin to a hydrostatic skeleton, to give the soft slug some structure. This highlights how printed channels can be used to make truly soft robots without any rigid components. The slug drive also demonstrates how the ability to pattern and layer the dielectric material makes it possible to neatly integrate the connections of the HASEL actuators. Inkjet printing makes it possible to integrate complete circuits into soft robots eliminating the need for external connections.

2 Fundamentals of electrostatic transducers and inkjet printing

2.1 Dielectric elastomer (DE) transducers

2.1.1 DE fundamentals

DE transducers are compliant capacitors which deform when a voltage is applied. The effect was first documented by Röntgen in 1880 when he sprayed electrons onto a piece of rubber and noted that this resulted in a large deformation. Röntgens experiment was repeated in 2010 by Keplinger et al. (Figure 2.1). Keplinger's suspended a piece of rubber on a frame and sprayed electrons on to the surface with a pair of moving combs. The combs spray electrons onto the rubber surface where they become trapped. The opposite charges attract one another and compress the piece of rubber. Since the rubber is incompressible it decreases in thickness and increases in area. The mass is lowered due to this area change. The experiment by Röntgen was an excellent demonstration of spraying charges and static electricity but is not very practical as an actuator. The sprayed charges cannot be removed. This problem was later solved by Pelrine et al. in 1998 who added compliant electrodes onto the rubber and described the basic equation (2.1) for the compressive pressure p generated due to an electric field E. An equation for the stain in the thickness direction (2.2) and in the planar directions (2.3) are also given. Note that the equations are only valid for low strains because the initial thickness was used to deduce these formulas. In addition the material properties ε and Y are non linear.

$$p = \varepsilon_0 \varepsilon E^2 \tag{2.1}$$

p = actuation pressure
ε_0 = permittivity of free space $8.85 \times 10^{-12}\,\mathrm{F\,m^{-1}}$
ε = relative permittivity
E = electric field

$$s_z = -p/Y = -\varepsilon_0 \varepsilon E^2/Y = -\varepsilon_0 \varepsilon (V/z)^2/Y \tag{2.2}$$

s_z = strain in thickness direction
Y = Young's modulus
V = Voltage
z = Thickness of membrane

$$s_a = (1 + s_z)^{-0.5} - 1 \tag{2.3}$$

S_a = in-plane strain ($s_a = s_x = s_y$)

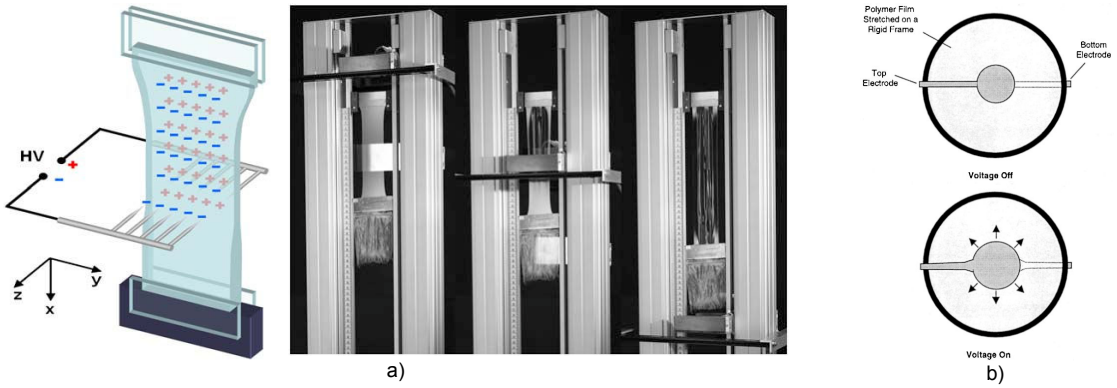

Figure 2.1 – (a) An experiment conducted by (Keplinger et al., 2010) to replicate an experiment conducted by Röntgen. The experiment shows how electrostatic charges can be sprayed on to an elastomer using combs. The opposite charges squeeze the elastomer causing it to elongate. (b) In 2010 Pelrine et al. showed how more practical devices can be built using compliant electrodes. A diagram (view from above) shows a frame with a pre-stretched dielectric elastomer film and circular electrodes. When a voltage is applied the electrodes squeeze the dielectric film causing it to expand. The figures have been modified from Keplinger et al. (2010) and Pelrine et al. (1998)

2.1.2 DE applications

Since Pelrine's work there has been an explosion of DE based devices. DE transducers are extremely versatile given that they can be used as actuators (DEA), as sensors (DES), and as generators (DEG) (Carpi et al., 2008). A few examples have been selected to demonstrate the versatility of DE transducers and also point out the key benefits. Figure2.2a shows a soft DE sensor sheet made from a thin silicone membrane sandwiched between two carbon based electrodes (Xu et al., 2015). By measuring the capacitance of the sensor it is possible to measure the average strain of the sensor. Xu et al. (2015) further developed the sensing technique making it possible to sense localised deformation

by using a multi-frequency capacitance sensing technique based on a transmission line model. Figure2.2b shows a DE stack actuator (Kovacs et al., 2009). By using the contraction in the z-direction it is possible to achieve a high force actuator. The displacement of a single DE layer is small, but by combining many in series the total elongation can be increased. Figure2.2c shows an electrically tunable lens (Maffli et al., 2015). The lens consists of a fluid filled core surrounded by a planar DE actuator. The actuator controls the tension on the fluid filled lens thus changing its shape and focal length. The tunable lens is very fast at adjusting its focal length because a silicone dielectric material was used. Figure2.2d shows a VHB based (commercial acrylic adhesive) DEA undergoing an extreme change in area 488% (Huang et al., 2012). The test consisted of a planar DEA under constant force loading. This was achieved by hanging individual weights off the side of a table. The actuator failed due to electro-mechanical instability shortly after reaching 488%. By designing a material which stiffens at high strains the electro mechanical instability can be avoided, making it possible to achieve reliable actuators with high strain capabilities (Zhao and Suo, 2010). Figure 2.2e shows a DE generator in a wave pool (Moretti et al., 2019). The device consists of tube closed on one end with a deformable DEG. When the tube is lowered into water the air is compressed, thus deforming the DEG. When waves pass, the DEG membrane expands and contracts, generating energy. To summarise, soft DE transducers can be designed for high force, high strain, or both. In addition, DE actuators can move incredibly fast when non visco-elastic materials are used. Due to these unique properties, DE transducers are used in many fields including: wearables (Atalay, 2018; Frediani et al., 2014), haptics (Phung et al., 2015), soft robotics (Jung et al., 2007), optics (Maffli et al., 2015), biomedical (Poulin et al., 2016), and energy harvesting (McKay et al., 2015).

2.1.3 DE fabrication

DE transducers are normally fabricated by first producing the dielectric film and then patterning electrodes on either side of the film. The dielectric film of a DET must be thin, uniform, have a high breakdown strength, and ideally should be defect free. Often the film is purchased which greatly simplifies fabrication. Purchased films are made in clean room environments and are more likely to be defect free. Three types of film are commercially available, acrylic based VHB from 3M, silicone based Elastosil from Wacker Chemie AG, and silcione EAP film from Parker Hannifin Corporation. VHB is the material mentioned earlier which produces high strains, however the material is highly visco-elastic and unreliable. VHB is a industrial grade pressure sensitive adhesive and apart from stickyness the quality of the film cannot be guaranteed. Elastosil and the EAP film from Parker Hannifin are silicone based films which are intended for DE transducers. Silicone films have a lower visco-elasticity making them well suited for high frequency actuation. Although silicone films produce lower actuation strains than VHB. Typically silicone DE actuators produce 10% strain but under certain conditions have been shown to produce strains up to 85% (Akbari et al., 2013).

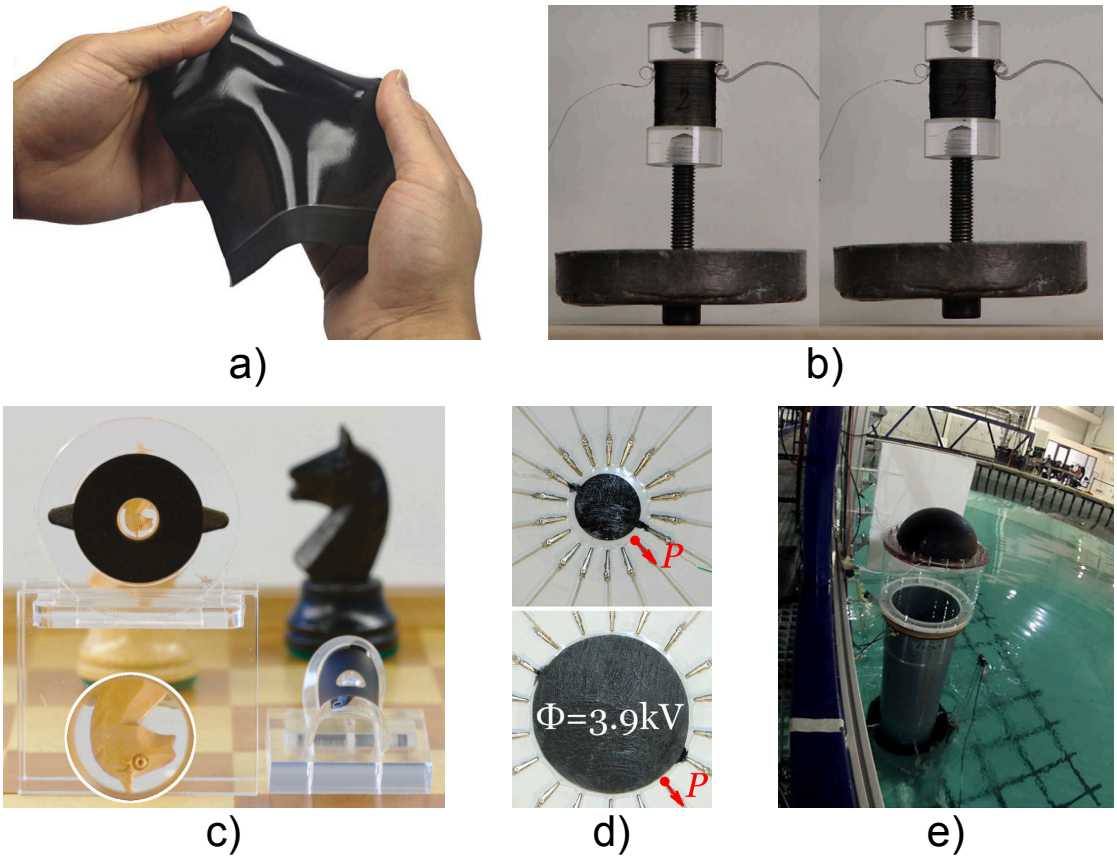

Figure 2.2 – A collection of dielectric elastomer devices and demonstrations (a) A compliant DE sensor. Stretchable sheets of material like this can sense their own deformation (Xu et al., 2015) (b) A DE stack actuator lifting a heavy weight (1 kg mass). The actuator reduces in length by 10% when actuated (Kovacs et al., 2009) (c) A tuneable DE lens. Silicone dielectric is used to create an extremely fast and bendable lens (Maffli et al., 2015) (d) An experiment to demonstrate the large deformations possible with DE actuators. A DE with constant force loading was shown to have an area expansion of 488% (Huang et al., 2012) (e) a small-scale prototype of wave energy converter utilising a DEG to generate electricity. The generator was tested at realistically scaled sea conditions and was shown to generate a peak power output of up to 3.8W (Moretti et al., 2019). Images modified from original publications.

Films can also be prepared in the lab. There are a number of benefits to preparing your own films, such as having more silicones to choose from, preparing custom mixtures with additives, choice of release layers and substrates, and films can be prepared with a specific thickness and size. The two most common methods for producing films are casting and spin coating. A process to make silicone films by casting is shown in Figure 2.3(A-F) (Rosset et al., 2016). Silicone is cast onto a PET substrate which has been coated in a water soluble release layer - in this case Polyacrylic acid (PAA). The silicone is then cured in an oven. Once cured, the membrane is laser cut to size and an adhesive support frame is added. The PET substrate can then be removed in vat of hot water. With this process it is possible to make high quality films down to a few microns. High

quality films can also be produced by spin coating (Lotz et al., 2011; Duduta et al., 2016). Spin coating is well adapted for creating stacks (Schlaak et al., 2005). One of the main limitations of spin coating is the size of the membranes which can be produced.

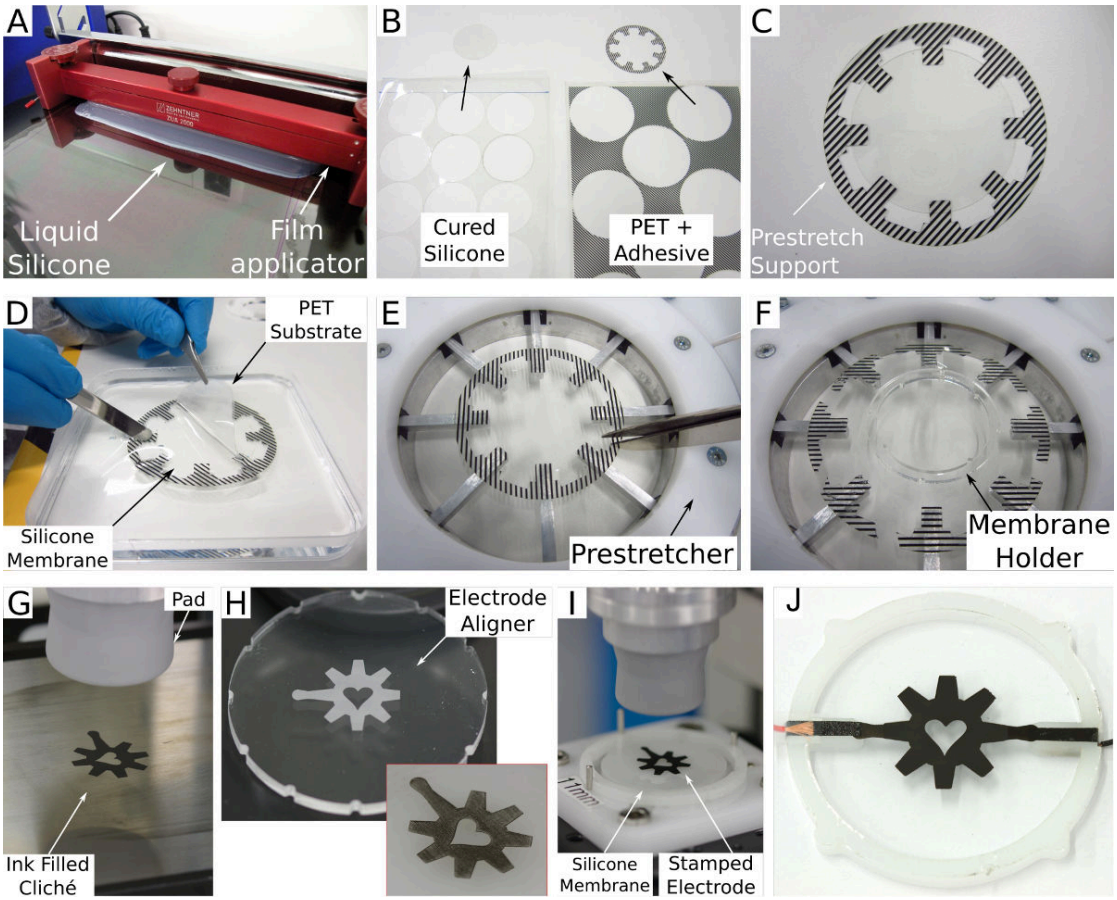

Figure 2.3 – Overview of silicone based DE demonstration actuator fabrication process. (A) Casting of silicone membrane on a PET substrate covered with a water soluble release layer(B) Laser cutting of cured silicone membranes and adhesive frames to pre-stretch the silicone membranes (C) Attachment of adhesisve pre-stretch support to silicone membrane (D) Removal of PET substrate from silicone membrane by dissolution of release layer (E) The free hanging membrane is attached to the prestretcher and the pre-stretch support is trimmed between the fingers (F) The membrane is stretched and a frame lined with adhesive is placed on the pre-stretched film (G) Cliché filled with conductive ink and the soft silicone stamp used to transfer the electrode ink (H) Laser etched electrode aligner align the printing plate. Inset figure shows example of a well-aligned electrode.(I) Printing plate with a silicone membrane loaded. The electrode has already been patterned (J) Finished device with two electrodes and electrical connections. When actuated the cog expands and the heart cutout becomes smaller. Reproduced from Rosset et al. 2016

The electrodes of a DEA must be stretchable, thin, conductive, and pattern-able. Most conductors are not stretchable. The most compliant conductors are conductive liquids. DE actuators have been made using liquid metal alloys (Pekas et al., 2012), electrolytes

(Keplinger et al., 2013; Christianson et al., 2018), and ionic liquids (Chen et al., 2014).However it is difficult to form thin layers with liquid metals, electrolytes dry out, and many ionic liquids are toxic. For this reason engineers have devised ingenious ways of making solid conductors stretchable. One way is to structure metals so that they deform more easily. DE actuators actuators have been made with corrugated silver electrodes (Jones et al., 2010), ion implanted titanium (Dubais and Alexandre, 2006) and gold electrodes (Rosset et al., 2008), and buckled silver electrodes (Low and Lau, 2014). However the most popular way to fabricate DE actuators is by producing conductive composites. Conductive composites are made by combining a conductive powder with a grease or an elastomer. Carbon black is a commonly used material for DE electrodes because it is readily available, cheap, and non toxic. Carbon black has been combined with silicone oils and silicone elastomers to make compliant electrodes (O'Brien et al., 2007)). To form more conductive and thinner electrodes carbon nano tubes have also been combined with silicone elastomers (Kim et al., 2012). Conductive powders such as carbon black can also be directly applied to a membrane, however without encapsulation the performance of the electrodes cannot be guaranteed. Powdered electrodes without encapsulation degrade more rapidly due to ablation (Yuan et al., 2009).

The electrodes are patterned on to the dielectric film using one of four ways: painting, masking, stamping, and transfer printing. Painting is the most primitive method to pattern electrodes. Often this technique is used to quickly prototype DEA. Painted electrodes are irregular in thickness and have poorly defined edges (O'Brien et al., 2007; De Saint-Aubin et al., 2018). Masking is a replication technique where a mask or screen is used to pattern the electrode mixture. The mask is placed on the dielectric membrane and the mixture is deposited over the full area. When the mask is removed only the exposed areas remain. The mixture can be deposited by airbrushing, or with a squeegee as in screen printing (Fasolt et al., 2016; Rizzello et al., 2016). One disadvantage of this technique is that the masks become soiled over time. Masks generally need to be cleaned or replaced regularly to ensure high quality electrodes. Stamping is a technique where the mixture to be printed is transferred to the substrate with a soft rubber stamp. The design can either be on the stamp (the stamp has been moulded to be in the shape of the electrode) or on the ink pad. When the design is on the ink pad a smooth rounded silicone stamp is used and the design is etched into the ink pad. This process is called pad printing and is illustrated in Figure 2.3(G-J) (Rosset et al., 2016). The design is etched into a metal sheet, called a cliché, which is filled by a sliding ink-cup. The blank stamp is then pressed on the cliché to pick up the the mixture and transfer it to the membrane. The main drawback of this technique is that it is a contact printing method. Contact printing methods are not suitable for free standing membranes. Transfer printing refers to any reproduction technique where the components of a DET are patterned when cured. The materials are prepared in large films and are cut to shape using a blade cutter or a laser cutter. The materials are then aligned and laminated. A recent publication showed how laser ablation could be used to pattern intricate electrodes and then transfer

it to a membrane (Araromi et al., 2015).

2.2 Hydraulically amplified self-healing electrostatic (HASEL) transducers

2.2.1 HASEL fundamentals

Hydraulically amplified self-healing electrostatic (HASEL) (Acome et al., 2018b) transducers are essentially DE actuators with a portion of the dielectric replaced with a liquid (Figure 2.4). Introducing a liquid into the structure reduces the stiffness of the actuator thus increasing the strain achievable at the same voltage (Figure 1.4). In addition, introducing fluids into a DE actuator makes it possible to tune the displacement and force of the actuator. There are two types of HASEL actuators, the basic HASEL actuator (Acome et al., 2018b) and the Peano HASEL actuator (Kellaris et al., 2018). The two actuator configurations are shown in Figure 2.5. Both actuators work by applying a high voltage. When the voltage is sufficient the electrodes compress the dielectric fluid and displace it. The difference between the two HASEL actuators is the type of materials used in their construction. The shell material of HASEL actuators is made from stretchable materials. The shell material of Peano HASEL actuators is made flexible, but not stretchable materials.

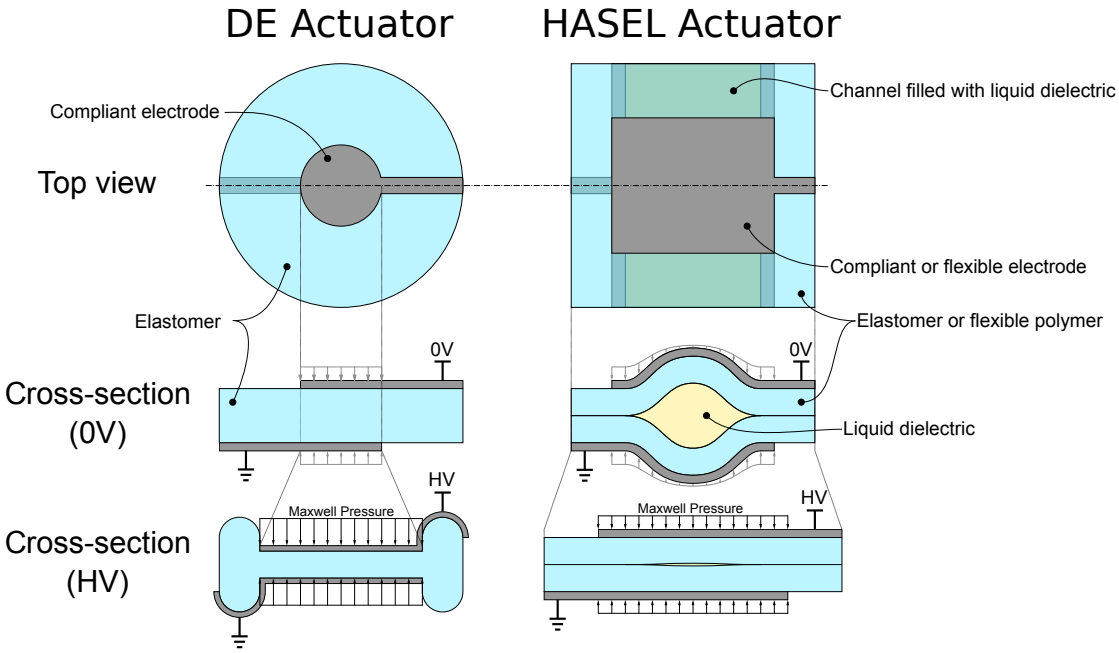

Figure 2.4 – Comparison of DE and HASEL actuators

HASEL actuators are an attractive technology because they solve many of the challenges faced by DE transducers. HASEL actuators are less susceptible to breakdown. When

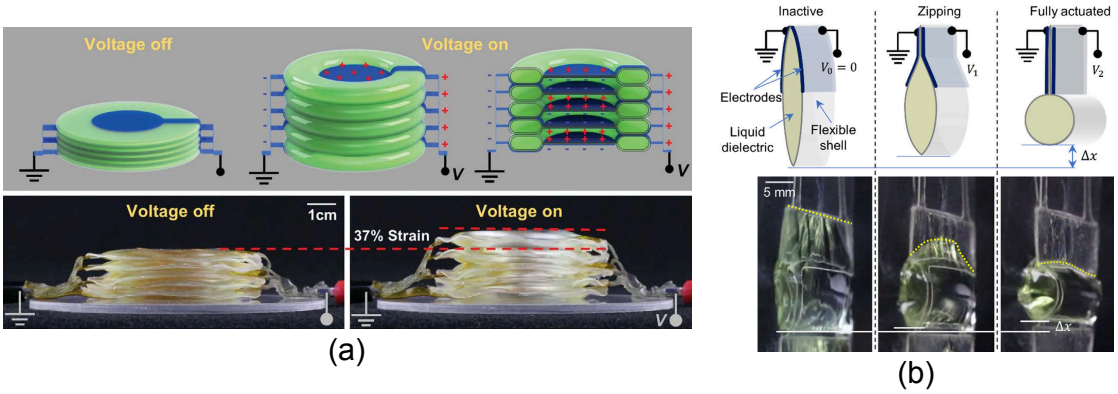

Figure 2.5 – (a) A stack of 5 donut like HASEL actuators (Acome et al., 2018b)). When actuated the stack expands by 37% (b) (B) A schematic of a single pouch Peano HASEL actuator (Kellaris et al., 2018). The leftmost picture shows the pouch in its inactive state (0V). The middle picture shows what happens when a voltage is applied.The Maxwell stress causes the electrodes to zip together starting at the top of the pouch where the electric field is at its highest. The rightmost picture shows the actuator in the fully actuated state. The actuator in the actuated state is shorter than the actuator in the inactive state. This displaces the liquid dielectric into the bottom of the pouch, leading to contraction of the structure. (D) As the voltage increases, the zipping progresses until the actuator reaches a fully contracted state, with the electrodes completely zipped together.

dielectric breakdown occurs the conductive path is broken up due to the fluid motion of the liquid dielectric. Note that this is only true for non zipping HASEL actuators. If breakdown occurs in a region without fluid the breakdown will be permanent. Another benefit of HASEL actuators is that there are more high performance materials to choose from for fabricating the devices. Non-stretchable materials have much higher breakdown strengths, up to 700 V/µm (Kellaris et al., 2018), than stretchable ones, around 100 V/µm. HASEL actuators can therefore be operated at higher electric fields and generate higher forces. Many choices are also available for the dielectric fluid. Dielectric fluids are available with different dielectric permittivity, breakdown strength, viscosity, and volatility. It is therefore easier to tune the properties of a HASEL actuator.

2.2.2 HASEL applications

HASEL transducers are in their early stages of development and we have yet to see the true potential of the technology. Most of the work on HASEL actuators has been conducted by Keplingers group. Keplingers group has developed some basic actuator configurations to produce expanding and contracting actuators (Kellaris et al., 2018; Acome et al., 2018b). The donut actuator shown in figure 2.5a expands on actuation and has been used in stacks to make a gripper (Acome et al., 2018b). The bag like Peano HASEL actuator in figure 2.5b contracts on actuation and have been used to make an animated lever arm which can move large distances (Kellaris et al., 2018). Custom

shaped actuators have also been produced to produce more complex devices (Mitchell et al., 2019). A scorpion with a curling tail has been developed consisting of a Peano HASEL actuator and a bending pouch actuator (Figure 2.6a). The scorpion demonstrates quite nicely the how the actuator can be distanced from the end effector. Of course this type of arrangement is slower because the liquid has to travel larger distances. A donut actuator with four individual quadrants has been developed to make a tilting platform. Many of these quadrant actuators have combined to make a tilting trunk (Figure 2.6b). The trunk is able manipulate light objects such as chip packets, ping pong balls and a balloon. HASEL devices which do not have a restoring force are unstable, hence the trunk has three elastic bands to return the trunk to the vertical position when no voltage is applied. Other groups have also started to explore HASEL actuators. A gripper made from bending Peano HASEL actuators was developed to pick up light and fragile objects (Park et al., 2019) and preliminary work has been conducted on using HASEL actuators for braille displays (Sirbu et al., 2019). To date HASEL transducers have only been used as actuators. It remains to be seen if HASEL transducers are also suitable for sensing.

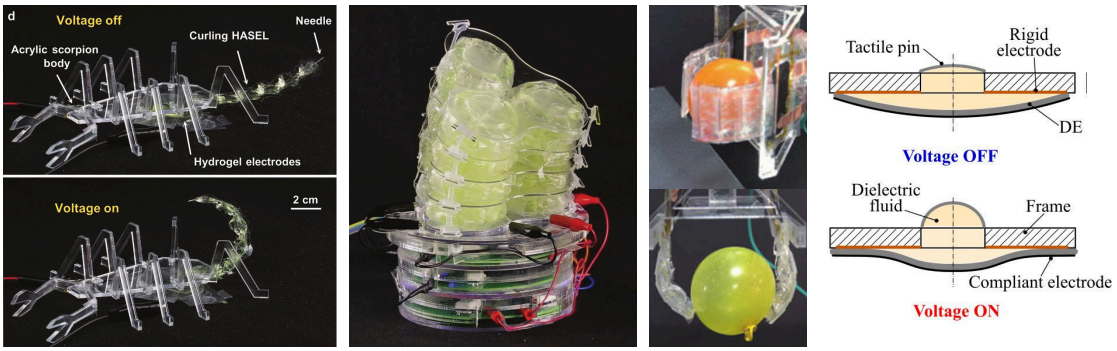

Figure 2.6 – (a) A curling actuator inspired by a scorpion (Mitchell et al., 2019). A Peano-HASEL actuator in the rear of the animal squeezes dielectric fluid into the tail. The tail curls because of a strain limiting layer on one side of the tail (b) Terry the trunk without the gripper attached (Mitchell et al., 2019). The trunk consists of stacked quadrant donut HASEL actuators. The platform has three degrees of freedom and can be used as a robotic arm (c) A gripper made from a Peano HASEL based transducer similar to the scorpion tail (Park et al., 2019). The gripper is pictured grasping a light balloon (d) A drawing of a prototype tactile actuator based on Peano HASEL type actuation (Sirbu et al., 2019). The tactile pin is able to transmit forces of up to 17 mN, between 1-3 Hz, with displacements in the millimetre range when unrestricted.

2.2.3 HASEL fabrication

HASEL transducers consist of three elements: the dielectric shell, the dielectric liquid, and the electrodes. The dielectric shell can be fabricated from stretchable and flexible materials. Stretchable materials are used when a truly soft device is required. Stretchable materials also provide a restoring force. To date the only stretchable materials which have been used for HASEL actuators are Sylgard 184 and Ecoflex 00-30 (Acome et al.,

2018b). One of the main drawbacks of using stretchable materials is that the electrodes must also be stretchable. Making stretchable electrodes which adhere well to silicone is not trivial and for this reason recent work has focused on HASEL transducers made from thin flexible shells instead. Thin flexible foils are available with higher dielectric constants and higher breakdown strengths and are readily available (Kellaris et al., 2018). Presently plastic films from the food packaging industry are used such as biaxially oriented polypropylene (BOPP) and thermoplastic polyurethane (TPU) Polyester film. These films are convenient because they can be purchased on a roll lined with a thermopolymer, allowing them to be easily heat sealed to form a liquid tight shell. Other groups have reported using Polyethylene film which is cheap and readily available. For the dielectric liquid modified vegetable oils such as Envirotemp FR3 (Acome et al., 2018b) and mineral oils such as Drakeol 7 (Kellaris et al., 2018) and Mictrans A (Park et al., 2019) have been used. The type of electrode depends on the type of dielectric shell. For stretchable HASEL actuators ionically conductive polyacrylamide (PAM) hydrogels have been used (Kellaris et al., 2018; Acome et al., 2018b) and carbon black/silicone composites (Sirbu et al., 2019). For flexible dielectric shells almost any conductor can be utilised, including vacuum-deposition process Aluminium electrodes (Kellaris et al., 2019), Copper foil (Sirbu et al., 2019), Carbon based conductive tapes (Park et al., 2019), and carbon black in a fluoro-elastomer resin (Mitchell et al., 2019). Although metal electrodes sound ideal they have been shown to ablate and completely lose electrical contact after just 20,000 cycles (Kellaris et al., 2019).

2.3 Inkjet printing

Inkjet printing is digital printing process where small droplets are jetted onto a substrate to reproduce a graphical information (Derby, 2010). The first traditionally ink-jet printing was developed for to print text and images, however the technology is now used as a more general fabrication tool. Ink-jet printing has been used to print electronics (Raut and Al-Shamery, 2018), biological materials (Derakhshanfar et al., 2018), and foods (Voon et al., 2019). Essentially any material which can be processed in liquid form.

A basic ink-jet system consists of three critical parts. A nozzle to dispense controlled volumes of liquid. A system to move the print-head or the substrate. And a computer to coordinate droplet ejection and the movement of the stages. The most common types of ink-jet printing are thermal ink-jet and piezo-electric ink-jet. Thermal ink-jet uses a thermally induced bubble to create a pressure wave and eject droplets whereas piezo-electric ink-jet printers use piezoelectric crystal to deform the printing channel and expel liquid droplets. Ink-jet printing is an interesting fabrication method because high resolution patterning of thin layers is possible. Furthermore ink-jet printing has all the benefits of digital fabrication, including automation, repeatability, and rapid prototyping.

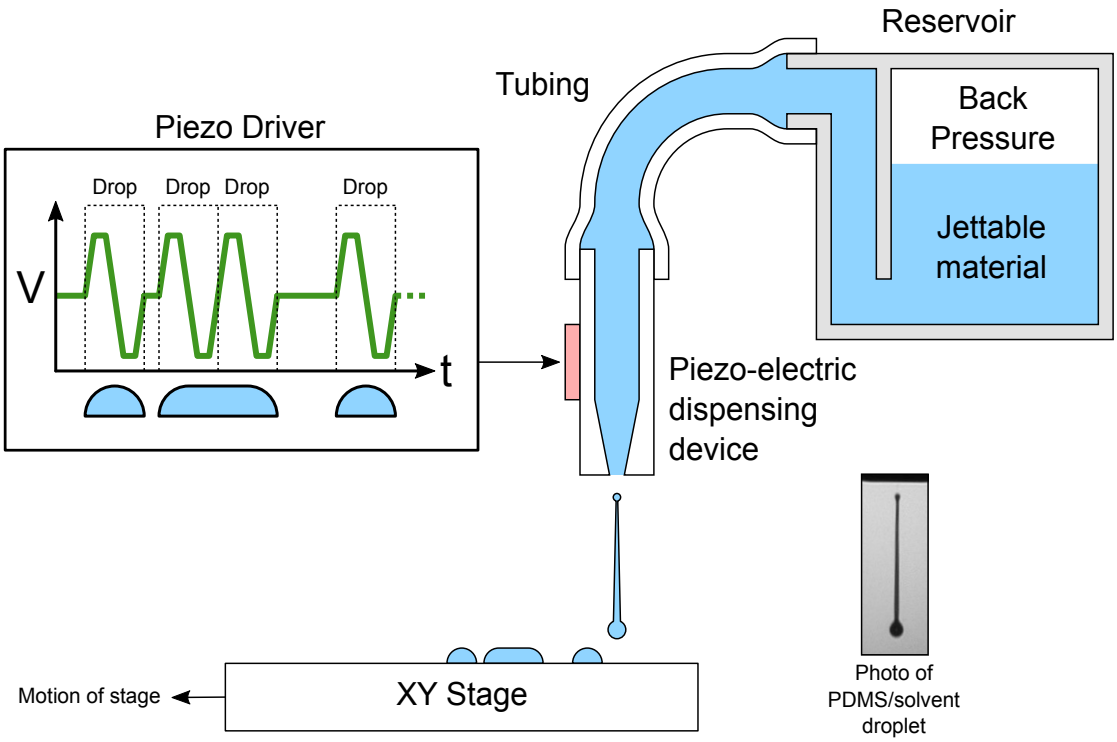

Figure 2.7 – A piezo-electric inkjet printing system consists of a dispensing nozzle and an XY stage. The jetting and the motion of the XY stage are controlled by a computer. The back pressure in the reservoir is set to maintain a level miniscus.

The principle of ink-jet printing is relatively simple but the process of producing a functional materials is not. Consider the venn diagram in Figure 2.8 (Rosset and Shea, 2013).First the material must be prepared as a liquid which is homogeneous and stable over time. If the material is unstable the jetting will not be stable. The material to be printed must be formulated in such a way that it can pass through the nozzle. It must have the correct viscosity, surface tension, and particle size to be expelled by the nozzle. Whether or not a fluid is jettable can be estimated by the dimensionless Ohnesorge number $Oh = \frac{\eta}{\sqrt{\rho\sigma d}}$ (McKinley and Renardy, 2011). Where η is the shear viscosity, ρ is the density, σ is the surface tension, and d is the jet diameter. At Oh values below 0.1 satellite droplets form. At Oh values above 1 the liquid is too viscous and becomes difficult to jet. However this equation was developed for Newtonian fluids and may not accurately predict droplet formation of polymer solutions and particle dispersions (McKinley2011). The interactions of the droplets with the substrate must also be considered. When a droplet hits the substrate the behaviour of the drop is influenced by the bulk material properties, the surface properties, and the environment. Bulk properties are important when the solvent is absorbed by the substrate. The surface properties are important if the droplet rests on the surface. The affinity of the materials determines whether droplets wet the surface or coalesce into larger droplets. Most often it is desirable to print lines or polygons which require some degree of wetting. The forces

between the droplet and the substrate must be higher than the forces between touching droplets. If this is not the case the droplets will coalesce and it will not be possible pattern the material. Once the droplets are on the surface they must be converted into a functional material. This may involve drying (Baechler et al., 2016), curing (Hamad et al., 2016; McCoul et al., 2017), sintering (Wu et al., 2014). Whatever process is used, it must be compatible with all of the materials in the structure.

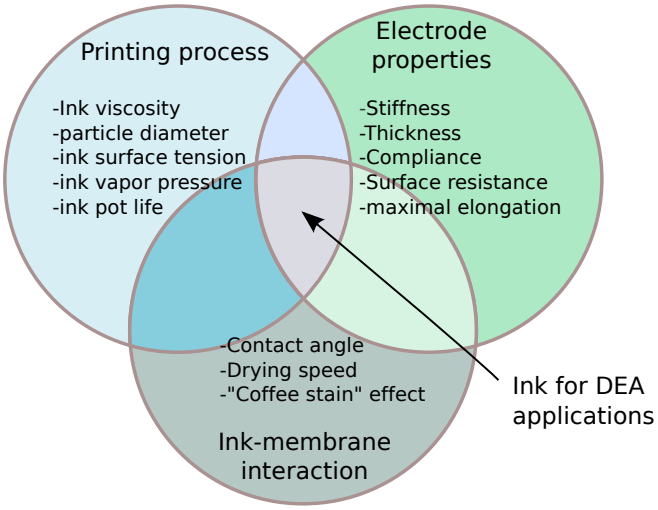

Figure 2.8 – A venn diagram showing the main points which must be considered to print functional materials. The fluid to be printed must have the right properties to be jetted, the jetted material must interact suitably with the materials being printed on, and the material must have sought-after properties once printed. It is only when the fluid properties, the material interactions, and the final material properties have been considered and correctly implemented that a functional material results (Rosset and Shea, 2013)

The ink-jet printing system used in this work is a Jetlab 4XL (MicroFab Technologies Inc.). The main parts of the printing system are shown in figure 2.9a On the Jetlab 4XL the print head remains stationary and the printing plate is moved. The distance between the print head and the printing plate can be adjusted with the z-stage before printing. The printing plate is mounted on top of the x and y stages and can be moved with an accuracy of ± 30 µm, a maximum speed of 50 mm/s, and an acceleration of 1500 mm/s^2. The printing plate on the Jetlab 4XL can be heated to 120 °C. When the printing plate is heated the temperature of the print-head also rises. This is problematic when jetting liquids which are volatile. To prevent the print head from heating up too much a cooling system has been retrofitted. Two pipes were attached to a hole, originally intended for a heater and thermocouple, to pass chilled water through the print-head. The Jetlab 4XL printing system has two cameras. The observation camera to observe droplet generation. The observation camera is attached to the printing plate. Jetting cannot be observed whilst printing. The inspection camera is located next to the z-stage and is used for alignment purposes and to inspect the print job. The piezoelectric dispensing nozzle is mounted vertically in the print head.

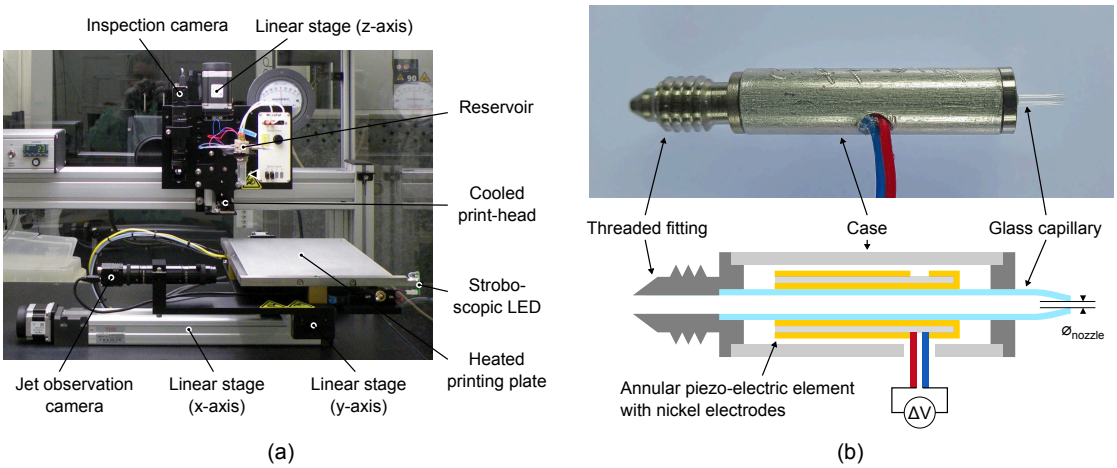

Figure 2.9 – The printing equipment used in this work (a) Jetlab 4XL with a printing area of 210 mm × 260 mm. The system has a heatable printing plate and has been retrofitted with a circulating chiller to cool the print head (b) A photograph of an MJ-AT-01-50-8MX piezo-electric dispensing nozzle. The diamter of the case is 4mm and the diameter of the orifice is 50 µm.

A photograph and a diagram of a piezo-electric dispensing nozzle are shown in figure 2.9b. On the Jetlab 4XL system nozzles are available with orifice diameters ranging from 20 µm to 80 µm. The dispensing nozzle in the photo is a MJ-AT-01-50-8MX and has a nozzle diameter of 50 µm. The viscosity is recommended to be between 0.5 - 40 cp (MicroFab Technote 99-02). If the viscosity is below 0.5 cp residual oscillations in the nozzle result in satellite formation. If the viscosity is too high, the drive voltage may not be sufficient to eject a droplet. The surface tension should be in the in the range 20 - 70 dy/cm. Surface tension has a small effect on the drive voltage required. Higher drive voltages are required for high surface tension liquids. Finally liquids containing particles must be small enough not to change the physical properties of the fluid. Microfab suggest that particles should be less than 5% of the orifice diameter.

To eject droplets with a piezo-electric dispensing device the back pressure must be set and a suitable waveform must be selected. The most basic waveform is a unipolar waveform consisting of a rise in voltage. When a positive voltage is applied to the annular piezo element the crystal increases in circumference and widens the glass capillary (Figure 2.9). The widening of the capillary creates a negative pressure wave which travels from the centre of the capillary outwards (Liu et al., 2012). If the fall in voltage, and the contraction of the capillary, is suitably timed to match the return of the pressure wave it will reinforce it. after it has reflected from the supply end of the capillary the pressure wave is amplified which increases the chances of a droplet being ejected . A bipolar waveform is normally used to reduce residual oscillations in the capillary which may lead to additional droplets being ejected (Tsai and Hwang, 2008; Gan et al., 2009). If the piezo transducer is centred on the glass capillary the echo time is two times the dwell time. Because droplet ejection is a resonant behaviour the speed of

the ejected droplet can be used to identify the optimal dwell time. The maximum speed is often desired because this increases the probability of droplet ejection. The rise and fall times are usually defined by the hardware. For the Jetlab 4XL rise and fall times of 3 to 5 µs are usually used. Finally the voltage is set to achieve maximum droplet velocity without generating satellite droplets. Note that jetting is highly sensitive to back pressure. To ensure repeatable results the back pressure should be set to achieve a level meniscus. If the pressure is too negative then the liquid will wet the front surface of the nozzle. This inverted puddle absorbs the energy of the droplet and prevents it from detaching. If the pressure is too high then the back pressure will overpower gravity and withdraw the fluid column back into the reservoir. The latter is hard to detect because there are no indicators for identifying excessive back pressures. In both cases jetting stops, however it is better to have a low back pressure because the jet normally does not start when the print job is started. With excessive back pressures the jetting will randomly stop in the middle of a print job without prior warning.

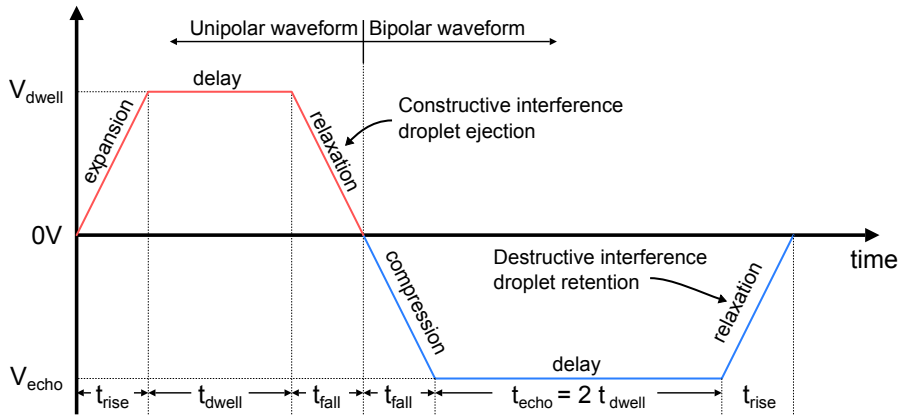

Figure 2.10 – Unipolar (red) and bipolar (red + blue) jetting waveform. A bipolar waveform reduces residual oscillations and reduces the chances of stray droplets.

Inkjet printers normally have two options for printing designs, vector printing and raster printing. Vector printing on the Jetlab 4XL is referred to as poly-line printing. In poly-line printing the user defines a set of printing lines composed of straight line segments and arcs. When the design is printed the jet is activated and the printing plate moves to trace out the path. This mode is used when the design can be represented as a sequence of lines. Raster printing on Jetlab 4XL is used to print monochrome bitmap images. Raster mode is used primarily when printing large filled in areas. The white pixels in the image encode a droplet and the black pixels represent a space. When printing a bitmap image the distance between pixels must be defined and the speed of printing (Figure 2.11). The distance between the droplets in a row is defined in this thesis as droplet spacing (DS). The distance between the printed row is referred to as the line spacing (LS). To deposit more material the image can be printed multiple passes (P). The printing plate (PP) temperature and the print head (PH) temperature are also important parameters when ink-jet printing.

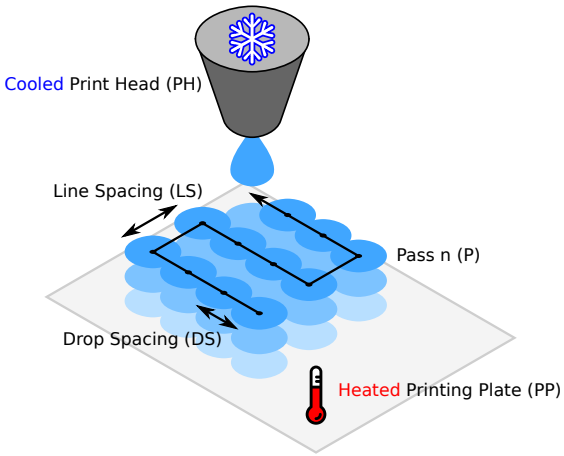

Figure 2.11 – The terminology used in this thesis to define patterning of droplets. When raster printing the Droplet Spacing (DS) and Line Spacing (LS) are specified in micrometers. When vector printing only DS is specified. The number of passes refers the number of times the printer passes without curing or drying in between. The word layer refers to a slice of n passes consisting of the same material. The Printing Plate (PP) and Print Head (PH) temperature is always given in degrees Celsius.

Part I

Formulation and characterisation of inkjet printed materials

3 Carbon black binder-less electrodes

3.1 Summary

In this chapter an ink-jet printable carbon black based electrode is presented. The shape of the printed electrode is measured. In addition the electrical properties of the electrode are explored with static (un-stretched) and dynamic tests (cyclic stretching). The electro-mechanical properties of the electrode are investigated using an in situ test setup. In situ testing gives representative results of the electrode under biaxial and high voltage stretching conditions.

3.2 Electrode requirements

Electrostatic transducers require electrodes which are conductive, compliant, thin, and pattern-able. Meeting these requirements is challenging as good conductors are generally stiff solids. Fortunately the electrodes for electrostatic transducers do not have to have a conductivity comparable to metals. Instead the conductivity must be sufficient to charge a electrostatic transducer in a reasonable time-frame. Generally the resistance of DE and HASEL transducers is in the hundreds of kilo-ohms range. Despite the high resistance it is possible to charge these devices in the kilo-hertz range because the capacitance is low. Consider a DE actuator with an area of 1cm^2 and a thickness of 60 µm with a capacitance of approximately 45 pF. The actuator and the connections leading up to it can have a resistance up to 3.5 MΩ while operating at 1kHz. The required mechanical properties, compliance and thickness, differ for the two types of electrostatic transducers. For DE transducers it is important that the electrode is stretchable and as thin as possible. The electrode has a Young's modulus which contributes to the stiffness of the DE structure. For example if the electrodes have the same stiffness as the dielectric material then a pair of electrodes with one tenth of the thickness of the dielectric layer increase the stiffness of the actuator by 20%. Generally the stiffness of the electrodes is higher than the stiffness of the dielectric meaning that the thickness plays an even

greater role. For HASEL actuators the compliance of the electrodes is also important. However the HASEL electrodes have less stringent requirements. HASEL actuators do not require electrodes which stretch by the same extent as DE electrodes. Consider a HASEL actuator which is integrated into a soft system consisting of a 1 mm thick silicone substrate. When the sheet is bent to a radius of 10 mm the surface of the silicone is strained by 5%. Similarly when it is bent to a radius of 5 mm the strain is increased to 10%. HASEL electrodes therefore can reach strains similar to DE electrodes when they are integrated into a soft system. Finally to make soft machines with many integrated transducers and interconnections the electrode must be pattern-able. It is difficult to define an exact resolution because it very much depends on the application. For devices on the centimetre scale it is often desirable to have sub millimetre accuracy with the placement of electrodes and routing. In this chapter we present a method which has the ability to produce electrodes with a placement accuracy ±25 µm and a feature size of 200 µm.

3.3 Material selection

Carbon black remains one of the most popular electrode materials for electrostatic transducers. As a material it is readily available, it is cheap, easy to process, and non toxic. Electro-mechanically it also performs well, it has a high conductivity, performs well under cyclic conditions, and is very compliant. There are many materials which outperform carbon black on specific aspects, but few which perform as well in all sectors. For this reason carbon black was chosen as the conductive material in this work.

Carbon black can be used as an electrode in one of three ways, as a powder, as a grease, or in a composite (De Saint-Aubin et al., 2018). Powered carbon black electrodes have a high conductivity and are extremely compliant. Unfortunately carbon black in powdered form is difficult to handle, difficult to pattern, and does not adhere well to most dielectric materials. For these reasons it is rarely used in powdered form. The most common way to use carbon black is when it is mixed with a grease to form a conductive paste. carbon black can be dispersed well in viscous silicone oils and petroleum jelly. Grease electrodes are very compliant and are easier to handle. The main disadvantage of grease electrodes is that the electrode is not fixed and can easily smudge. In addition the grease which is a high viscosity fluid can migrate out of the electrodes and penetrate the dielectric material. This is especially true for silicone based dielectrics. Over time the grease seeps into the dielectric and causes it to weaken leading to accelerated degradation. Carbon black in a silicone composite addresses the main problems of powdered and grease electrodes. silicone composites can be cured to form an elastomeric electrode which adheres well to the dielectric. Silicone composite electrodes are more practical, but adding silicone into the mixture comes at the cost of a reduction in conductivity, an increase in stiffness, and an increase in thickness.

Despite the disadvantages of powdered electrodes it may be the perfect candidate for ink-jet printing. The handle-ability and pattern-ability of powered electrodes can be improved by processing the material in liquid form. By adding a solvent it is easier to handle, grind, and pattern the carbon black. The solvent also helps in producing thinner electrodes. The solvent acts as a diluent reducing the concentration of carbon black. On drying the solvent evaporates leaving behind a thin, highly conductive carbon black electrode. Finally the problem of adhesion can be addressed encapsulating the electrodes with a thin layer of printed silicone.

Dispersing pure carbon black in a low viscosity solvent is challenging (Waarden, 1950; Rwei et al., 2002). Carbon blacks are available in two forms, paint blacks and conductive blacks. Paint blacks have a high number of oxygen-containg groups which improves their disperse-ability. However the addition of these groups also increases electrical resistivity of the carbon black (Nelson and Wissing, 1986). Conductive blacks are generally high structure black which have not been oxidised (Huang, 2002). The high structure improves the conductivity, but the lack of oxygen groups makes dispersing these blacks very challenging. Conductive blacks can only be dispersed in a low viscosity solvent by adding a surfactant. Like soap a surfactant creates an interface between the carbon black particles and the liquid. The dispersant must be chosen so that half of the molecule is carbo-philic, likes carbon surface chemistry, and the other half must be solvo-philic, similar to the solvent.

The solvent in the electrode mixture must be selected to achieve good wetting on silicone surfaces. The surface chemistry of silicone is such that most polar solvents will coalesce on the surface. The only solvents which wet silicone are non-polar solvents such as hydrocarbons and siloxanes. These solvents penetrate the silicone network and cause it to swell (Lee 2003). In part the liquids do not coalesce on the surface because the solvent which has penetrated the silicone acts as an anchor holding on to the liquid on the surface. This approach for wetting is usually avoided when patterning electrodes because the swelling can be so aggressive that it causes the dielectric membrane to wrinkle and deform. However when ink-jet printing, only small volumes are transferred to the printing plate and the swelling rapidly diminishes. The solvents with the highest swelling power and best wet-ability are siloxane solvents. Siloxanes have the same structure as PDMS and thus have a very high affinity to PDMS. Furthermore, siloxane solvents are available in different molecular weights meaning that it is possible to choose a suitable viscosity and volatility. A low molecular weight siloxane mixture, OS-2 Silicone cleaner and surface prep solvent (Dow), was chosen for the electrode mixture. It consists of 65% Hexamethyldisiloxane and 35% Octamethyltrisiloxane. The solvent mixture has a boiling point of 109° C, a viscosity of 0.6 cP at 25° C, and a vapour pressure of 4.2 kPa at 25° C. The low viscosity makes it easy to jet this solvent. The vapour pressure, which is comparable to isopropyl alcohol, leads to quick drying electrodes and minimal swelling.

To disperse unmodified carbon black in the siloxane solvent a special dispersant is required. The dispersant must be soluble in OS-2 and must have an affinity for carbon black. There are a number of silicone based dispersant which are designed for dispersing pigments or polar liquids in silicone oils. The one used here is a water-in-silicone emulsifier Belsil SPG 128 VP (Wacker). The dispersant consists of a silicone backbone and a glucose polymer group. The silicone part serves as the solvo-philic end of the dispersant and the glucose polymer group serves as the carbo-philic part.

The final properties of the electrode depend very much on the properties of the dispersant and how much is used. Belsil 128 is a 20% active solution in a low volatility solvent (cyclopentasiloxane). Once the solvent has evaporated the dispersant forms a gel like substance with some elasticity.

3.4 Preparation of electrode mixture

The electrode mixture is prepared in a four step process. The carbon black is first combined with the dispersant in a planetary mixer (Thinky ARE-250). This ensures that the ingredients are combined without losing any materials on stirring utensils. The high forces also help to break down the carbon black pellets and remove any air from the mixture. The coarse paste is then milled using a three roll mill (Exakt 50i). A three roll mill uses high shear forces to break down particles. Three roll milling is used because pastes processed in this way have narrower particle distribution than ball milling, thus reducing the chance of large particles ending up in the final mixture. The fine paste that is produced is then added to the siloxane solvent and sonicated (Sonorex RK 102H) to disperse the paste uniformly. The process to prepare the electrode mixture is shown below.

1. 5 g Ketjenblack EC-300J (Akzo Nobel) is added to 45 g Belsil SPG 128 VP (Wacker Chemie AG) in a planetary mixer and combined for 7 min with a rotational speed of 2000 RPM

2. The paste from step 1 is then passed through the roll mill three times at the minimum gap setting.

3. 8 g of the mixture from step 2 was combined with 20g of Dowsil OS-2 Silicone Cleaner and Surface Prep Solvent (Dow) in a sonicator for 10 mins

The electrode mixture was left to sit for 20 minutes to let large particles settle to the bottom. After 20 minutes the mixture was drawn out with a syringe and transferred to a clean printer vial.

3.5 Jetting profile

To jet the electrode mixture a 50 µm nozzle was used. Using a small nozzle improves the resolution of the printed electrodes. The basic waveform from section 2.3 was adapted in order to reduce the chances of the nozzle clogging. The dwell time was selected to achieve maximum droplet ejection velocity and the echo and dwell voltages were maximised to ± 70V. These adaptations increase the likely hood that jetting will start even after long pauses. The echo time was reduced to 1.5× the length of the dwell time. Reducing the echo time prevents the tail of the drop from diverging from the vertical path and creating satellites. When printing the electrode mixture the printing plate is heated to achieve a higher printing resolution. When wider lower thickness electrode lines are required the printing plate is heated to 40°C, otherwise for high resolution electrodes the printing plate is set to 80°C. In both cases the print head is cooled to 10°C to reduce the rate of nozzle evaporation and clogging.

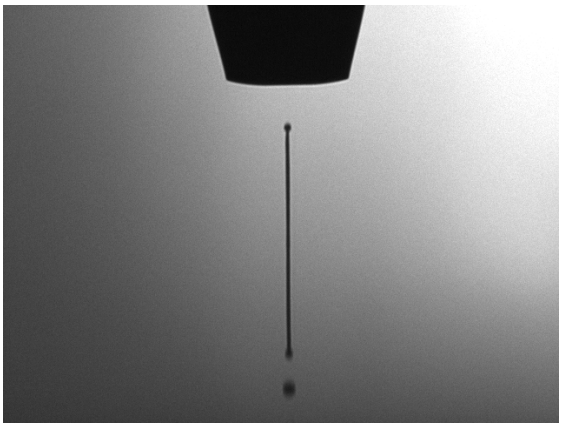

Figure 3.1 – Stroboscopic image of a jet of the standard electrode mixture (Section 3.4) being ejected from a 50 µm piezo-electric nozzle. The droplet was generated using the adapted waveform with the jetting pramaters RT 5 µs, DT 20 µs, FT 10 µs, ET 30 µs, RT2 5 µs, DV 70 V, EV, -70 V, PP 40°/80° C, PH 10° C. The backpressure was adjusted to level the miniscus when the jetting was off. The long tail of the generated droplet breaks up into smaller droplets but remain on the vertical path.

3.6 Shape of printed electrode

The electrode is printed either in raster mode or in vector mode. Raster mode is used for large filled in regions such as the electrodes of an actuator, the electrical contacts used to apply power to the soft machine, and for connections which are very long or need to carry a high current (a bus powering multiple actuators). These type of features are printed in raster mode and are encoded as monochrome bitmap images. The bitmap is printed row by row where each pixel represents a single droplet. To reduce printing time the raster printed electrodes are printed on-the-fly, bidirectionally, at a speed of 50

mm/s. A droplet and line spacing of 100 µm is genrally used. This spacing produces enough overlap between the droplets and the lines to produce a continuous conductor.

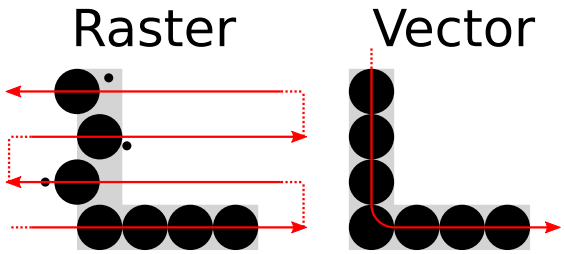

Figure 3.2 – A diagram to demonstrate the differences in print quality when printing in raster and vector modes. In raster printing mode the printer jets droplets row by row on the forward and backward strokes. There is some misalignemnt beween the droplets jetted on the forward and backward strokes resulting in jagged edges for conductors which are perpendicular to the printing direction. Sattelites are also more likely to be generated because the printhead is inactive for most of the stroke which leads to partial drying of the nozzle. When vector printing the printhead moves along the path of the conductor. The droplets are well aligned and there are no satellites because the printer is continuously jetting.
Raster versus vector printing

Vector printing is used whenever narrow and long conductors are required. In vector mode the print head follows the path of the conductor. The motion of the stages are very accurate (±25 µm) thus producing conductors with repeatable width and conductivity. This is especially true for conductors which are not aligned with the motion of the printer. An example of this is shown in Figure 3.2. When printing an *L* shaped conductor in vector mode the shape has crisp edges, both on the horizontal and the vertical part. Conversely an L shaped conductor printed in raster modes has jagged edges on the vertical part. This is because there is misalignment between the droplets jetted on the forward and on the return stroke. In addition the long pauses between jetting on the vertical part of the *L* increases the number of satellites produced because jetting has to constantly start and stop. For these reasons vector printing is used whenever well defined, accurately placed, and narrow electrodes are required. This includes electrical connections which span large distances, narrow electrodes where the alignment to other features is important, and closely spaced conductors where contact is not allowed (serpentine strain sensors).The vector printed electrodes are normally printed with a droplet spacing of 50 µm and a speed of 5 mm/s. The droplet spacing is relatively small to maximise the amount of material which is deposited and thus increase the conductivity. The speed of the printer is limited primarily by the acceleration of the printer. When printing small arcs the printer must accelerate rapidly in order to maintain the correct tangential velocity. The speed was chosen based on the maximum acceleration and minimum turn radius. The maximum acceleration of the jetlab 4XL is 250 mm/s^2. For a minimum turn radius of 100 µm the maximum speed is 5 mm/s.

To measure the behaviour of the electrode mixture on silicone (Sylgard 184) some vector

and raster lines were printed. The vector printed tracks were printed with a droplet spacing of 50 µm or 100 µm at a speed of 5 mm/s. The raster printed electrodes were printed with a droplet and line spacing of 50 µm or 100 µm at a speed of 50 mm/s. The experiment was conducted two times, once with the printing plate at 40° C and a second time with the printing plate at 80° C. At both temperatures the print head temperature was cooled to 10° C. The results of these test prints are shown in Figure 3.4 (profile) and in Figure 3.3 (light field microscope images of corresponding conductors). Both figures illustrate clearly that increasing the spacing of the droplets and increasing the temperature of the printing plate decreases the width of the printed conductors. The light field images also show that using a small spacing (DS and LS of 50 µm) for printing electrodes results in a very thick electrode, close to 10 µm which cracks on drying. These printing parameters should be avoided as cracks result in sudden resistance spikes when stretching the conductor.

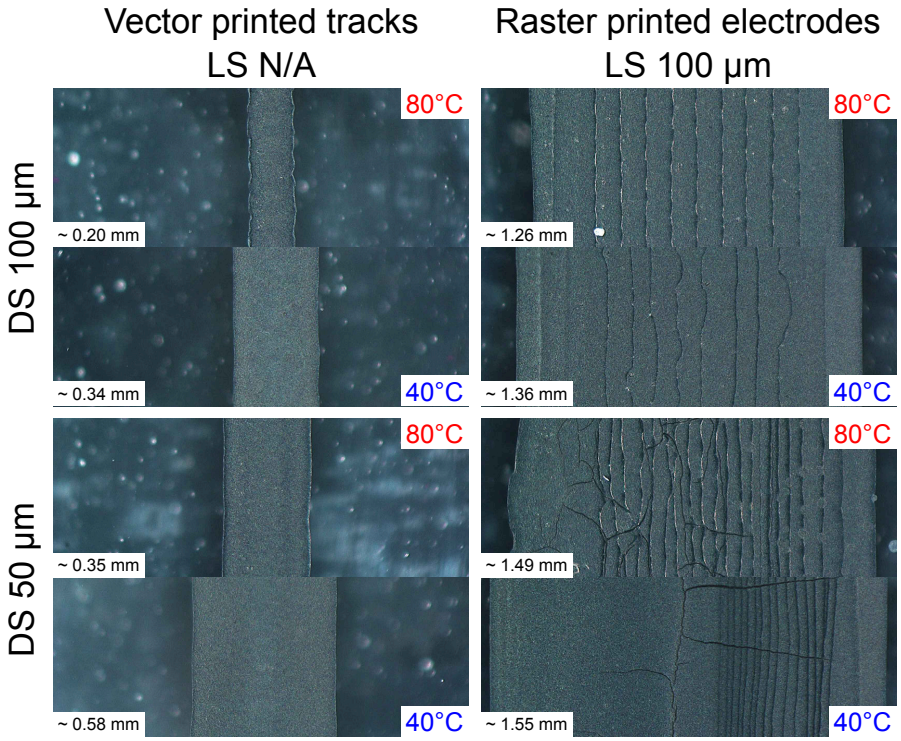

Figure 3.3 – Light field images of vector printed traces (left column) and raster printed electrode (right column) at different droplet spacings and substrate temperatures. The approximate width of each conductor is also given in the bottom left of each image. The traces and electrodes in the first row are printed with a Droplet Spacing (DS) of 100 µm. The traces and electrodes in the second row are printed with a droplet spacing of 50 µm. The temperature of the printing plate was set either to 40° C (blue) or 80° C (red). The printhead was cooled to 10°C for printing all conductors.

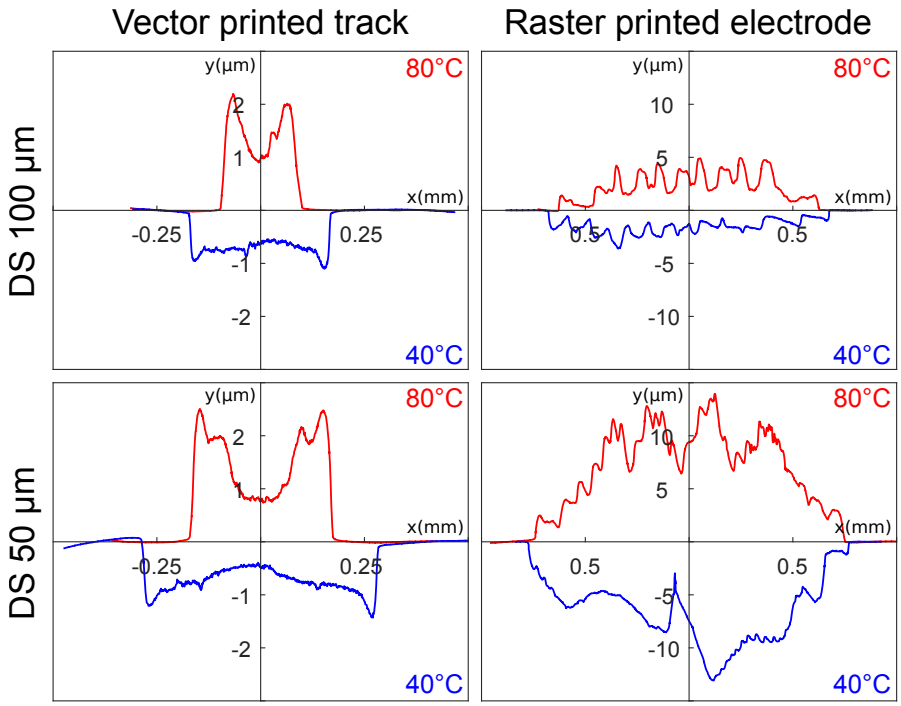

Figure 3.4 – Profile of vector printed traces (left column) and raster printed electrodes (right column) at different droplet spacings and substrate temperatures. The traces and electrodes in the first row are printed with a Droplet Spacing (DS) of 100 µm. The traces and electrodes in the second row are printed with a droplet spacing of 50 µm. The temperature of the printing plate was set either to 40° C (blue) or 80° C (red).

3.7 Resistance of printed electrode

In this section the resistance of the printed carbon black electrode is presented. The resistance of the electrode must be considered in both the static (unstretched) and dynamic (cyclic stretching) case. To determine the resistance of the electrode in the static case a set of lines, vector and raster, were printed on a constrained silicone substrate. The lines include extra contacts which enable more accurate four wire resistance measurments. To determine the performance of the electrodes when stretched the Novel Electrode Resistance Degradation (NERD) setup is used (Rosset 2018 and Saint-Aubin 2018). The NERD setup monitors the actuation strain and electrode resistance in a real DEA over many cycles. From this we can infer the resistance of the electrode at different stretch values and also get some insight into the compliance of the electrodes.

3.7.1 Static resistance measurements

The static resistance measurements were conducted on a sheet of constrained silicone. The silicone was constrained by placing a 0.6 mm sheet of cast Sylgard 184 (Dow) onto a 0.5 mm thick float glass wafer. Trapped air was removed by placing the glass-silicone substrate into a vacuum chamber. The glass silicone substrate was then loaded into the printer and six lines were printed onto the surface (Figure 3.5). The first three were raster printed with a length of 50 mm and a width of 1 mm, a droplet and line spacing of 100 µm, and a print-on-the-fly speed of 50 mm/s. The fly direction was aligned with the conductor and is inline with the direction of current flow in the sample. The last three conductors were printed in vector mode with a droplet spacing of 50 µm at a print-on-the-fly of 5 mm/s. Electrical contacts were printed over the top of the printed lines in the raster mode. The square contact pads were printed to inject current into the printed lines and the speech-bubble-like contacts were printed to measure the voltage across a known length of the conductor. The exact spacing of the voltage pick up points is 35 mm. Two samples of this type were printed. One with the printing plate temperature at 40° C and the other with the printing plate temperature at 80° C. To make the four wire resistance measurements a small plastic connector was fabricated with a laser engraver. The connector consist of a 3 mm thick block with 8 holes. Winding wire is slipped through these holes so that a short piece of wire is protruding out of the bottom of the block. A small rectangle was also engraved to ensure that the block does not contact the line being measured. The plastic connector is placed on the sample using a small magnet which applies constant pressure and ensures a good connection. The resistance was measured using a 10V power supply and two multimeters. One multimeter is placed in series with the power supply to measure the current through the printed line. Another was placed in parallel to measure the voltage generated across the speech bubble contacts.

The resistance for the different modes of printing is represented differently. For vector

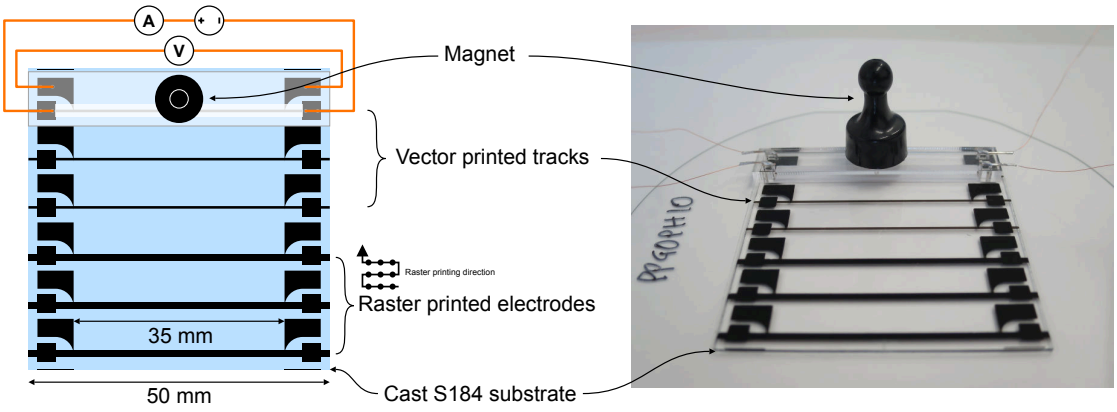

Figure 3.5 – Setup and sample used for making static resistance measurements of ink-jet printed electrode. The diaphragm on the left depicts the static resistance sample. It consists of six horizontal conductors. The bottom three are 1 mm wide raster printed electrodes and the top three are vector printed traces. The raster printed electrodes were printed with a droplet and line spacing of 100 µm, the vector printed traces were printed with a droplet spacing of 50 µm. The four contact points are used to make a four wire resistance measurement. The current was injected into the square contacts and the voltage was read across the speech bubble like contacts. A photo of the sample with the plastic connector is shown on the right.

printed conductor the resistance is given as a function of the length of the conductor and was calculated with the following formula $R = \frac{1}{35} \times \frac{V}{I}$. For raster printed electrodes the resistance is given in sheet resistance. The sheet resistance can be calculated by dividing the total resistance by the number of squares $R_{sheet} = \frac{width}{35} \times \frac{V}{I}$. The results are shown in Table 3.1. Each result is the average of 3 measurements. The table shows that for both vector printed traces and raster printed electrodes the resistance is lower at the elevated printing temperature of 80° C. This is because conductors printed at elevated temperatures are narrower and thicker. In thick conductors there are more percolation paths in the z-direction which help to decrease the resistance of the conductor. Another interesting point to note is the low sheet resistance of the raster printed electrodes. The raster printed electrodes have a sheet resistance of 3.3 kΩ/sq at 40° C and 2.9 kΩ/sq at 80° C. These results are much lower than the results I have previously reported (Schlatter et al., 2017). Since 2018 there have been a number of changes which may have contributed to lowering the resistance. The processing of the electrode mixture has been improved. The electrode is now processed with a three roll mill which requires less dispersant and thus increases the percentage of carbon. Also the electrode mixture is no longer filtered with a centrifuge which also increases the concentration of carbon black. The way the electrode is printed has also changed. The electrode is now printed at elevated temperatures resulting in thicker electrodes. All of these changes increase the conductivity in the printed electrode. It is also important to note that these samples were printed and measured on a rigid substrate. It may be that the conductivity drops significantly after the first deformation (peeling a membrane off the substrate).

Temperature	Resistance per millimeter of Vector printed traces	Sheet resistance of Raster printed electrodes
40° C	17 kΩ/mm	3.3 kΩ/sq
80° C	14 kΩ/mm	2.9 kΩ/sq

Table 3.1 – Average resistance of printed vector printed electrode traces and raster printed electrodes at different printing plate temperatures.

3.7.2 Dynamic resistance measurements

In this section the aging of inkjet printed electrodes is studied using the NERD setup (Rosset et al., 2017). The NERD setup was designed and built by Samuel Rosset and samples were produced and tested by the author (Samuel Schlatter).

The NERD setup was used to measure the resistance of the electrode when stretched. The setup is designed to measure the resistance of an electrode under true operating conditions. This is achieved by measuring the resistance of the electrodes which are a part of an actual DE actuator. In-situ measurements like this are more representative than uniaxial stretch tests because the electrodes are subjected to true operating conditions, including biaxial strain and high voltages. An additional advantage of doing in situ measurements is that silicone based DE actuators can actuate very fast. This means that the degradation of a DEA can be studied in a reasonable time frame. With the NERD setup it is possible to monitor the evolution of electrode restance and stretch to one million cycles in a matter of hours.

The NERD setup (figure 3.6) consists of a High Voltage Power Supply (HVPS), a digital multimeter, a USB microscope, and the sample DE actuator, and a computer. The HVPS is a computer controlled high voltage power supply which can generate square wave voltages up to 5kV. More information describing its function and how to assemble one of these power supplies can be found on the website petapicovoltron.com and in the hardwareX article (Schlatter 2018). The digital multimeter (Keithley 2000) is used in 4-wire mode to measure the resistance of the electrode. Using a 4 wire measurement approach eliminates the contact resistance and the resistance of the tracks leading to the actuator. The USB microscope is used to measure the strain of the actuator. Finally a computer is used to control the HVPS, the multimeter, and the USB microscope with a labview application. The application completely automates the testing of the DE actuator. Before the test begins the user must set up the image tracking, enter the maximum actuation voltage (V_{test}), and define the test parameters. The test parameters define the speed and number of cycles in each phase of the test. The test begins with the ramp phase. The ramp phase measures the resistance and strain at 8 voltage levels between 0V and V_{test}. The voltage is held constant for 5 s before taking the measurement. Typically the ramp phase occurs every 50'000 cycles. The ramp phase is followed by the fast actuation phase. Here the DEA is subjected to a square wave between 0V and V_{test}

at 50 Hz to quickly accumulate cycles. The fast actuation phase occurs every 2'000 cycles. Following each fast actuation phase is a slow acquisition phase. The slow acquisition phase records the resistance and strain of the DE actuator at 0V and at V_{test}. The voltage is held constant for 5 s before taking the measurement. Generally the test is conducted for a total of one million cycles.

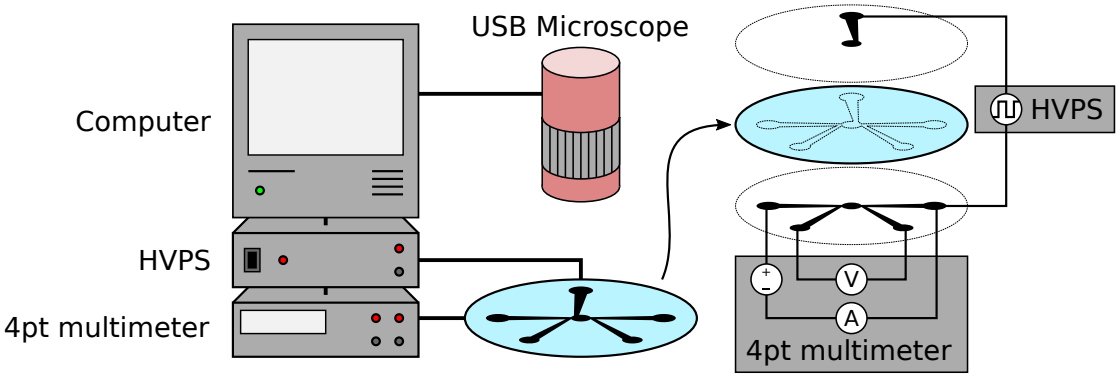

Figure 3.6 – NERD setup is an in-situ test setup to measure the degradation of DEA electrodes. The setup consists of a high voltage power supply, a four wire multimeter, a USB microscope, and a computer to automatically control all of the equipment. The NERD actuator is a 4 mm wide circular actuator with additional connections to measure the electrode resistance. The four wire connections are on the ground side of the actuator. A current is injected into outside contacts and the voltage across the central circular electrode is measured across the inside contacts. With the NERD setup the degradation of the electrode can be measured while the DEA is actuating.

It should be noted that the electrode formulation and process used in the study which follows are not identical to formulation and process presented in sections 3.4 to 3.7.1. One, the electrode mixture in 2018 contained a higher percentage of dispersant because it was ground with a ball mill. High surfactant content increase the compliance of the electrodes. Two, the electrode mixture was filtered using a centrifuge. Filtering removes conductive particles and therefore increases the resistance of the electrode. Three, the electrodes were printed with a droplet and line spacing of 50 µm. Higher droplet density increases the cross-sectional area of a printed electrode and therefore reduces its resistance. Four, Sylgard 186 (Dow) was used as the dielectric material. Different silicones have different surface properties and therefore affect the flow of the printed materials. However, despite these differences, the following tests still reveal a lot about the dynamic stretching behaviour of electrodes based on carbon black and Belsil 128 dispersant.

A NERD actuator is shown in figure 3.6 on the right. It consists of a prestretched membrane made of Sylgard 186 (Dow) with two inkjet printed electrodes. The electrode on top consists of a 4 mm circle with a single connection to the HVPS. The electrode on the underside consists of a 4 mm wide circle with 4 arms to make four wire resistance measurements on the centre circle. The multimeter applies a low voltage (<10 V) to the outside arms of the bottom electrode and measures the current through this circuit

(typically 700 nA in the 100 MΩ setting). Simultaneously the voltage is measured across the inside arms of the bottom electrode and the resistance is calculated with ohms law. The resistance measured by the multimeter is the resistance of the 4 mm circle electrode on the ground side of the actuator. Initially it was unclear if the printing direction would have an effect on the resistance and stretch of the electrode and hence samples with different printing orientations were prepared (figure 3.7). Printing orientation refers to the alignment of the printed lines with respect to the direction of the measurement current. Samples where the printing orientation are inline with the measurement current are denoted with the letter *I*. Samples where the printing orientation is perpendicular (or transverse) is denoted with the letter *T*. And samples where the printing orientation is cross-hatched are denoted with the letter *X*. Cross hatched samples are prepared by printing two layers of electrodes, once inline and a second time transverse. Since the cross-hatched electrodes consist of two printed layers, additional samples of the inline and transverse samples were also prepared for fair comparison. The number of passes is denoted with the letter *L*, either one layer *1L* or two layer *2L*.

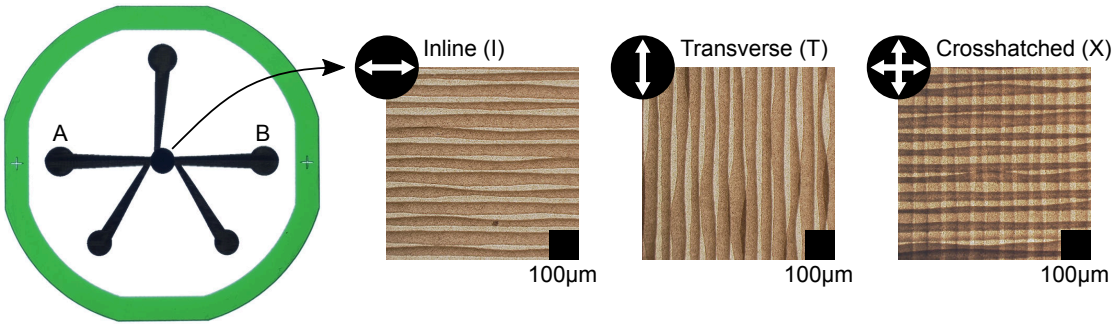

Figure 3.7 – A photograph of a NERD actuator and the terminology for printing orientation. Electrodes where the raster printing direction is inline with the measurement current (flows from A to B) are referred to as inline printed electrodes. Electrodes where the printing direction is perpendicular to the measurment current are transverse printed electrodes. Finally electrodes which are printed in both directions are referred to as cross-hatched electrodes.

First the performance of single layer inline and transverse printed electrodes were tested to a biaxial actuation stretch of 5%. The stretch is defined as the diameter of the actuator at voltage *V* divided by the diameter of the actuator at *0V*. Before the test is started the DE actuator is ramped close to the maximum voltage to determine the voltage required to achieve a linear stretch of 5%. This voltage, V_{test}, is then used for the entire test.The samples were then subjected to one million cycles with the test parameters described earlier. The results for single layers samples stretched to 5% are shown in Figure 3.8. The colours red and blue correspond to different samples. The first row of plots shows the absolute resistance of the electrode at 0V (dotted lines) and at V_{test} (solid lines). The resistance of the inline samples at 0V increases slightly from ~36kΩ to ~44kΩ after a million cycles. The resistance at V_{test} begins at ~107kΩ, reduces sligthly in resistance in the first ten thousand cycles, and slowly increases to ~108kΩ after a million cycles.

The resistance of the transverse samples at 0V begin at ~32kΩ and increase slightly to ~43kΩ after a million cycles.The resistance at V_{test} begins at ~170kΩ, reduces drastically in the first ten thousand cycles, and increases steadily to ~195kΩ after a million cycles. The stretch of the inline sample at 0V increases slightly by ~0.5%. The stretch at V_{test} decreases slightly from ~4.4% to ~4.2%. The stretch of the transverse samples at 0V increases slightly by ~0.4%. The stretch at V_{test} decreases slightly from ~4.5% to ~4.3%. The behaviour of single layer inline and tranverse samples at 5% is similar, however the resistance at V_{test} rises more rapidly in the transverse samples.

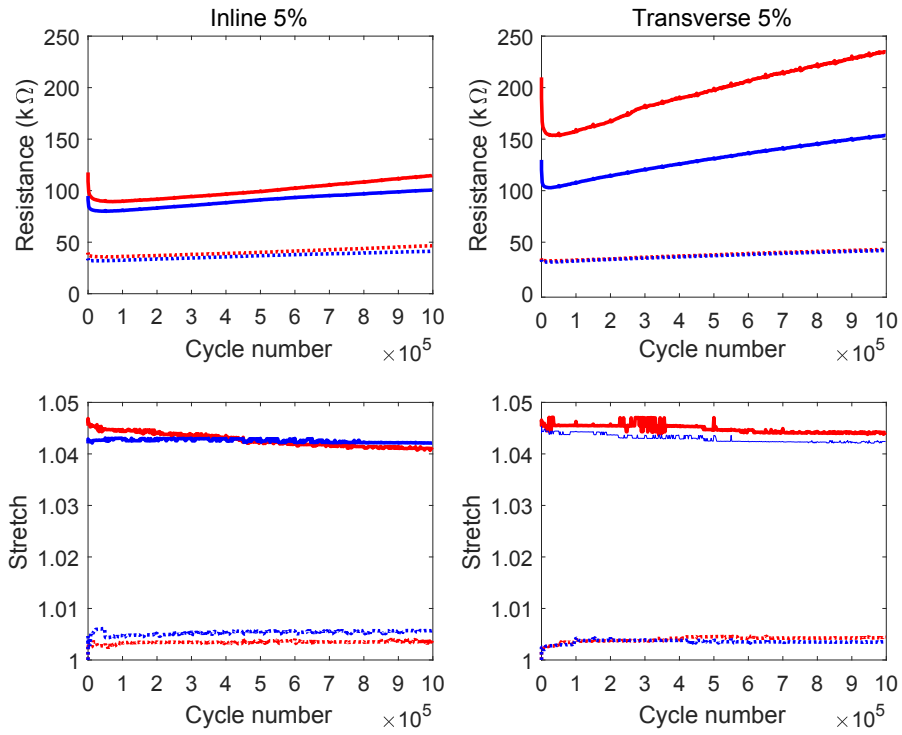

Figure 3.8 – The evolution of resistance and actuation stretch of single layer inkjet printed electrodes when stretched to 5% over one million cycles. The columns correspond to actuators with a different printing orientation. The resistance and stretch data in the left column is for electrodes where the printing orientation is inline with the measurement current. The resistance and stretch data in the right column a sample where the printing orientation is perpendicular to the measurement current. For each printing orientation two samples were tested (red and blue). The dotted and solid lines are the measured values at 0V (OFF) and V_{test} (ON) respectively.

The test was repeated at 10% stretch for two more samples, one with inline orientation and another with transverse printing orientation (Figure 3.9. The samples were also subjected to one million cycles. The resistance of the inline sample at 0V increased steadily from ~30kΩ to ~2.13MΩ after a million cycles. The resistance at V_{test} begins at ~233kΩ, increases rapidly to ~8MΩ at 500k cylces, and reduces back to ~3.38MΩ after a million cycles.The resistance of the transverse sample at 0V increases steadily from ~30kΩ to ~2.81MΩ. The resistance at V_{test} increases rapidly from ~371kΩ to ~16.1MΩ after a million cycles. The stretch of the inline sample at 0V increased rapidly in the

first 100k cycles and plateaus to 2.2%. The stretch at V_{test} reduces steadily from 8.9% to approximately 5% after 400k cycles, it then drops drastically to ~2%. The same stretch as at 0V. The stretch of the transverse sample at 0V increased rapidly in the first 100k cycles and plateaus to 1.6% after a million cycles. The stretch at V_{test} reduces steadily from 9.2% to approximately 5.6% after a million cycles. These results show that the inkjet printed carbon black electrode degrades rapidly when stretched to 10%. The inline electrodes failed to produce any stretch after 500k cycles. The transverse electrode sample continued to function at 1M cycles, however the stretch range has been severely reduced to less than half of the original value (9.4% to 4%). The effect of high stretch and cycling is also visually apparent on the electrodes (Figure 3.10. The samples which were subjected to 10% stretch show signs of electrode burning an ablation after a million cycles.

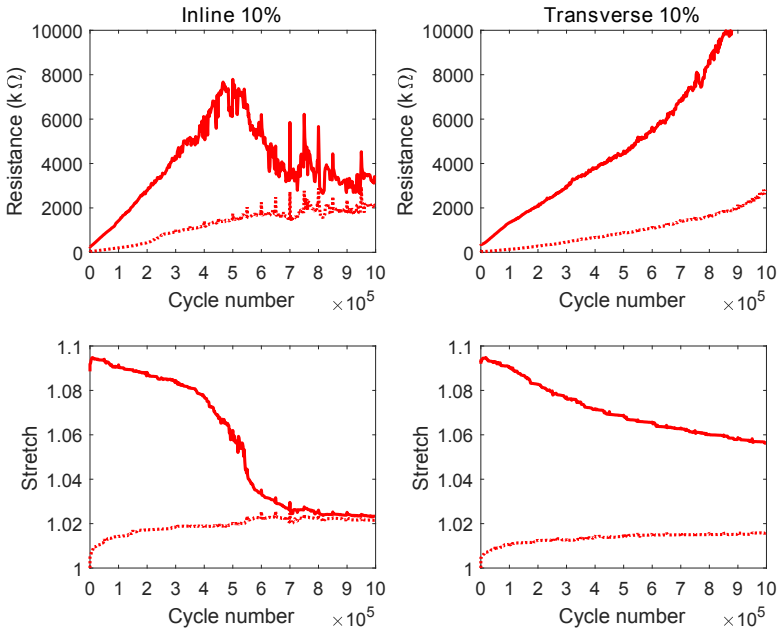

Figure 3.9 – The evolution of resistance and actuation stretch of single layer inkjet printed electrodes when stretched to 10% over one million cycles. The columns correspond to actuators with a different printing orientations. The resistance and stretch data in the left column is for electrodes where the printing orientation is inline with the measurement current. The resistance and stretch data in the right column are for samples where the printing orientation is perpendicular to the measurement current. For each printing orientation two samples were tested (red and blue). The dotted and solid lines are the measured values at 0V (OFF) and V_{test} (ON) respectively.

A set of two layer NERD samples were also produced to determine the sensitivity of different thickness and printing orientations on the elctrode resistance. Two layer inline and transverse samples were fabricated by printing the same electrode twice. The crosshatched sample was prepared by printing an inline electrode followed by

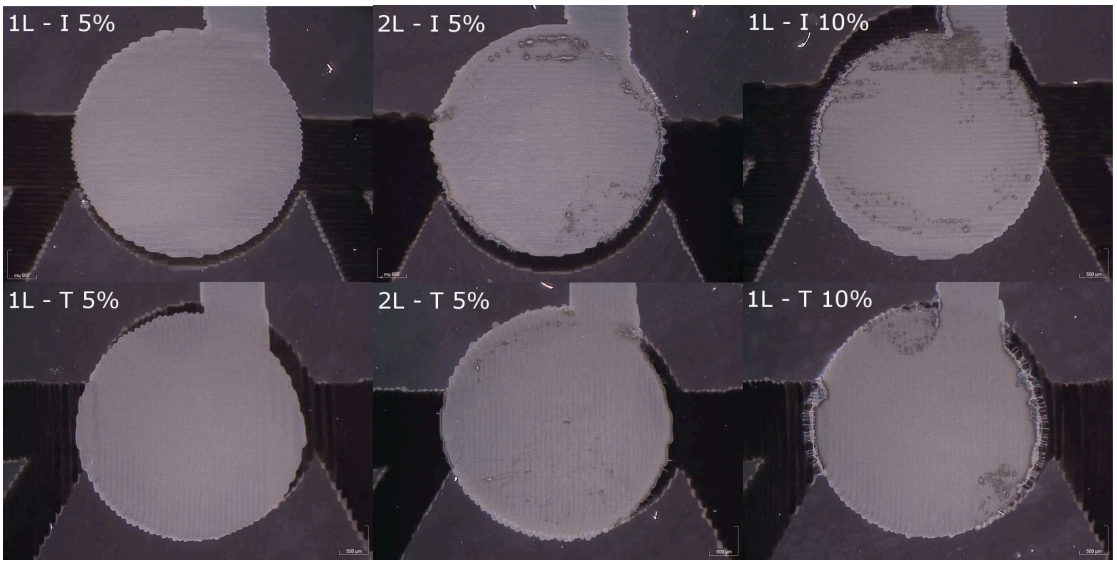

Figure 3.10 – Light field microscope images of inkjet printed electrodes of different layer thicknesses (1L or 2L) and printing orientations (I or T) exposed to cyclic stretch of 5% or 10% stretch for one million cycles. The images show visible degradation on the 2L electrodes and the electrodes which were stretched to 10%

a transverse electrode. The samples were submitted to the same test as above but only the data from the first ramp phase was extracted for each sample. The relative resistance change as a function of stretch of single and bilayer electrodes is shown in Figure 3.11. The plot shows that one layer inline and transverse electrodes undergo the smallest relative change in resistance, followed by the two layer inline and transverse electrodes, and finally the two layer crosshatched electrode. The plot clearly illustrates that thickness has a profound effect on electrode resistance when stretched. The thick electrodes generally increase in resistance more quickly when stretched and are more likely to burn out than thin electrodes.

From the dynamic tests one can make the following conclusions:

- single layer electrodes can withstand 5% stretch for one million cycles without a drastic resistance increase or loss in actuation strain.
- single layer electrodes cannot withstand 10% stretch for one million cycles. A drastic increase in resistance and loss of actuation stretch was observed. However the electrodes are suitable for devices which only need to operate for a few hundred thousand cycles.
- The 2-layer electrodes are more sensitive to stretch than the 1-layer electrodes.
- The difference between inline and transverse printed electrodes is not significant but the cross-hatched electrodes are clearly worse.

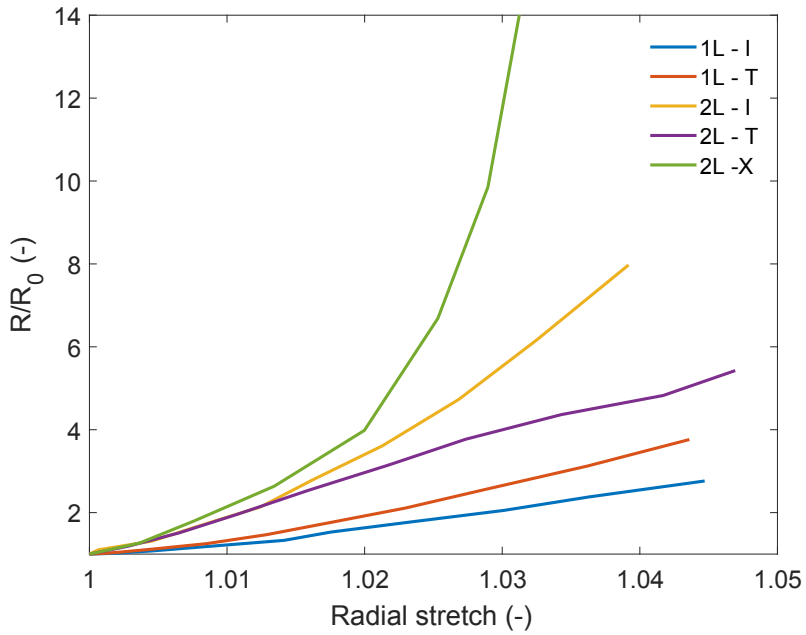

Figure 3.11 – Relative resistance change of electrodes of different layer thicknesses (1L or 2L) and printing orientations (Inline I, Transverse T, Crosshatched X). The 2L electrodes increase in resistance more quickly than 1L electrodes. The transverse printed electrodes increase in resistance more quickly than the Inline printed electrodes, and the crosshatched electrodes increase in resistance more quickly than the transverse printed electrodes.

3.8 Printing on non-silicone substrates

The electrode mixture was designed to be printed on to silicone based materials. To ensure good wetting a low surface tension siloxane solvent was used. The benefit of this mixture is that relatively thin electrodes may be printed on silicone without any surface treatment. However there is a large drawback to this approach: the same mixture cannot be used on other materials with different surface and bulk properties. When the electrode material is printed on to silicone a large portion of the solvent is absorbed by the silicone substrate, thus limiting the spread of the electrode. On other materials the solvent isn't absorbed and remains on the surface for longer. As a consequence, the resolution of a printed electrode is poor when printed on non-silicone substrates (Figure 3.12). One way to overcome this problem is to heat the printing plate and evaporate the siloxane solvent more rapidly. In this section the spread of the electrode mixture on two different substrates, a polyester substrate coated with a release layer and a silicone substrate, is compared.

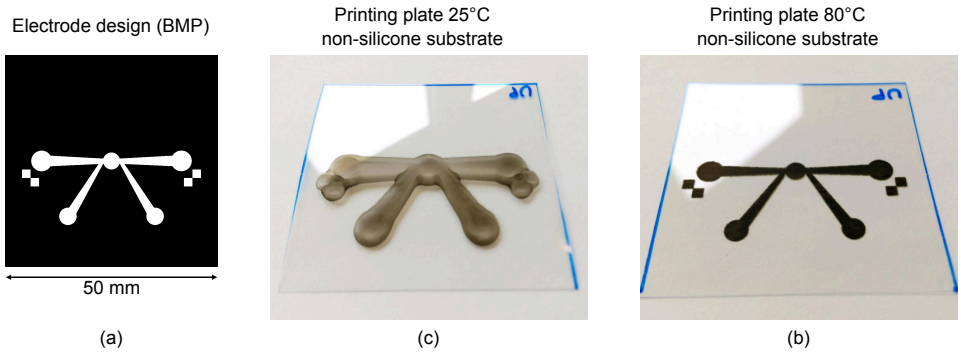

Figure 3.12 – (a) BMP image of the low voltage sensing side of a NERD actuator. The Jetlab4 printer jets the white pixels and holds on the black pixels.(b) The spread of the electrode mixture on a PET substrate coated with a PAA release layer. The electrode was printed at room temperature. (c) The spread of the electrode mixture on a PET substrate coated with a PAA release layer. The electrode was printed at 80° C.

The polyester substrate (Melinex ST-506, DuPont Teijin Films) was coated with a thin layer of PAA (PolyAcrylicAcid 25% soln. in water MW 50,000, Chemie Brunschwig). A mixture of 20 wt% PAA in isopropanol was used. The release layer was applied with a threaded rod (Zehntner ACC378.022) at a speed of 8mm/s. The silicone substrate was prepared in a similar way. However a layer of silicone (Sylgard 186, Dow) was cast on top of the release layer. The silicone had a dry film thickness of approximately 50 µm. The different substrates were placed next to each other and an array of electrode droplets was printed on the substrates. Note that an earlier version of the electrode mixture was used for this experiment (Schlatter et al., 2017). The experiment was repeated at 8 different printing plate temperatures, starting at room temperature and increasing to 95°C in 10°C increments.

The average droplet diameter was measured for each of the samples and plotted against temperature. The results are shown in Figure 3.13. The plot shows that there is a large difference in droplet diameter depending on the substrate. On the polyester substrate the diameter is almost two times higher than the droplet diameter on the silicone substrate. A linear regression is also indicated on the plot. The linear regression may be used to estimate the temperature required to achieve the same printing resolution on silicone. To obtain a droplet size of approximately 300 microns when printing on polymer substrate a printing plate temperature of approximately 110°C is required.

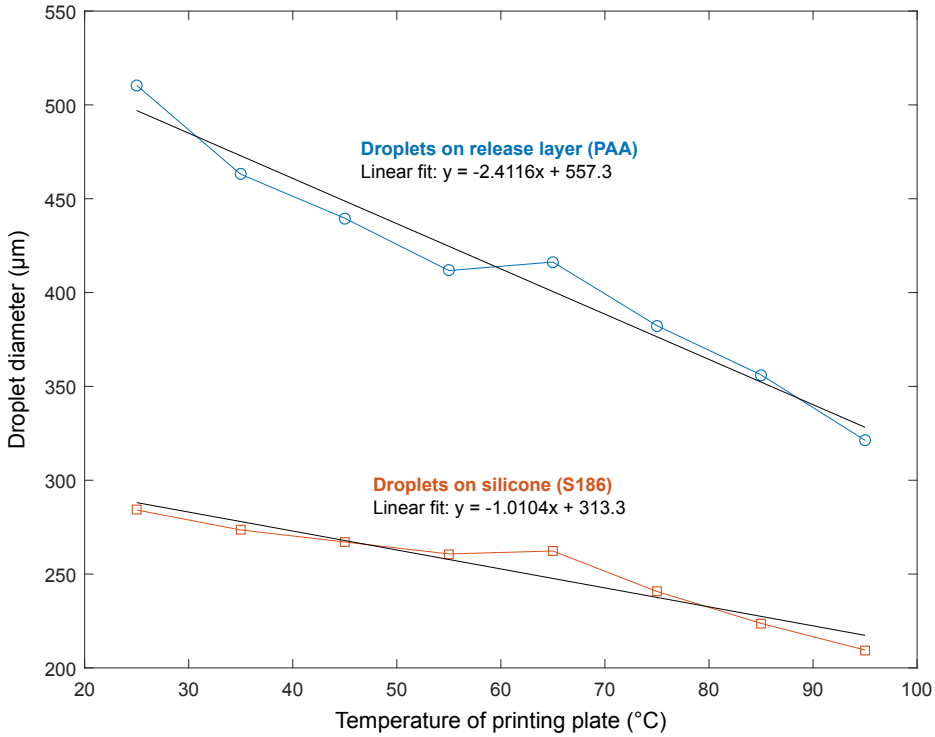

Figure 3.13 – The spread of the electrode mixture on different substrates and different printing plate temperatures. One of the substrates consists of PET coated with a PolyAcrylicAcid release layer. On PAA the siloxane isn't absorbed and spreads more. The second substrate consists of a PET substrate coated with Sylgard 186. The silicone absorbs the siloxane solvent in the electrode mixture, thus reducing its spread.

The maximum printing plate temperature on the Jetlab 4XL is 120°C. At this temperature the nozzle begins to heat up and jetting becomes more erratic. For this reason a more conservative printing plate temperature of 80°C was used to print an electrode. A close up image of a printed electrode (Figure 3.14) shows that heating the printing plate does indeed improve the resolution of the printed electrodes. However, on a polymer substrate at elevated temperature the electrode mixture behaves differently. The electrode mixture at elevated temperatures forms features that resemble tears. These tears are most likely due to the dispersant heating up and becoming more mobile. The differences in electrode thickness may negatively affect the conductivity and cyclic

properties of the electrode.

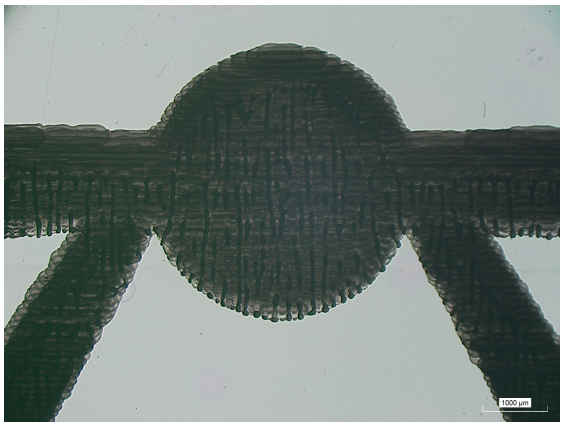

Figure 3.14 – A microscope image of an electrode printed at 80° C (printing plate temperature) on a PAA coated substrate. The high temperature cause the to spread differently than on a silicone substrate. The irregular profile may affect the conductivity and cyclic properties of the electrode.

3.9 Inkjet printed MWCNT electrodes

Carbon nanotubes have a higher conductivity than carbon black (Yu et al., 2011). Carbon nanotubes may therefore be better suited for electrostatic actuators because the electrodes may be thinner. In this section the conductivity and thickness of inkjet printed Multi Walled Carbon Nano Tubes (MWCNT) is investigated.

A low viscosity mixture of MWCNT was prepared by diluting Aquacyl (AQ0302, Nanocyl SA.) with ethanol. Aquacyl is a dispersion 3 wt% of MWCNT in deionised water with an ionic surfactant. The mixture may be dispersed in water and alcohols. Ethanol was selected because of its low surface tension and high volatility. A ratio of 4 g: 36 g ratio of Aquacyl to ethanol was used, giving a 0.3 wt% dispersion. Rheology modifiers may be added to improve the jettability of this mixture (Baechler et al., 2016).

The MWCNT electrode mixture was printed with a 50 µm piezoelectric nozzle on a Jetlab4 XL printer. The electrodes were printed on 20 µm thick Elastosil frame with the backing intact. An array of arrays was printed to create 6 electrode lines with a width of 2 mm. The arrays were printed with droplet and line spacing from 50 µm to 100 µm increasing in 10 µm increments. In total two samples were printed. One sample consisted of 1 Pass and the other was printed in 2 passes (the second pass is aligned with the first, no offset). Both samples were printed on the fly at a velocity of 50 mm/s. Due to the water content in the electrode mixture the printing plate was heated to 80°C. This prevented the printed electrode mixture from coalescing. The following printing parameters were used RT 5 µs, DT 20 µs, FT 10 µs, ET 30 µs, RT2 5 µs, DV 70 V, EV, -70 V, PP 80° C, PH 10° C.

The electrode resistance was measured with the 4 point (4-pt) probe shown in Figure 3.15. The 4-pt probe consists of a right angle gold coated header pin soldered to a piece of Vero board. The outer most pins are connected to power supply of which the current is measured. The central pins were connected to a high impedance voltmeter. Before taking a reading the backing of the Wacker membrane was gently removed. The header was then lowered on to the electrodes until contact was made. The exact pressure is not important because the silicone adheres to the header pins and prevents the sample from stretching even if more pressure is applied. The results of the resistance measurement are shown in Figure 3.15. The plot shows that the resistance of the 2 pass sample is approximately two times that of the single pass. For the single pass electrodes the resistance increases from 4 kΩ/sq (DSLS50) to 15 kΩ/sq (DSLS100). For the two pass electrodes the resistance increases from 1 kΩ/sq (DSLS50) 8 kΩ/sq (DSLS100).

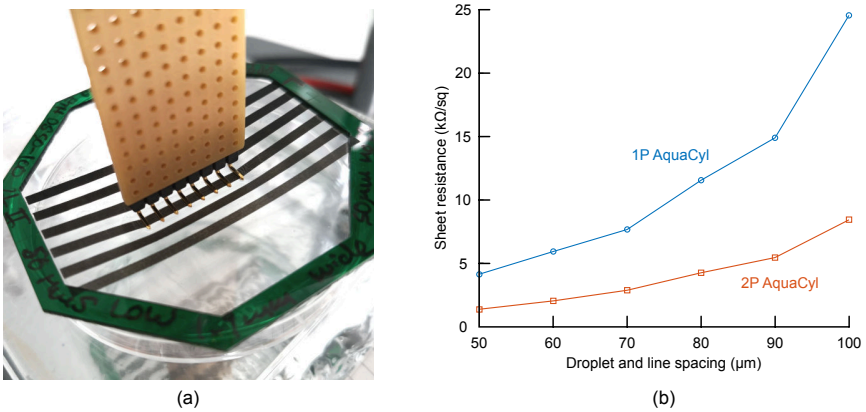

Figure 3.15 – (a) Measurement setup showing 4-pt probe in contact of inkjet printed MWCNT electrodes. Electrodes were printed on to a sheet of Elastosil (film 2030 250/20, Wacker Chemie AG). The backing was removed before the resistance was measured (b) Sheet resistance of inkjet printed MWCNT electrodes at different line (LS) and droplet spacings (DS), where LS=DS. Sheet resistance was measured for single pass (1P) and two pass (2P) electrodes. Second pass is parallel to first without any offset.

The thickness of the printed electrodes was also measured (Figure 3.16). The measurement was conducted on a laser confocal microscope (3D Laser Scanning Confocal Microscope VK-X1100, Keyence AG). The thickness of the single pass electrode decreases from approximately 500 nm (DSLS50) to 100 nm (DSLS100). The thickness of the two pass electrode decreases from 1000 nm (DSLS50) to 200 nm (DSLS100).

The MWCNT electrode has a higher conductivity than the Carbon black electrode presented in section 3.7.1. The carbon black based electrode has a sheet resistance of 3 kΩ/sq at a thickness of 3 µm. The MWCNT has a sheet resistance of approximately 4 kΩ/sq at a thickness of 0.5 µm. MWCNT electrode has a approximately the same sheet resistance as the carbon black electrode, but at one sixth of the thickness.

During the testing it was noted that the MWCNT electrode is very brittle. This is most likely due to the ionic surfactant in Aquacyl which is a solid when dry. This means that the printed electrode fractures when stretched by only a small amount (Figure 3.15). The same was reported by Baechler et al. (2016).The brittle nature of these electrodes suggests that MWCNT electrodes based on Aquacyl may degrade more rapidly when undergoing cyclic stretching. However further experiments are required to confirm this.

3.10 Conclusion

In this chapter a method to print carbon black based electrode directly on to silicone was introduced. A stable and ink-jet printable electrode mixture was presented. The electrode mixture consists of carbon black, a dispersant, and a siloxane solvent. The siloxane solvent has a high affinity to silicone. No surface treatment is needed to pattern the electrode mixture on silicone. The electrode mixture does not contain a binder and is thus highly conductive. The sheet resistance was shown to be as low as 2.9 kΩ/sq in static measurements (unperturbed electrode). The dynamic behaviour of the printed was also tested. However its should be noted that the dynamic results were from a recipe with a higher dispersant to carbon black ratio. The dynamic in-situ tests revealed that the electrodes can withstand biaxial stretching to 5% for 1 million cycles. The electrodes may be stretched to 10% but degrade more rapidly. The printed electrodes are therefore better suited for electrodes which are subjected to lower strain, such as Peano HASEL actuators. The shape of the electrode was also measured. Vector printing traces at 80° C produces narrow traces with a width of 200 µm. Printing at 40° C produces wider traces, but of a lower thickness (as low as 1 µm). The spread of the electrode mixture was also characterised on non-silicone substrates. Printing on non-silicone substrates is not recommended because the electrode mixture spreads producing a low resolution electrode. The flow may be counteracted by heating the printing plate. However, the electrical properties of such an electrode have not been characterised and may vary greatly from the properties of an electrode printed on silicone. For comparison purposes a MWCNT electrode was also presented. The MWCNT electrodes have a lower resistance (down to 1.4 kΩ/sq) and are thinner than the carbon black electrodes (down to 128 nm). The MWCNT electrode is very brittle and is likely to have poor cyclic properties without any additives. The techniques developed in this chapter can be used to pattern high resolution electrodes and electrical interconnections.

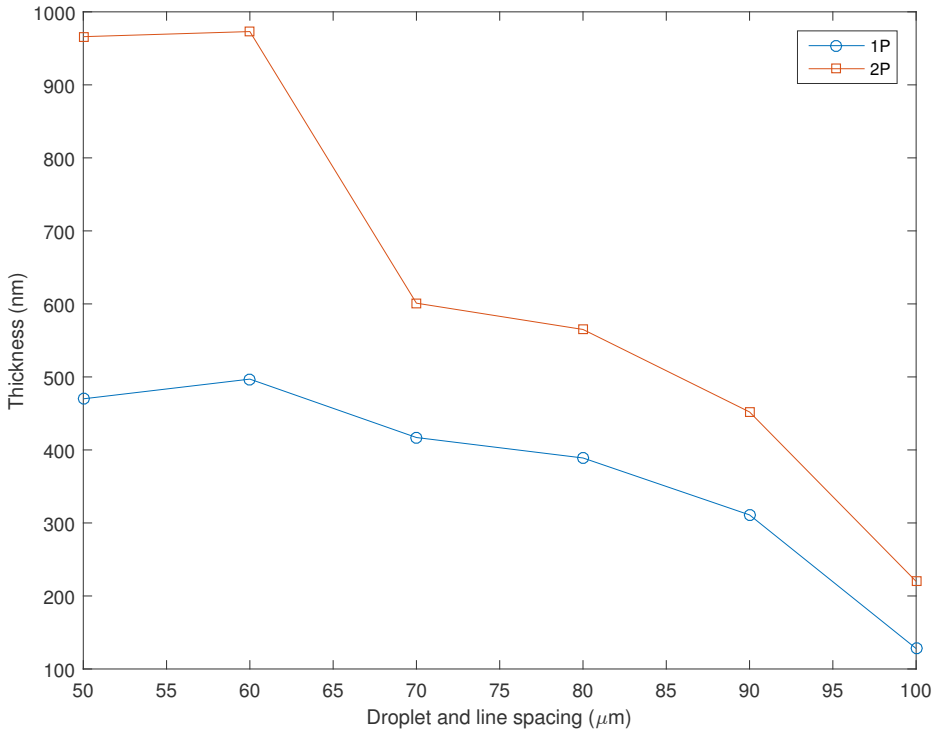

Figure 3.16 – Thickness of MWCNT electrode printed with different printing parameters. Printing 2 passes (2P) produces thicker electrodes than 1 pass electrodes (1P). The second pass was printed parallel to the first without any offset.

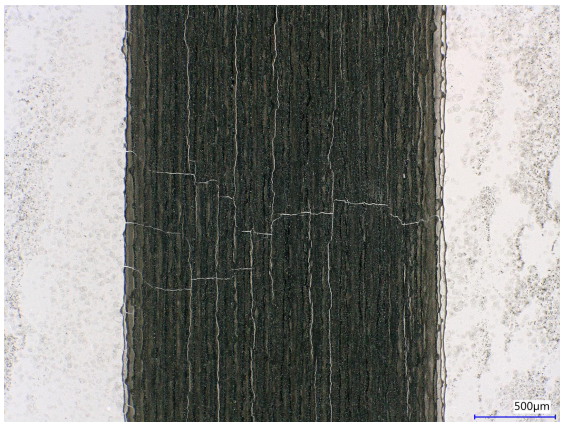

Figure 3.17 – Cracking of inkjet printed MWCNT electrode made from Aquacyl. Sample shown here is a 2 pass electrode printed on Elastosil film (2030 250/20, Wacker Chemie AG) at 80° C.

4 Sacrificial channels

4.1 Summary

In this section chapter and ink-jet printable sacrificial material is presented. The material can be dissolved to form channels in thin layered silicone structures. The shape of the printed sacrificial layer is characterised and a process to rapidly open the channels is presented.

4.2 Sacrificial channel requirements

A channel is formed by an absence of the surrounding material, in this case silicone. Since the silicone is a a low viscosity fluid it is not possible to create a channel by simply leaving a space while printing, subsequent passes will fill in the space. Instead a material has to be printed to reserve the space during printing and can be removed once the surrounding material has cured. This material, the sacrificial material, can be printed in two ways: As 3D shape with the same cross section as the desired channel, or as a 2D shape to create a barrier between the printed silicone layers so that they can later be peeled apart. In this work the latter approach has been selected because it is more suited for ink-jet printed soft machines.

Thin sacrificial channels are more suited for ink-jet printed soft machines. Firstly ink-jet printing is not suited for producing large aspect ratio structures. The solid content of ink-jet printable mixtures is usually less than 20% which means that the printed layers are microns thick. It would therefore take hundreds of passes to produce one millimetre thick channel. Second, HASEL actuators can more effectively close a flat channel. Zipping generally relies on having a thin dielectric from which zipping can occur. The zipping is also more effective at closing a channel if the channel can fully collapse. Thin sacrificial channels are therefore better for creating HASEL based devices. Third, flat channels simplify the fabrication of the structure. When high aspect ratio

structures are printed one must take into account the profile of the structure when printing subsequent layers. This makes the design of devices much more complicated. A levelling procedure could be used to fill in any holes and level the surface. Although this increases printing time without any added functionality. Finally, flat channels can be opened more rapidly than 3D channels. Flat channels produces a thin layer in between dielectric layers. These can be opened by injecting a liquid and peeling the channel open and later dissolving the sacrificial material with a solvent. This is a more rapid process than waiting for diffusion to dissolve along a thick 3D channel.

Taking the points above into consideration the sacrificial material must have the following properties. The sacrificial channel must be thinner than the printed dielectric layers so that the sacrificial channels do not lead to uneven layers. The sacrificial channel must be pattern-able at high resolution so that complex fluidic networks can be patterned, preferably down to hundreds of micrometers. The sacrificial material must not be soluble in the solvent used to dilute the silicone. Finally, to open the channels the material must be readily be soluble in a solvent at room temperature.

4.3 Material selection

Plastic, or polymers, are well suited as sacrificial materials. Polymers form a dense barrier, are plastic meaning that thermal stresses, solvent swelling, and mechanical stresses are unlikely to cause the material to crack or rupture, and many polymers can be solvating and on drying recover their original mechanical properties. A few polymers were considered, including PolyAcrylic Acid (PAA), PolyVinylPyrrolidone (PVP), PolyVinyl Alcohol (PVA), Cellulose Acetate (CA), and Ethyl Cellulose (EC). Most of these polymers are soluble in common solvents and form a rigid barrier on drying. However not all of these polymers have the right properties for printing sacrificial channels. For example PAA and PVA are less soluble at room temperature and require time and heat to dissolve. CA is readily dissolved in acetone, but this solvent is too volatile leading to erratic jetting and rapid clogging of the nozzle. PVP is highly soluble in many solvents including water but was eliminated because it was interfering with the curing mechanism of UV cure silicones. Although no additional experiments have been conducted to determine if it interferes with the curing mechanism of Sylgard 184. The material with the most desirable properties was EC (Sigma Aldrich 200689 10cp 48% ethoxyl). EC is available as a low molecular weight solid which is soluble in most alcohols, dissolves rapidly at room temperature, and does not dissolve in the solvent used to dilute the dielectric mixture.

The solvent was chosen based on its solubility, volatility and surface tension. The solubility of ethyl cellulose depends on ethoxyl content. Ethyl cellulose with more than 46-48% is readily soluble in common solvents such as methanol, ethanol, isopropanol, acetone, toluene, and ethyl acetate. Of these solvents Ethanol was selected because it

has a reasonably high volatility and good wetting properties on silicone due to its low surface tension. The vapour pressure of ethanol is higher than water but lower than isopropanol. The printed ethyl cellulose therefore rapidly dries but does not evaporate at a rate which leads to nozzle clogging.

4.4 Preparation of sacrificial material

The sacrificial material was prepared by combining the solvent, the polymer, and a plasticiser. The plasticiser was added to improve the ductility of the ethyl cellulose to reduce the probability of the sacrificial layer from cracking (Hyppoelae 1996). The materials are combined by transferring 0.05 g of the plasticiser, Dibutyl Sebacate (Sigma aldrich 84840 more than 97.0%), in a conical test tube. To this 32 g of ethanol was added and the conical test tube was shaken to combine the materials. Finally 0.5 g of ethyl cellulose (Sigma Aldrich 200689 10cp 48% ethoxyl) was weighed and added. The conical test tube was rapidly closed and shaken to prevent the ethyl cellulose from forming lumps. This mixture can be sonicated for 10 mins at elevated temperature for immediate use or left to dissolve for 24 hrs before use. The mixture was left to rest for at least 20 mins before use. The resting period allows any large dust particles to settle to the bottom of the conical test tube. After 20 mins the mixture was drawn out from the top of the test tube and transferred to a printer vial ready for printing.

4.5 Jetting parameters

For printing the sacrificial material a 80 µm piezoelectric nozzle (MJ-AT-01-80 from MicroFab Technologies, Inc.) was used. The 80 µm nozzle is a good compromise between speed of printing and resolution. Although the resolution of the printed sacrificial channels could be improved by using a smaller nozzle. The printing waveform presented in section 2.3 was modified to reduce the chance of nozzle clogging. The dwell time was selected to maximise the speed of droplet ejection DT = 20 µs, the echo time was reduced 1.5×DT to reduce the tail of the droplet from diverging from the vertical path ET = 30 µs, and the voltage was maximised to prevent clogging during long pauses DV = EV = ±70V. Surprisingly the jetting parameters for the sacrificial material are the same as the jetting parameters for the electrode material despite the larger nozzle. This is likely to be the case because the viscosity of the sacrificial material is different. The sacrificial material was printed using a printing plate temperature of 40° C and a print head temperature of 80° C. A photograph of a drop being ejected from a 80 µm nozzle is shown in Figure4.1.

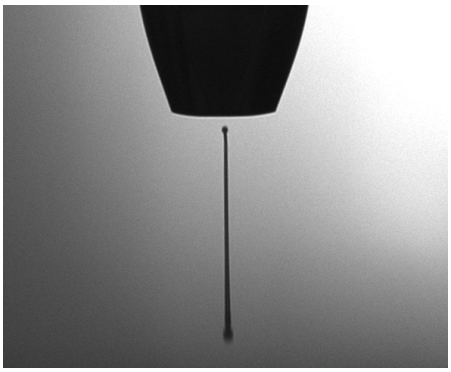

Figure 4.1 – Stroboscopic image of the standard sacrificial mixture (Section 4.4) being ejected from a 100 µm piezo-electric nozzle. The droplet was generated using an adapted waveform with the jetting pramaters RT 5 µs, DT 20 µs, FT 10 µs, ET 30 µs, RT2 5 µs, DV 70 V, EV, -70 V, PP 40° C, PH 10° C. The backpressure was adjusted to level the miniscus when the jetting was off. The long tail of the generated droplet breaks up into smaller droplets but remain on the vertical path.

4.6 Patterning sacrificial channels

The sacrificial material is more challenging to print than the electrode and dielectric materials. Unlike OS-2, ethanol is not readily absorbed by silicone, and is therefore not anchored to the surface. If too much liquid is deposited too rapidly the liquid will coalesce. However by selecting a suitable drop spacing, speed of printing, and elevating the temperature of the printing plate it is possible to pattern the sacrificial material without it coalescing. Figure 4.2 shows a series of lines printed with a speed of 50 mm/s when the printing plate was set at 40°C and the print head was cooled to 10°C. A large droplet spacing of 200 µm reveals the size of the drops.Lone droplets have a diameter of ~150 µm. When the droplet spacing is reduced to 150 µm the droplets make contact and form a bulging line with a width of ~130 µm. At a droplet spacing of 100 µm the droplets form a relatively straight line with a width of ~170 µm. Reducing the droplet spacing further to 50 µm leads to low frequency undulations and a much wider line of ~190 µm.

Printing a polygon is not as straight forward as printing individual lines. Polygons are raster printed and consist of parallel lines. When printing the sacrificial material subsequent passes can redissolve the material which were just printed. The effect is especially a problem when bi-directional printing is used. When printing bidirectionally, the sacrificial material does not have enough time to dry before the printer turns around and starts printing the next line. The sacrificial therefore tends to coalesce on the edges of a printed polygon. To avoid this the sacrificial material was printed uni-directionally. Unidirectional printing means that the printer is only jetting on the forward stroke and does not jet on the return stroke. In addition the printer was forced to travel the full width of the print job. This is achieved by drawing a 1 pixel wide border to force the

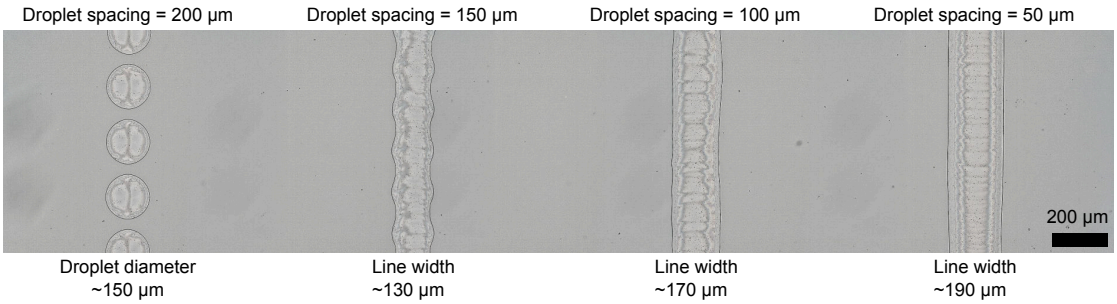

Figure 4.2 – The width of ink-jet printed sacrificial lines on Sylgard 184 (Dow) with decreasing droplet spacing. The droplet spacing is reduced from 200 µm to 50 µm in 50 µm increments. The approximate diameter or width is noted above each line.

printer to travel to the edges of the print job. Forcing the printer to always travel the same distance ensures that each pass has the same amount of time to dry resulting in more repeatable printing results. A picture of a 2 mm wide printed sacrificial channel and its profile is shown in Figure 4.3. The raster printed channel was printed with a droplet and line spacing of 100 µm, a print-on-the-fly speed of 50 mm/s, and the printing plate and the print head at 40°C and 10°C respectively. The sacrificial channel shown in the figure consists of two layers of printed sacrificial material. On occasion droplets fail to be ejected leaving a hole in the sacrificial layer. Holes can prevent the channel from opening and must be avoided. The easiest way to prevent holes in the sacrificial layers is to print two layers on top of eachother. The probabability that two holes are perfectly aligned is extremely unlikely. The average thickness of the sacrificial channel shown in the figure is 1.9 µm.

4.7 Opening of channels

A layer of silicone must be printed first to cover the sacrificial channel. Inkjet printing of silicone is covered in chapter 5.

Before the channels can be opened and filled fluid connectors must be added. The type of connection depends on the nature of the device. For thin devices a perpendicular connection is made and for thick devices an in-line connection is made (Figure 4.4). For thin devices (without a thick silicone base) it is difficult to access the channels from the edges. For this reason a hole is left in the printed dielectric layer and a silicone tube is attached to the top surface. The tube is first dipped in RTV silicone and the excess silicone was dabbed off. The tube is then placed over the top of the printed hole and the silicone runs down the side to create a seal. For thick devices the channels can be accessed from the edges. First the device is trimmed with a razor blade to produce a clean edge. The device is then submerged in ethanol and a tapered silicone tube is gently forced into the channel. Once the tube is inserted and secured the device is placed in an

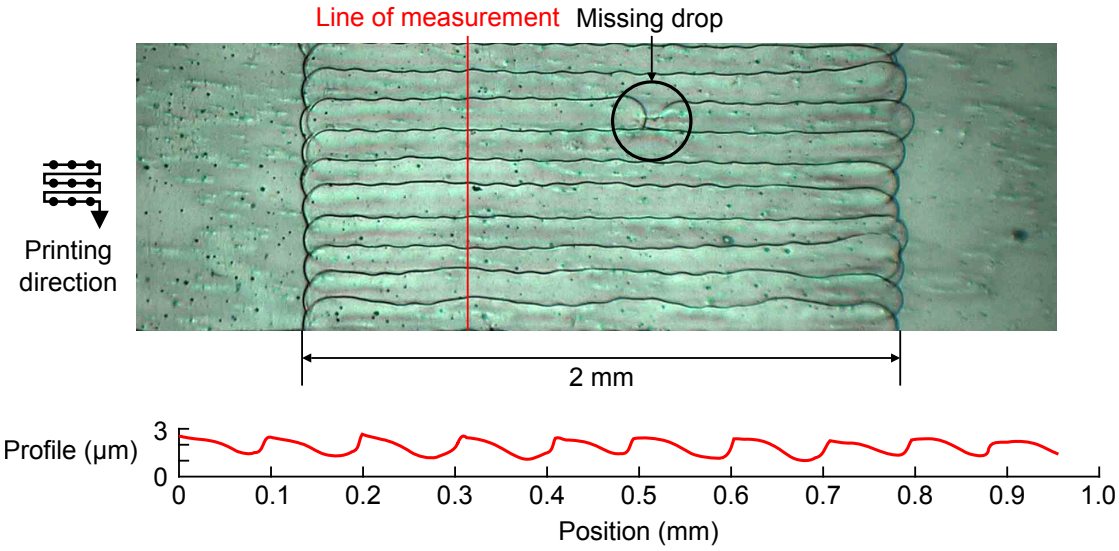

Figure 4.3 – Profile of an ink-jet printed sacrificial channel. The photograph shows a 2 mm wide channel printed in raster mode with a droplet and a line spacing of 100 µm. The sacrificial channel was printed in two passes to avoid holes in the printed sacrificial layer. The average thickness of the sacrificial channel is 1.9 µm.

oven to evaporate the ethanol. Silicone is applied around the tube to hold it in place. The silicone wicks into the space between the printed silicone layer and the thick silicone base to produce a robust fluid connection.

The channels are opened by peeling the layers apart with a pressurised fluid. The process is illustrated in Figure 4.5. A basic channel consists of two printed dielectric layers and one sacrificial layer. The sacrificial layer does not bond to the underlying silicone and the silicone bonding to ethyl cellulose is also poor. When a fluid is injected into the channel these weak interfaces are peeled apart. The ethanol then floods into the channel dissolving the thin film of ethyl cellulose. The processes is relatively quick and channels can be opened at a rate of millimetres per second. Once a channel has been completely opened the sacrificial material can be flushed out using more ethanol. To ensure the channel is completely rid of ethanol the device is dried before the final dielectric fluid is injected.

4.7.1 Printing channels which are easier to open

Up to this point the process to print a sacrificial channel has been described. The sacrificial material contains a plasticiser to prevent cracking and is printed in two passes to reduce the probability of holes blocking the channels. The process is fairly robust, however sacrificial channels may be printed in a cross hatched orientation to further ease the opening of channels.

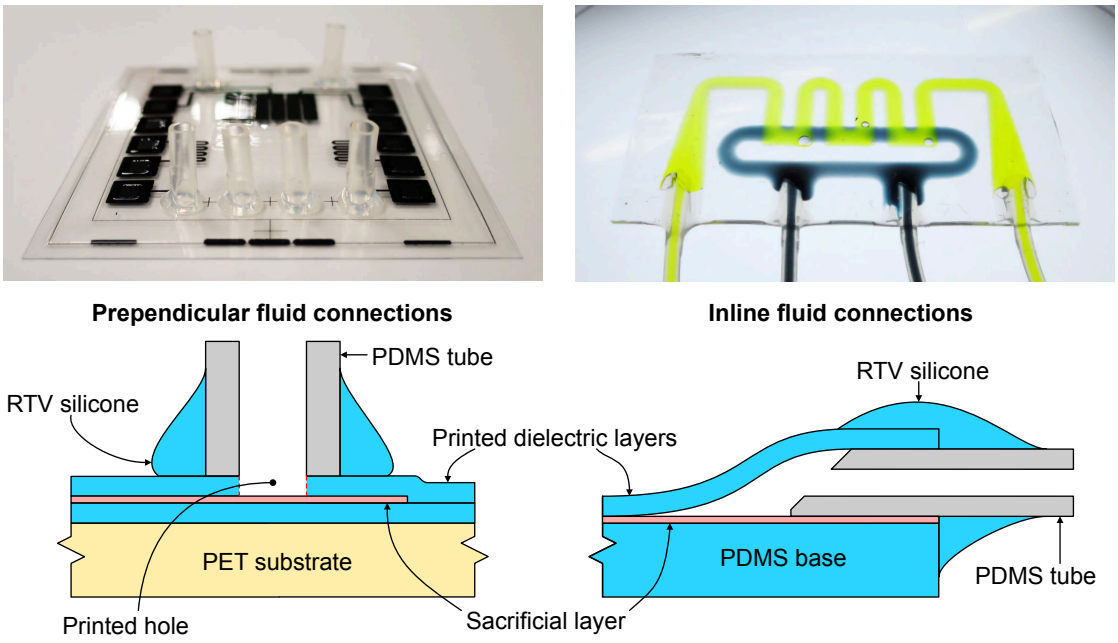

Figure 4.4 – Photograph and diagrams showing how fluid connections are made. On thin devices perpendicular connections are made by gluing 1 cm silicone tubes on to the surface using RTV silicone. On devices with a thick silicone base the tubes are inserted on the edges creating an inline connection. The tubes are fixed in place using RTV silicone.

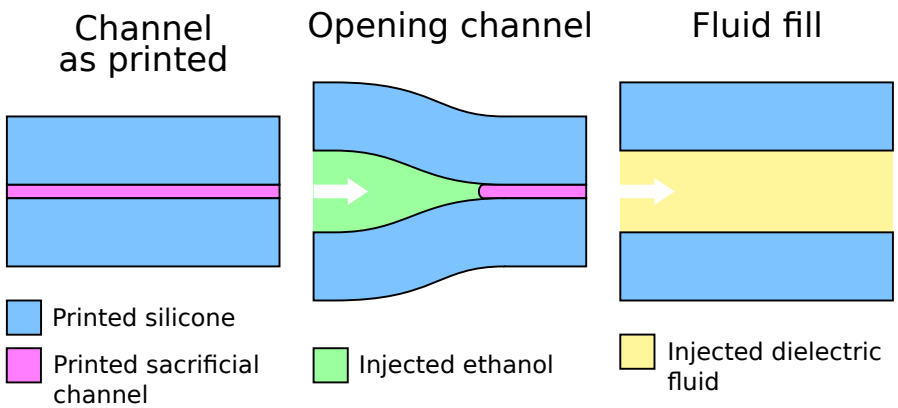

Figure 4.5 – A diagram showing how the channels are opened. A channel is formed by printing a silicone-sacrificial-silicone sandwich. The bonding between the silicone and sacrificial layers is weak. When ethanol is injected the layers peel apart forming a channel.

A single layer of printed sacrificial material is extremely fragile. When printing the sacrificial material on silicone it is susceptible to the coffee stain effect. The dissolved polymer is deposited at the edges of the printed lines (Figure 4.6a). The edges are much thicker than at the centre of the printed lines. The cross section of a single pass sacrificial layer is shown in Figure 4.6b. The thickest part is approximately 1.4 µm thick and the thinnest part has negligible thickness. The thin part is extremely fragile and susceptible to cracking.

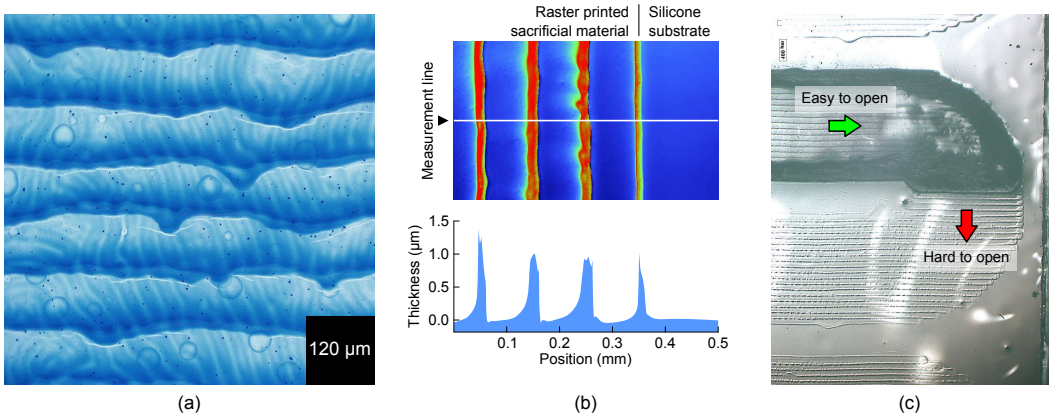

Figure 4.6 – (a) A microscope image of a 1 pass sacrificial layer in between two printed dielectric layers. The blue die in the sacrificial material makes the cracks in the thin parts clearly visible. The ripples were caused by drying and thermal stresses. (b) Surface plot and profile of 1 Pass printed sacrificial layer. The plots show how the polymer is deposited at the edges creating thick and thin regions which are prone to cracking (c) A 2 mm wide sacrificial channel printed in 1 Pass. The channel opens easily when the peeling is parallel to the printing direction. However the channel is difficult to open when the peeling is perpendicular to the printing direction

Single layer sacrificial channels were difficult to open. In particular the channels were often blocked at the turn around points. A turn around point is where a channel makes a 90° turn (Figure 4.7c). The thin regions of the printed sacrificial material presented an obstacle to opening the channel. It is not clear if this is because of the thin regions and cracking or the steep peeling angle at the edges of the printed lines. Printing two passes (parallel) reduces the problem but does not eliminate the problem completely.

The sacrificial layer may be printed in a crosshatched configuration to ease the opening of channels. A crosshatched sacrificial layer is printed in two passes, however the second pass is printed perpendicular to the first. This produces a sacrificial channel with the same roughness in the x and y directions. Crosshatching may be applied to the whole channel or to the regions where the channel makes a 90° turn. Figure 4.7 shows two microscope images of cross hatched channels. Partial crosshatching may be preferred when a channel is long and narrow to reduce printing time.

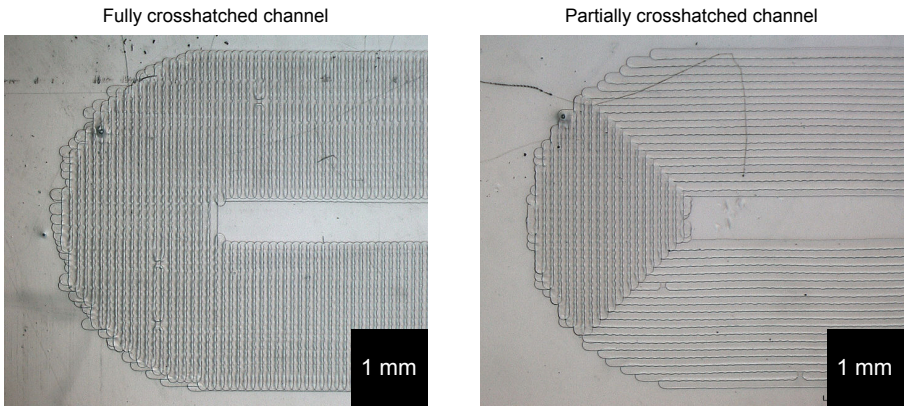

Figure 4.7 – Crosshatched sacrificial channels to ease the opening of channels. (a) Cross hatching may be applied to the entire channel. (b) Crosshatching may be applied only to the turn around points in the channel to reduce printing time.

4.8 Alternative techniques to fabricate channels

In this section two alternative ways to produce channels are presented. The first, glue-line, is an approach which uses ink-jet printed silicone as a glue layer to bond silicone membranes together. The second, soft-lithography, may be used to make high resolution channels using an SU-8 mould.

4.8.1 Glue-line channels

The glue-line approach uses ink-jet printing in vector mode to print a line of glue to bond two prefabricated silicone layers together (Figure 4.8). The process has some advantages over printing the whole structure: First, the glue-line approach is much faster because prefabricated membranes may be used; Second, the use of prefabricated membranes produces channels with more uniform dielectric layers; Third, Pre-stretched membranes may be used for the dielectric layers; Lastly, the channels are easy to open because the bonding between the membranes is weak. There are also disadvantages to this approach which are summarised at the end of this section.

A glue-line channel may be fabricated with un-stretched or pre-stretched membranes. Un-stretched membranes make very compliant channels which readily deform under pressure. Prestretched membranes produce channels which are less compliant and deform less under pressure. Pre-stretch may be necessary for devices with integrated DEA.

The un-stretched glue-line channel shown in Figure 4.8b was fabricated with the following procedure. First the frames were prepared. A sheet of Plexiglas was lined with a silicone adhesive (Arclear 8932, Adhesive Research) and laser cut into the shape of an

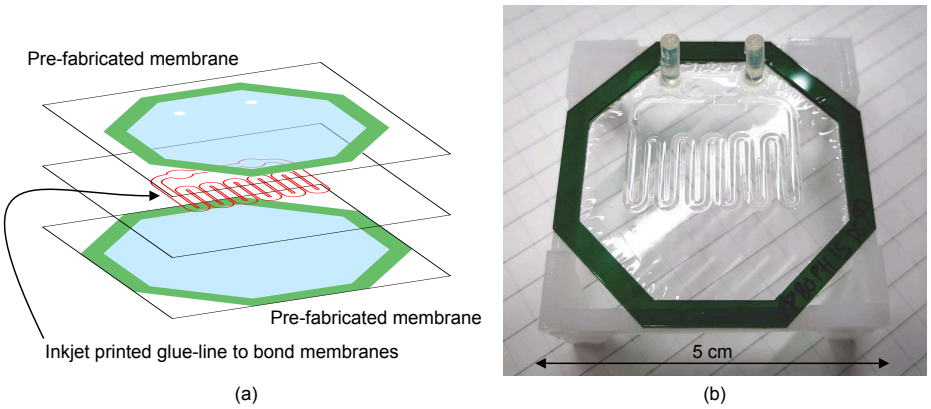

Figure 4.8 – (a) Glue-line channels are produced by bonding two prefabricated membranes together with a line narrow line of silicone glue. (b) A photograph of a serpentine channel made with two 20 µm Elastosil membranes laminated with the glue-line method.

octagon. The frames were designed to fit inside each other. Second, the frames were attached to a 20 µm thick Elastosil film (Elastosil 2030 250/20, Wacker Chemie AG). The frames were cut out with the backing intact. Third, the glue line was printed onto the larger of the two membranes. The dielectric mixture from section 5.4 was used. The line was printed in vector mode with a droplet spacing of 50 µm at a speed of 5 mm/s. The droplet spacing and the temperature of the printing plate may be varied to control the width of the glue-line (Figure 4.9). Four, the small membrane was prepared. A template was used to puncture holes through the membrane. The backing was gently removed and the small membrane was placed on to the large membrane. It is best to bring the membranes together at an angle to avoid trapping air. Once assembled the glue-line was cured at 80° C for approximately 1 hour. Fluid connections were made according to the procedure detailed in section 4.7.

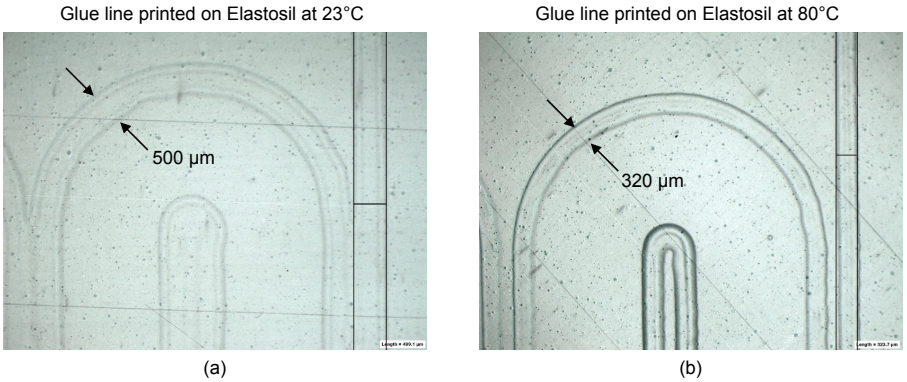

Figure 4.9 – Width of ink-jet printed glue-line on Elastosil membranes. (a) The glueline has a width of 500 µm when the printing plate is at room temperature. (b) The glue-line has a width of 320 µm when the printing plate is at 80° C.

When working with pre-stretched membranes the process is slightly different. First,

the membranes are pre-stretched and adhesive frames are added to hold on to the membranes. If wide glue lines are acceptable the pre-stretched membrane may be suspended on the printing plate. If narrower glue lines are required the membrane may be placed directly on the metal printing plate or a metallic film may be added as a temporary backing layer (Figure 4.10). Using metal as a backing layer improves the conduction of heat and reduces interference from static electricity produced by peeling off the original backing layer. For the top membrane a temporary PET layer is applied to the pre-stretched membrane. With the temporary backing in place it is possible to puncture holes in the pre-stretched membranes for the fluid connections. The temporary PET backing layer is removed before the membranes are laminated. The laminated structure is cured in an oven.

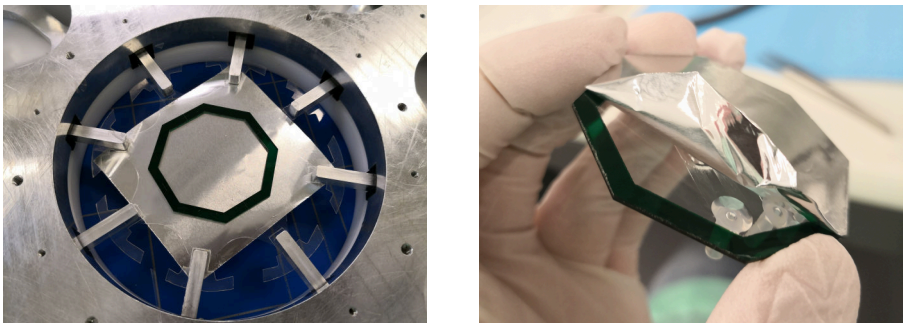

Figure 4.10 – Use of a metal backing on pre-stretched membranes to improve heat transfer and dissipate static electricity. Static electricity is generated when removing plastic backing of Elastosil films (a) Aluminium foil is added after pre-stretching membrane (b) Aluminium foil is peeled off after all layers have been printed.

This method for making channels in thin silicone membranes is fast and the membranes are more uniform than ink-jet printed membranes. However, there are a number of reasons why this technique was not adopted for complex multilayer devices. A major problem with this approach is that the channels may be glued shut when silicone is printed on subsequent layers. Silicone is a very porous material and the printed silicone mixture may penetrate through cured silicone layers. When this occurs the surfaces in the channel are bonded together and are impossible to open. This was observed when the device in Figure 4.11 was fabricated. Electrodes were printed on top of the serpentine channel along with an encapsulation layer. After curing the encapsulation layer it was no longer possible to open the channel. The picture shows a wire being inserted into the channel to force the channel open. A solution to this problem is to print the electrodes and encapsulation layers before laminating the structure. However, the electrode and dielectric materials contain a siloxane solvent which causes the membranes to swell and deform. Laminating layers which are not flat is challenging. For this reason the glue line approach is not recommended for multi-layer devices with electrodes and encapsulation layers.

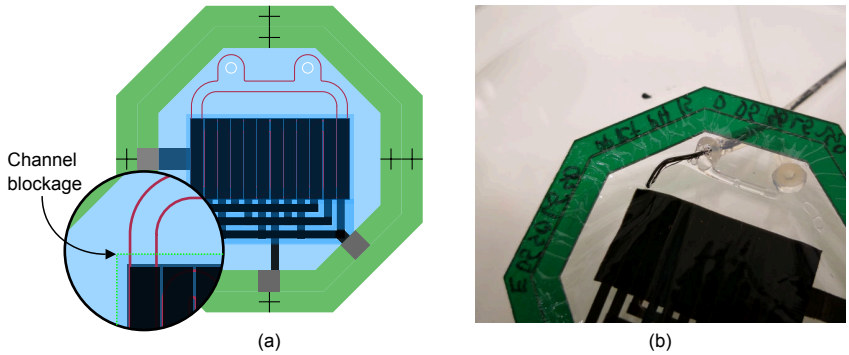

Figure 4.11 – Silicones printed on the outside of a glue-line channel penetrate through the dielectric membranes and glue them shut (a) A multi-layer glue-line structure with ink-jet printed electrodes and a silicone encapsulation layer. The magnified view shows where the encapsulation layer crosses the glue-line channel (b) A photo of the same device with the blocked channel. The photo shows a wire being used to force the channel open. The channels were permanently bonded shut due to encapsulation layer.

4.8.2 High resolution moulded channels by soft lithography

Soft lithography may be used to make high resolution channels in silicone. However, the conventional fabrication techniques are typically used to create thick pieces of structured silicone.In this section a fabrication technique is presented to create thin structured silicone membranes. Thin membranes with channels are compliant and may be used to make structures with integrated electrostatic transducers.

To mould silicone with soft lithography a master mould is required. The master mould is fabricated with conventional photo lithography techniques. In short, a photo resist is spin coated on to a silicon wafer, exposed to UV radiation through a mask, and then washed with a developer to leave a cured micro-structure. A photograph of a master mould is shown in Figure 4.12. The process used to make the master mould is summarised in the appendix section A.1.

The silicone is micro-structured by pouring silicone on to the master mould. Simply pouring the silicone on to the mould produces a thick piece of silicone with a micro-structured surface. A method to remove the excess silicone is therefore required. One way to do this is to use a spin coater. However initial experiments showed that spinning resulted in non-uniform silicone membranes (Figure 4.13). Streaks or unevenness was particularly prominent around the large border grooves. The impact of these grooves may be reduced by making narrow grooves (< 100 µm). However, the problem is not completely eliminated and results in thin regions which cause the structured membrane to tear more easily (Figure 4.13c).

Blade casting would be a more suitable way to create a flat silicone layer. Unfortunately a film applicator was not available at the time of these experiments. Instead a flat and

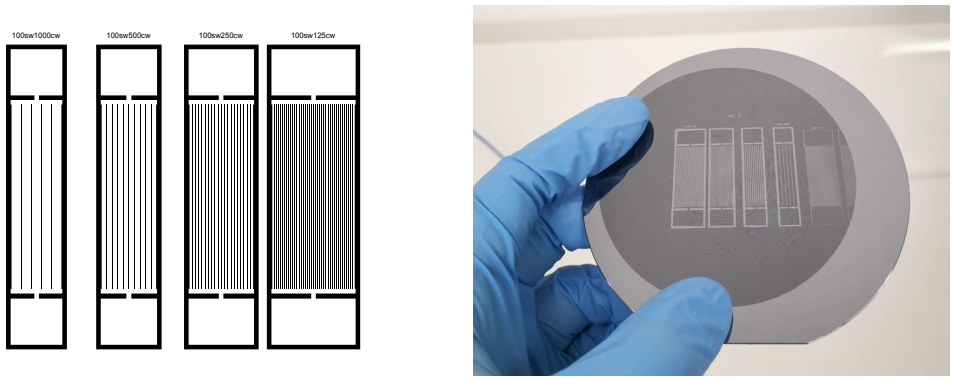

Figure 4.12 – SU8 master mould (a) Design of photo-lithography mask to test channels with a seam width of 100µm, channel widths from 1000 µm to 125 µm, and border width of 500 µm (b) SU-8 mould for soft lithography.

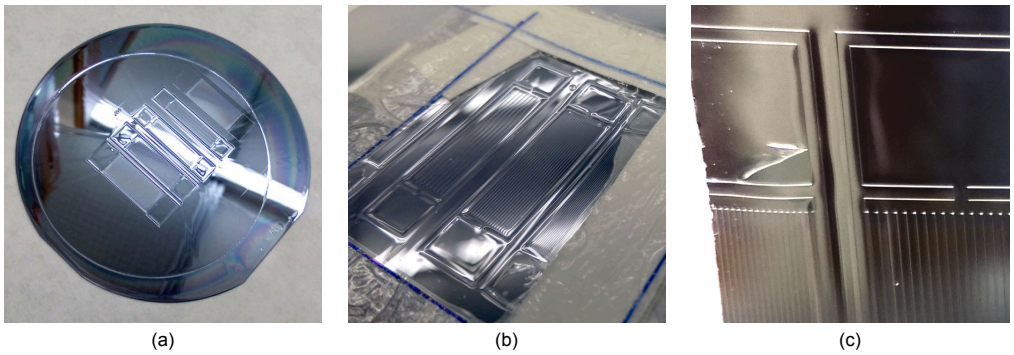

Figure 4.13 – Thin film of Sylgard 184 on SU-8 master mould after spin coating. (a) Full wafer showing streaks due to large grooves on master mould. (b) Magnified view showing uneven surface of silicone membrane. (c) Silicone tearing at sharp edges during removal.

uniform silicone layer was produced by filling the mould up to the top surface and removing the excess material. A uniform membrane may then be laminated on to the top surface to create a thin and uniform structured membrane. Two methods based on this principle were tested (Figure 4.14).

The first, Method A, uses a sheet of PET coated with a sacrificial material (PolyVinylPyrrolidone) to push out the excess silicone. The silicone was cured with the PET sheet intact. After curing the PET sheet was removed with a small amount of isopropanol to aid the peeling. A prefabricated Elastosil membrane was plasma bonded on to the top surface using oxygen plasma bonding. The micro-structures could then be removed from the master mould. Finally the structured membrane was bonded to another Elastosil membrane to seal the channels.

The second method, Method B, used a squeegee to remove the excess silicone. Silicone was poured on to the master mould to fill all the grooves and the excess was removed with a squeegee. A relatively stiff squeegee with a perfectly straight edge must be used to remove all residue from the surface. Before the the silicone was cured a free hanging Elastosil membrane was laminated on to the back of the mould. This was accomplished by placing the free hanging membrane in close proximity of the mould and using a jet of compressed air to bring the materials together. The structured membrane was removed by adding a small amount of isopropanol to remove the micro-structured membrane. To seal the micro-structured membrane a layer of silicone glue was applied to a sheet of Elastosil. The structured membrane was lowered on to the sheet of Elastosil to seal the channels.

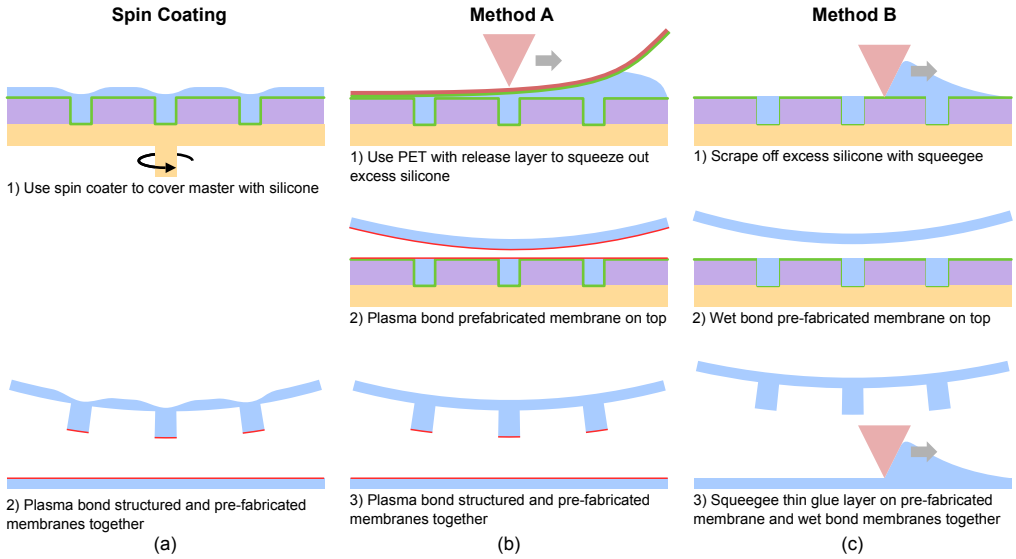

Figure 4.14 – Three methods to make a thin structured membrane using an SU-8 mould. (a) Spin coating used to remove excess silicone (b) Method A: Indirect removal of silicone with a scraper and a flexible sheet of material. (c) Method B: Direct removal of silicone with a squeegee.

All three methods have been used to make channels. However, each process has some advantages and disadvantages. Spin coating is a relatively simple method to make structured membranes with repeatable properties. The downside of spin coating is the uneven surface produced due to large features (grooves). The channels tend to burst at a low pressure because of this. In addition the oxygen plasma bonding was poor leading to de-lamination of the channels (Figure 4.15a). Method A is a promising way to create thin structured membranes. The main problem with this approach is the removal of the PET sheet. The thin silicone membrane between the SU-8 master and the PET sheet adheres well to both surfaces. The thin silicone membrane tears when the PET sheet is removed (Figure 4.15b). The uneven surface makes it difficult to create a good bond between the Elastosil membrane and the micro-structures. This problem may be reduced by using a better release layer. Method B was the most effective of all the processes. The bonding between the Elastosil membranes and the micro-structures is very strong. This makes it easier to remove the micro-structures from the master mould. Unfortunately the end result is less than perfect. Using a squeegee directly on the master mould introduces air bubbles into the mould (Figure 4.15c). The forces applied to the mould may also damage the micro-structures.

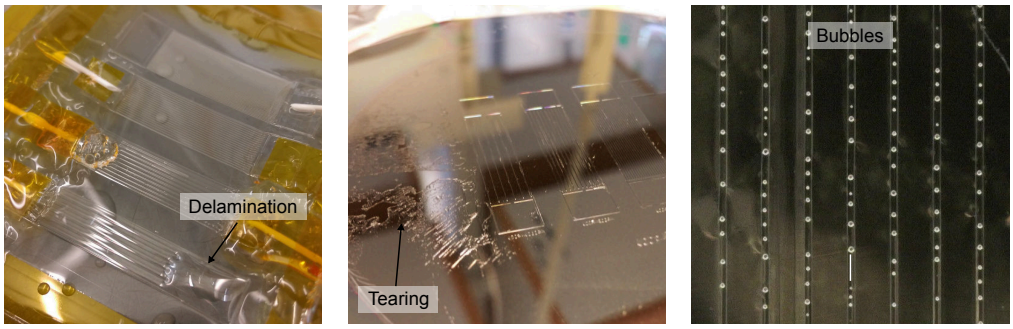

Figure 4.15 – Problems encountered whilst fabricating structured membranes. (a) De-lamination of plasma bonded membranes. (b) Tearing of thin film between SU-8 mould and flexible squeeze sheet. (c) Trapped air bubbles in the micro-structures.

In this section three different approaches to create thin structured silicone membranes were presented. Direct removal of the excess silicone, Method B, produced the best results. However, the squeegee process micro-structure with trapped air bubbles and streaks. A better way to form high resolution channels may with a film applicator. With a film applicator the speed of application and the thickness can be controlled. A film applicator would therefore produce a more uniform and robust structured membrane. Finally, to seal the channel the structured membrane must be bonded to a pre-cast silicone membrane. The strongest bond was obtained by using a thin film of silicone as a glue layer. The combination of casting and gluing may be used to create high resolution and robust channels.

4.9 Conclusion

In this chapter a ink-jet printable sacrificial material has been presented to produce channels in layered silicone structures. The solid content of the sacrificial mixture is less than 2% producing very thin sacrificial layers. The sacrificial layers can be rapidly printed, are well suited for zipping actuators, do not require post levelling procedures, and can be rapidly opened. The process may be used to print high resolution (features down to 150 µm) and complex networks of channels in thin silicone structures.

5 Silicone dielectric layers

5.1 Summary

In this chapter an ink-jet printable dielectric material is explored. A special process is developed to print thin uniform silicone membranes on substrates with different surface properties. The breakdown strength of the printed membranes is also measured.

5.2 Dielectric requirements

Electrostatic transducers require dielectric layers which are thin, uniform, clean,impermeable to the dielectric fluid, and have a high breakdown strength and electrical permittivity. Although thin dielectrics are not essential to produce working transducers they are important to reduce the operating voltage of electrostatic transducers. The driving voltage of a transducer has an effect on control electronics. In general the components for switching high voltages are expensive, more bulky, and there are less components to choose from. The size and weight of high voltage electronics also prevent miniaturisation and present an obstacle to producing untethered soft robots based on electrostatic actuation principles. In addition high voltage devices are perceived as dangerous. This is not true as we are exposed to 10 s of kilovolts on a daily basis due to static electricity. High voltage devices are only dangerous when the energy storage of a device is high enough to generate a current in the milliamp range.A good voltage limit for small devices is 5 kV. At this voltage there are commercially available electrical components to generate and control the transducers, it is possible to miniaturise circuits without arcing being a problem, and electrical shocks are only a nuisance. Furthermore 5kV corresponds to a thickness of 50 µm for silicone based dielectric materials with a field strength of 100 V/µm. The uniformity is extremely important when fabricating electrostatic transducers because it can lead to premature dielectric breakdown. Dielectric breakdown occurs at at the weakest link in a electrostatic transducer. The weakest link is either a region where the dielectric membrane is locally thinner than the surrounding material or contains

a piece of dust. For ink-jet printed printed dielectric materials uniformity must be given special attention because the material is formed drop by drop. Although the drop density can be closely controlled, the flow of the material is less predictable. Finally the material properties, dielectric breakdown strength and the electrical permittivity, are very important because these determine the performance of an electrostatic transducer. Equation 2.1 in section 2.1 demonstrates this. A high breakdown strength permits the use of a higher electric field E and thus a higher actuation pressure. Since the pressure is proportional to the electric field squared a small increase in dielectric breakdown strength can have a large effect on the maximum pressure. The electrical permittivity can also increase the actuation pressure. The electrostatic pressure is linearly proportional to the dielectric permittivity.

5.3 Material Selection

Silicone in its pure form is too viscous to print with an ink-jet printer. The viscosity limit for the piezoelectric nozzles on the Jetlab4 printer is about 40 cp. silicones with desirable mechanical properties such as Sylgard 184 and Sylgard 186 have a viscosity of 3500 cp and 66700 cp respectively. A solvent is required to reduce the viscosity of the silicones. In this section the selection of a suitable silicone and solvent is discussed

When choosing a silicone, a number of factors must be considered. The properties of the fluid so that it can be ink-jet printed to produce thin uniform films, the curing mechanism used to convert the silicone from a liquid to an elastomer, and the final physical properties of the silicone. The fluid property which is of the utmost importance is the viscosity (which is closely linked to chain length) of the silicone. The viscosity determines how much solvent is required to dilute the silicone and hence the final thickness of the printed dielectric. The viscosity also has an effect on the uniformity of the printed dielectric layer. Silicones with a low viscosity, often advertised as being pourable or self-levelling, will continue to level when printed. The choice of viscosity is a compromise between printability, self levelling and uniformity, thickness, and also resolution. Silicones with an extremely low viscosity will flow and reduce the resolution of the patterned dielectric. The curing mechanism must also be carefully considered. The curing mechanism determines where the dielectric material can be cured, the rate of curing, its compatibility with other printing processes and materials. Silicone is available with four different curing mechanisms. Addition cure which is a silicone consisting of two parts, and by adding a second part a cross linking reaction can take place. Moisture cure silicones which use water vapour in the atmosphere to complete a chemical reaction. UV cure silicones which use UV light to provide enough energy for a reaction to place at room temperature. Thermal cure silicones which use elevated temperatures to accelerate curing. Generally thermal cure silicones are addition cure silicones which can be heat accelerated and will cure eventually at room temperature. The curing mechanism dictates how the dielectric material is cured. Addition cure silicones can be cured within

the printer by using multiple nozzles (one for part A and another for part B) or printing the parts with the same nozzle sequentially. Moisture cure silicones can also be cured within the printer as the ambient humidity is sufficient for curing to begin. It is also possible to accelerate the curing by placing a humidifier into the printer enclosure. UV cure silicones can also be cured on the printing plate. By adding a UV light into the printer enclosure it is possible to cure printed layers by the flick of a switch. Thermal cure silicones can also be cured within the printer however the rate strongly depends on the curing temperature. Most ink-jet printers have heated printing plates. However, using a heated printing plate can have negative impact on jetting. The jetlab4 XL printer has a printing plate which can be heated to 120° C, however this temperature is rarely used. At 120°C nozzle clogging is accelerated and most plastic based substrates thermally deform leading to potential nozzle collisions. The effect of the curing mechanism on other printed materials must also be considered. For example the moisture cure mechanism may cause issues when water soluble materials are used and the curing process is accelerated with a humidifier. When using thermal cure silicones the curing temperature must be carefully selected to prevent thermal stresses in other materials. Thermal stresses can lead to deformation of printed materials. It may lead to cracking of the electrodes or cracking and bending of sacrificial layers. The curing mechanism may also be sensitive to chemical species in other printed materials. For example silicones which contain a platinum catalyst materials are sensitive to sulphur, amines and amine-containing compounds, and organometallic compounds. Additional materials that could lead to cure inhibition are vinyl plastics, chlorine-containing materials, certain epoxies, leather, clays, and vulcanized rubbers (Sommer and Sommer, 2014). Silicones which use a peroxide curing system may also be sensitive to oxygen.

Three types of silicones were tested at the beginning to determine the advantages and disadvantages of each curing mechanism. One of the three was a UV cure silicone, Silopren UV Electro 225-1 from Momentive Performance Materials Incorporated. We had previously printed this silicone to make thin dielectric layers (McCoul et al., 2017) and it looked to be a very promising material. However there were multiple issues with the material curing. When printing thin layers the proportion of photo-initiator had to be increased from the recommended 50:1 (base:initiator) to 2:1. We now understand that the increased photo initiator was required because the photo initiator is a peroxide precursor which is disabled when exposed to oxygen. The effect is especially pronounced when printing thin membranes because the surface area to volume ratio is extremely high when printing membranes. Curing was also inhibited when printing on the sacrificial material presented in Chapter 4. For these reasons work was discontinued with UV electro 225-1 because it was too sensitive to poisoning. The second was a moisture cure RTV, Dowsil 734 (formerly Dow Corning 734) from Dow. This flow-able silicone sealant was considered because it cures rapidly in ambient conditions (skin over time 7 min tack free time 13 min) and is very resistant to poisoning. Since the membranes printed are a few micrometers thick the silicone is cured throughout in less than 10 mins

and subsequent layers can be printed. However to print consistently for long periods of time is challenging. The mixture begins to cure in the reservoir and tubing as time progresses. This results in a viscosity change which eventually terminates the jetting. In part this challenge was overcome by using dry nitrogen as the back pressure gas, drying the solvent with molecular sieves, and adding a nitrogen curtain to the nozzle tip. With these changes it was possible to prevent the viscosity change and prevent build up on the nozzle. However significantly more work would have been required to design a nitrogen curtain which does not introduce turbulence. The third was a thermal cure silicone, Sylgard 184 from Dow. Sylgard 184 is a pourable encapsulant with good dielectric properties. This material has a long working time (1.5 hrs) and cure time (48 hrs at 25° C) and thus can be premixed and printed. Premixing the parts is preferable because it reduces printing time and improves film quality. Less care has to be taken when preparing the materials as moisture and light do not affect the curing of these elastomers. There is however one large drawback to using thermal cure silicones. In order to rapidly cure the printed layers the printed sample must be removed from the printing plate and placed in a high temperature oven (>100° C. Doing this increases the risk of exposing the samples to dust and makes printing stacks more tedious.Following the feasibility test S184 was chosen as it was the material easiest to prepare as it does not require shielding from moisture and UV light, seemed to be resistant to poisoning. Further more due to its low viscosity it produced flatter layers.

To reduce the viscosity of silicone a solvent must be added. The solvent must meet a number of requirements in order to be suitable for printing thin dielectric layers. Firstly the solvent must be miscible with the chosen silicone, Sylgard 184. In general non-polar solvents have the ability to solvate silicones , including ethyl acetate, toluene, xylene, chloroform, dichloromethane, siloxanes and most hydrocarbons. The chosen solvent must not interfere with the curing mechanism and must have a suitable viscosity (less than 40 cp) and volatility to jet with an ink-jet printing nozzle. The solvent also dictates how the mixture behaves on the surface. In general solvents which dissolve silicone also swell silicone (Lee 2003). Swelling indicates that the solvent has an affinity towards the material and can penetrate the elastmer network. The solvent is absorbed into the material raising the concentration of the solvent in the substrate. Since solvents also have a strong affinity to themselves any droplets on the surface are essentially anchored on the silicone surface. This phenomenon is particularly useful because it enables us to print on PDMS without any surface treatment. One must also consider the interaction of the solvent with the other printed materials, the electrode and the sacrificial material. Solvents such as ethyl acetate, toluene, xylene, chloroform will more readily dissolve these materials. For example if the solvent remains present for a long time it may begin to redissolve the electrode material. If the electrode material dissolves it may weaken the breakdown strength of the printed dielectric layer leading to failure at lower voltages. Also strong solvents have the ability to redissolve polymers which may be used as release layers, as stiffening materials, or to make channels. For

this reason it is best if the solvents have a high volatility and rapidly evaporate. If the solvents evaporate on contact there is insufficient time to dissolve the materials it lands on. This can be achieved by choosing a high volatility solvent and heating the printing plate. In summary the solvent must be miscible, low viscosity, high volatility, and must not dissolve other printed materials. The last requirement narrows down the list to siloxanes and hydrocarbons. Siloxanes are essentially short PDMS chains the best option for solvating silicones. Furthermore, liquid hydrocarbons are cytotoxic and require more careful handling. For this reason siloxanes are also preferred.

5.4 Preparation of dielectric mixture

The dielectric mixture was prepared in a four step process. First the two parts (A and B) were combined in a planetary mixer (Thinky ARE-250). While the mixing is ongoing a conical test tube was prepared with a known amount of OS-2. When the mixing is finished the pre-mixed PDMS was poured into the silicone solvent. This step is conducted as soon as possible to cool down the mixed silicone and prevent the curing from progressing. The mixture was then vigorously shaken to disperse the silicone in the solvent. Following this the mixture is left to rest for at least 15 mins to allow for any particulates to settle. Finally the mixture was transferred to a printer vial by extracting the mixture from the top with a syringe.

1. Combine 10 g base: 1 g curing agent in a planetary mixer for 2 min at 2000 RPM and de-foam for a further 2 min at 2200 RPM

2. Place 16 g of Dowsil OS-2 Silicone Cleaner and Surface Prep Solvent (Dow) in conical test tube

3. Pour 4 g of the pre-mixed Sylgard 184 into the conical test tube

4. Close and shake vigorously for 1 min to combine

5. Keep the mixture still for at least 15 mins before transferring the mixture to a printing vial with a syringe

5.5 Jetting profile

To ink-jet print the dielectric mixture a 80 µm piezoelectric nozzle was used (MJ-AT-01-80). A large nozzle diameter was used to increase the amount of material which can be transferred in a single printing pass. Using a larger nozzle makes it possible to produce thick layers more quickly and reduces the probability of the nozzle getting clogged. Some adaptations were made to the standard jetting waveform shown in section 2.3. Silicone is a high molecular weight polymer and requires a lot of energy to eject. For this

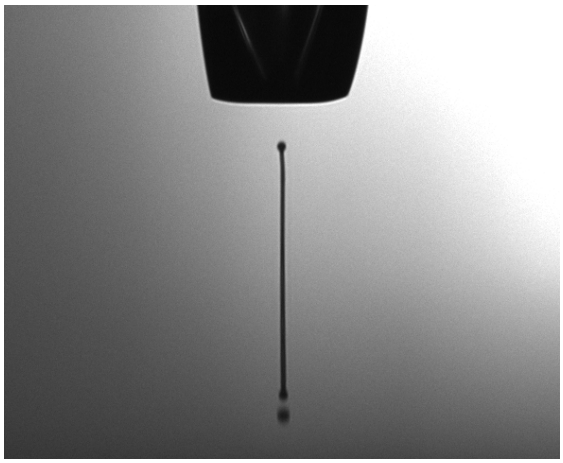

Figure 5.1 – Stroboscopic image of the dielectric mixture (Section 3.4) being ejected from a 80 µm piezo-electric nozzle. The droplet was generated using an adapted waveform with the jetting pramaters RT 5 µs, DT 27 µs, FT 10 µs, ET 41 µs, RT2 5 µs, DV 70 V, EV, -70 V, PP 80° C, PH 10° C. The backpressure was adjusted to level the miniscus when the jetting was off. The long tail of the generated droplet breaks up into smaller droplets but remain on the vertical path.

reason the maximum voltage 70V was used for the dwell voltage and the echo voltage. The dwell time was set to 27 µs to achieve maximum ejection velocity, and the echo time was set to 41 µs (1.5× dwell time). To reduce swelling and to more rapidly evaporate the solvent a printing plate temperature of 80° C is used. The print head was cooled to 10°C to reduce drying on the nozzle. An photograph of the jet is shown in figure ...explain tail

5.6 Patterning of dielectric layers

Patterning a dielectric material is challenging when printing on multiple materials. The materials printed in this work,silicones, electrodes and sacrificial materials all have vastly different surface and bulk properties.Surface properties determine how a material wets a surface and the bulk determines how solvents are absorbed. The areas where material properties change generally leads to unexpected flows of the freshly printed materials. These flows displace the printed materials from their intended position and lead to non-uniform printed layers. The concept is illustrated in Figure 5.2. When printing the dielectric mixture it is either deposited on silicone or on a region covered by an electrode or the sacrificial material. On the silicone the solvent is rapidly absorbed by the underlying silicone whereas On the covered region the solvent only has a single path to dissipate, evaporation. The different dissipation rates ultimately lead to different silicone concentrations. The concentration differences then lead to flows which redistribute the printed silicone. Unfortunately the flows occur at the transition regions where electrical fields and mechanical stresses are highest leading to dielectric breakdown or tearing of the film.

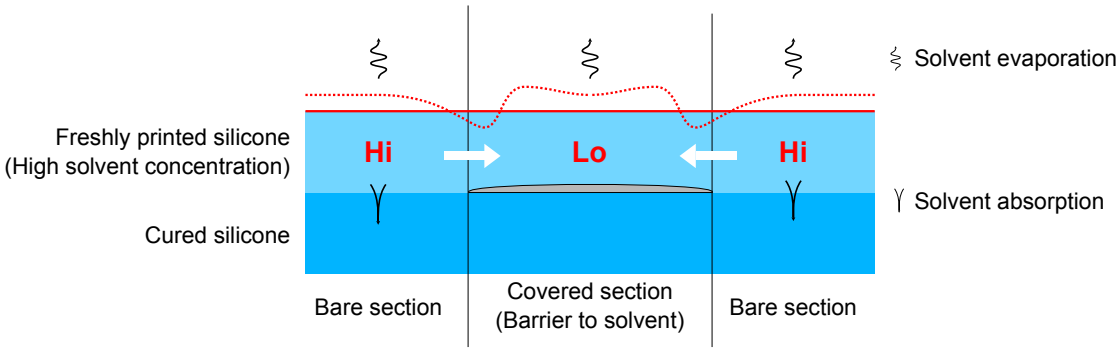

Figure 5.2 – A diagram showing how the dielectric mixture behaves when it is printed on a partially covered silicone surface. The dielectric mixture contains a solvent which has a high affinity to silicone. On the bare sections the solvent evaporates and is absorbed by the underlying silicone. On the covered region the solvent only evaporates. The concentration difference causes silicone to migrate creating a non-uniform dielectric layer.

Flows can be minimised by reducing the amount of solvent present on the printing plate. The extent of the flow is dependent on the viscosity of the mixture. Therefore by decreasing the amount of solvent, and thus increasing the viscosity, the flows can be reduced. The amount of solvent can be reduced by heating the printing plate and by reducing the rate of jetting materials. However reducing the rate of jetting increases the chance of nozzle clogging and thus a better approach is to deposit the material in multiple passes. Here the dielectric method is deposited in 5 passes (Figure 5.3). All the passes are printed with a droplet spacing of 50 µm and the printing plate temperature was set to 80° C. The line spacing was decreased on each pass starting with a line spacing of 500 µm, 500 µm again with offset, then 250 µm, 125 µm, and finally 62.5 µm. Each pass is offset to fill the valleys of the previous pass. The first layer is most affected by the material contrasts and thus has the biggest impact on the uniformity of the printed dielectric. Depositing less material at the start therefore minimises its impact. Subsequent passes are printed into solvent free silicone. Solvent free silicone has a higher viscosity. It is essentially like injecting low viscosity liquid into a paste. In addition the the later passes are no longer in directed contact with the underlying materials and are therefore less affected by material contrasts.

5.7 Uniformity of printed dielectric layer

In this section the uniformity of dielectric layers printed with the 5 pass method is investigated. Two samples were fabricated. One with a 1 mm electrode trace completely covered in silicone. From this the impact of material contrasts on the 5 pass method can be determined. The second sample was fabricated to determine the effect of holes on the local uniformity of the printed dielectric layer. A square hole of 1.6 mm was patterned directly on top of a 1 mm electrode trace. Holes like this can be used to make electrical

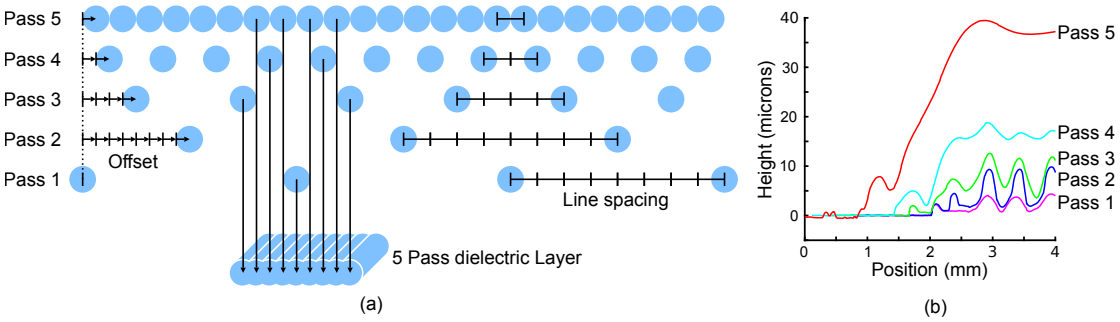

Figure 5.3 – The dielectric layer is printed in five passes to avoid flows due to material contrasts. Printing in multiple passes reduces the amount of solvent on the printing plate and thus reduces the mobility of the printed material (a) The first pass is printed with a line spacing of 500 µm and an offset of zero. The second pass is printed with a line spacing of 500 µm and an offset of 250 µm. The third pass is printed with a line spacing of 250 µm and an offset of 125 µm. The subsequent passes are printed with a lower line spacing and an offset to fill in any gaps. The end result is a uniform dielectric layer independent of the materials underneath (b) A cross section showing the surface profile of printed layers as more passes are added. Typically a membrane printed with the 5 pass method is around 30 µm.

vias between layers. The uniformity is around electrical vias is important because it determines how close parallel conductors can be placed.

Both samples were prepared in a similar manner. First a rigid glass substrate was prepared with a sheet of silicone on a rigid glass substrate to facilitate measurement. A float glass wafer with a thickness of 0.5 mm was used as the substrate. A cast 0.6 mm thick sheet of sylgard 184 was cut into 50 mm squares. This squares were placed onto the glass wafer and the bubbles trapped between the glass and the silicone square was removed by placing the assembly in a vacuum chamber. An electrode was then printed on to the silicone square. The electrode was printed with a droplet and line spacing of 100 µm with the printing plate at 80° C and the print head at 10° C. Following this the 5 pass method was used to pattern a dielectric layer over the top of the electrode trace. For one of the samples the dielectric was continuous, for the other the dielectric included 1.6 mm holes which were aligned with the underlying electrode.

The profile of the continuous dielectric is shown in Figure 5.4. The profile of the samples was measured with a laser confocal microscope (3D Laser Scanning Confocal Microscope VK-X1100, Keyence AG). The line of measurement is indicated in (b). The line of measurement is perpendicular to the printed electrode and also perpendicular printing direction of the dielectric layer. A plane fit was applied to the full measurement area to remove any tilt. The profile (c) shows that the dielectric layer has a height variation of maximum 1.34 µm. This corresponds to a height variation of less than 5%.

The profile of the dielectric layer with holes is shown in Figure 5.5. A plane fit was applied to the exposed electrode to remove any tilt of the sample. The lines of mea-

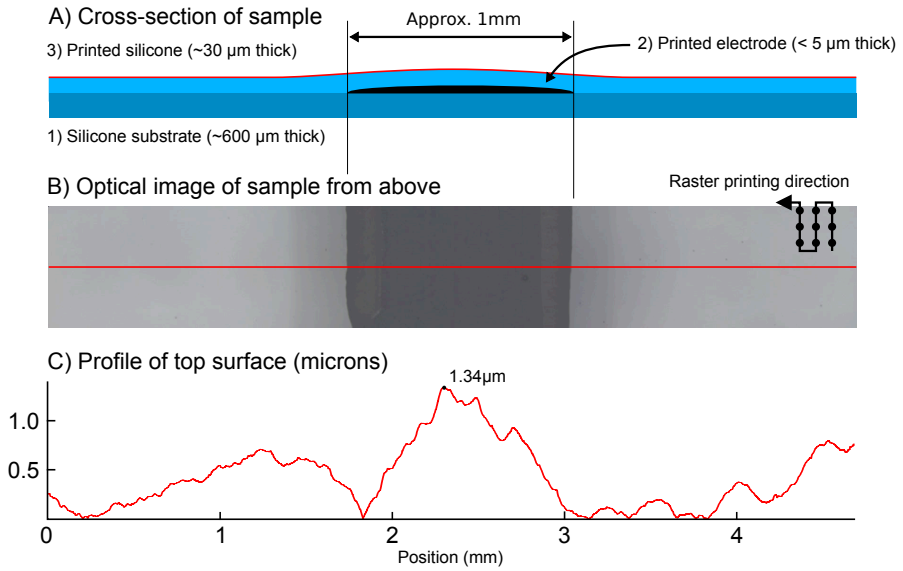

Figure 5.4 – Uniformity of dielectric material over a printed electrode. A test was conducted to determine the effect a 1 mm wide electrode has on the uniformity of a 5 pass printed dielectric layer. The surface profile shows that the dielectric layer varies by no more than 1.34 µm.

surement are indicated on the figure. The red line is parallel to the electrode and to the raster printing direction. The profile plot shows that the 5 pass dielectric layer is more than 30 µm thick and varies very little in the parallel direction. In addition the hole walls are relatively steep and reach a height of 30 µm in about 0.5 mm. The profile was also measured perpendicular to the electrode and the printing direction, indicated in blue. The profile plot shows that the 5 pass dielectric has an approximate thickness of 30 µm on the areas without an electrode. However the effect of the hole are much more pronounced. On the approaching side of the hole (tail of arrow = 0) the wall of the hole rises to 30 µm much more slowly than on the departing side (head of arrow ≈ 5 mm). On the approaching side the dielectric reaches a thickness of 30 µm in 1.5 mm and on the departing side in approximately 0.5 mm.

5.8 Breakdown strength of printed dielectric layers

In this section the breakdown strength of inkjet printed dielectric layers is investigated. First the breakdown strength of a dielectric layer printed with the 5-Pass method is measured. The breakdown strength of the 5-Pass method is then compared with dielectric membranes of fewer passes to determine the impact of printing multiple layers. Finally the breakdown strength of printed membranes is compared to the breakdown strength of cast membranes.

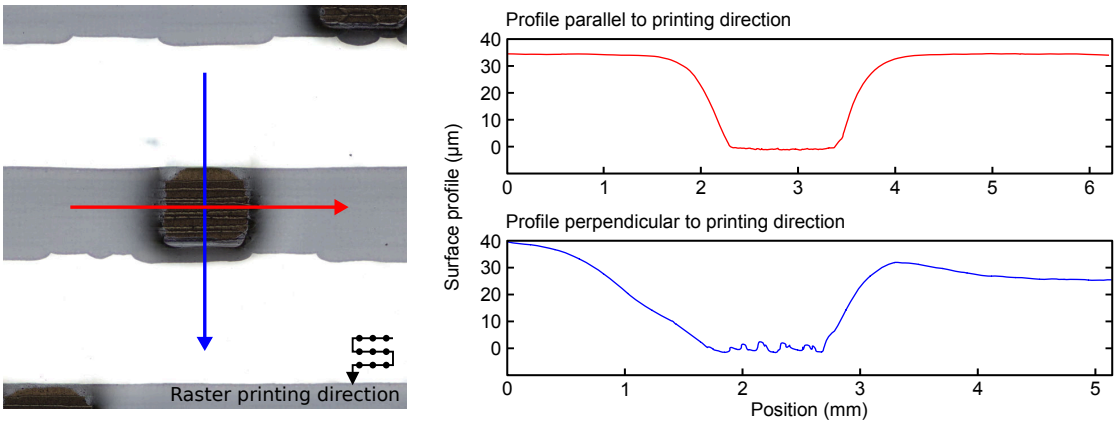

Figure 5.5 – The profile of a printed dielectric material around an electrical via. An electrical via is formed by leaving a hole in the printed dielectric layer so that an electrical cannection can be made to the electrode underneath. Here the profile is shown parralel to the printing direction (red) and perpendicular to the printing direction (blue)

5.8.1 Breakdown strength of 5-Pass dielectric layers

To measure the breakdown strength of a dielectric material two quantities must be measured: The voltage at breakdown and the thickness of the sample. Measuring the voltage is trivial; however, measuring the thickness is difficult. Typical DE electrodes are thick, not flat, and the structure is soft. These properties make it difficult to determine the thickness of the dielectric membrane where the breakdown has occurred. To overcome these problems breakdown testing is performed on a glass slide with gold sputtered electrodes. Gold electrodes are very thin (100's of nanometres thick) which means their thickness and surface roughness can be ignored. The glass slide provides a flat reference plane for measuring the thickness of the dielectric layers and also reduces the deformation of the dielectric layer when a voltage is applied. An additional benefit of using gold electrodes is that the location of breakdown is clearly visible. The gold electrodes ablate when breakdown occurs. The ablated regions are clearly visible under the microscope and may be used to detect the location of the breakdown and how many have occurred. This may be used to measure the thickness close to the breakdown site and reject samples where multiple breakdowns have occurred.

A photograph of a breakdown test sample is shown in Figure 5.6. The samples are fabricated on a 76 mm × 26 mm glass microscope slide. First the ground electrode is deposited in a gold sputtering machine (Jeol 1200 sputter coater). Following this a layer of silicone is printed directly on the glass slide using the 5-pass method described in section 5.6.Next, the silicone is cured in an oven at 100° C for 35 minutes. Finally the high voltage electrodes are deposited on top of the printed silicone layer. Laser cut PET shadow masks are used to pattern the gold electrodes.

The breakdown of each sample was detected manually. To record the breakdown a

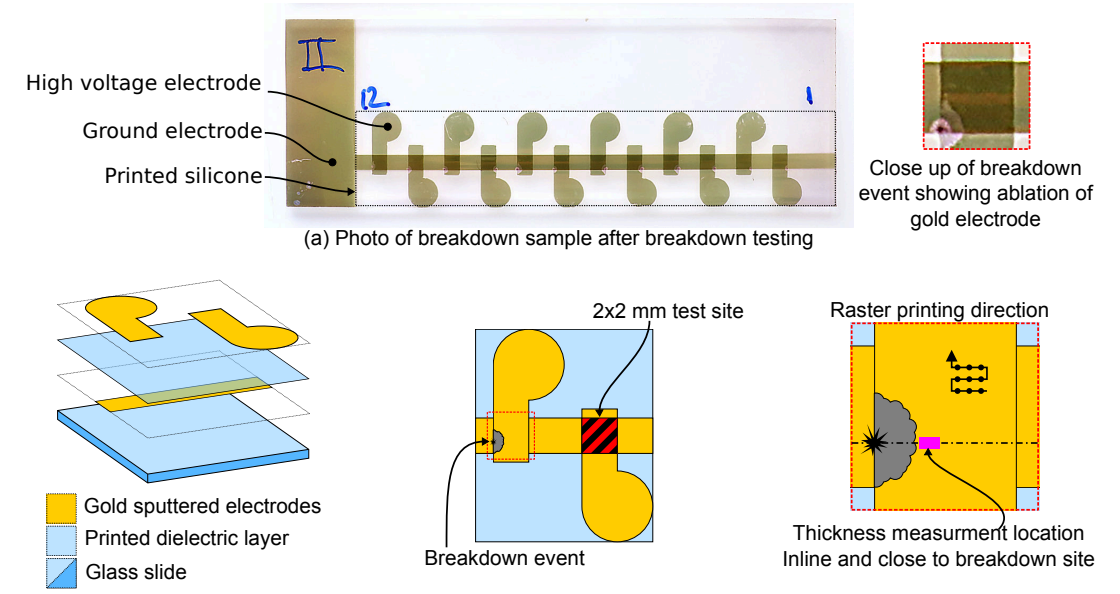

(a) Photo of breakdown sample after breakdown testing

(b) Cross section of breakdown sample

(c) Top view of breakdown sample

(d) Thickness measurement location

Figure 5.6 – A photograph and explanatory diagrams of the samples used for measuring the breakdown strength of the dielectric layer. The sample consists of a glass microscope slide, gold sputtered electrodes and a dielectric layer. The electrodes are patterned using a mask and the dielectric layer is printed directly on to the sample. The breakdown occurs in a 2 x 2 mm region where the gold electrodes overlap. The thickness of the dielectric material is measured using a confocal microscope on the same horizontal line as the breakdown crater.

high voltage power supply was used. An HVPS (See petapicovoltron.com or Schlatter et al. (2018)) was programmed to generate a stepped voltage ramp starting at 1 kV, increasing by 10 V every second. The voltage across the sample was monitored using an oscilloscope with a 100:1 attenuating voltage divider. When breakdown occurs a sudden drop in voltage can be observed on the oscilloscope. When a drop in voltage was observed the test was stopped and the previous voltage level was recorded. The same was repeated for the 12 test sites on the sample.

To measure the thickness of the printed dielectric layer a step is required. A razor blade was used to trim off the silicone close to the breakdown sites. A line was cut along the bottom edge of the ground electrode to create a clean edge. The razor blade was used horizontally to scrape off the silicone. The sample was coated with a thin layer of gold in a gold sputtering machine to make the surface opaque. This step is important to avoid measurement problems due to the translucent gold electrodes. This was achieved by placing the sample into a gold coater (Fine coater JFC 1200, Jeol Ltd.) to deposit approximately 30nm of gold across the whole surface. Finally the thickness, or step, was measured using an an optical profiler (Wyko NT1100, Veeco Instruments Inc.). The thickness was measured as close to the breakdown site as possible.

Two samples were fabricated and measured. The breakdown of the samples was measured from right to left. This is important so that the ground electrode is not damaged for subsequent breakdown measurements. It is also important to move the ground connection after every breakdown test. When a breakdown occurs the gold electrodes are ablated at the contact sites. This produces an air gap by the ground connection which may grow in size with every breakdown. At a certain point the measured breakdown will be dominated by the air gap and give false measurements.

The results of the two breakdown samples are shown in Figure 5.7. The data is represented with a box plot. The central mark indicates the median, and the bottom and top edges of the box indicate the 25th and 75th percentiles, respectively. The whiskers extend to the most extreme data points. The first sample had mechanically damaged breakdown sites which were omitted from the results. Hence the plot only shows 8 data points for sample 1. The median breakdown field of sample 1 was 64 V/µm and for sample 2 was 71 V/µm. The median of each group overlaps with the interquartile range of the other showing that groups are similar i.e. the same material and the same process.

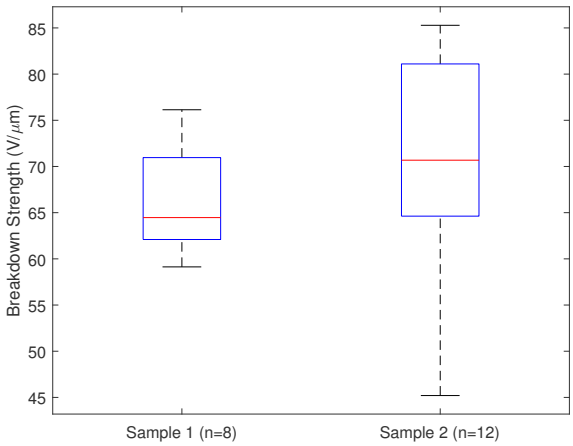

Figure 5.7 – Boxplot of breakdown strength. Sample 1 and Sample 2 were prepared in the same way.

The same results may be plotted on a 2 parameter Weibull plot (Figure 5.8). The Weibull plot may be used to determine the probability of failure at a given field. The 2 parameter Weibull distribution is shown in Equation 5.1 which gives the cumulative fraction of samples which will fail at a given electric field E, also known as the unreliability function. The unreliability of the samples was estimated with Bernard's approximation or Median Ranks (Equation 5.2).

$$F(E) = 1 - e^{-\left(\frac{E}{\eta}\right)^{\beta}} \tag{5.1}$$

E = Electric field in V/m
η = Characteristic life or scale parameter
β = slope or shape parameter

$$MR = \frac{i - 0.3}{N + 0.4} \tag{5.2}$$

i = rank number or index of ordered samples
N = is the sample size

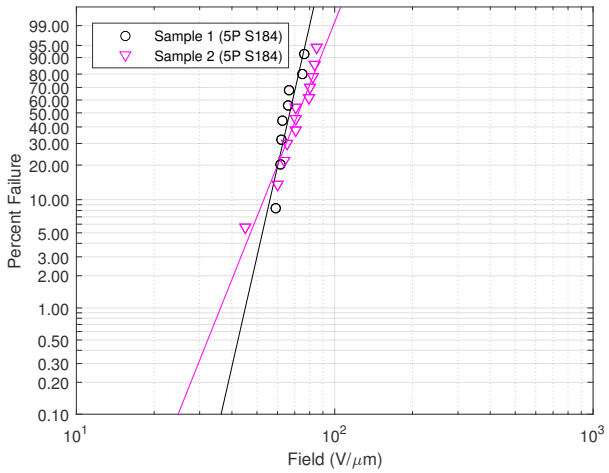

Figure 5.8 – Probability of failure of membranes printed with the 5-Pass method. Sample 1 and Sample 2 were prepared in the same way. Average thickness of samples 31 µm.

Sample 1 was calculated to have a characteristic breakdown strength of 69 V/µm and a weibull slope of 10.7. Sample 2 was calculated to have a characteristic breakdown strength of 77 V/µm and a Weibull slope of 6.1. The similar characteristic life and slope show that these two samples are very similar.

5.8.2 Impact of passes on breakdown strength

The data in the previous section gives the breakdown strength dielectric layers printed with the 5-pass method. However, it is not clear from the data if printing multiple passes has an impact on the dielectric strength of a printed dielectric layer. Is it better to print a dielectric layer in a single pass or in multiple passes? To answer this question some additional data is presented in this section. A dataset containing dielectric breakdown strengths for 1 Pass and 2 pass printed dielectrics is added to the Weibull plot in Figure 5.8.

The samples were prepared with the same protocol as presented in section 5.8.1. The only difference between the samples were the printing parameters. The silicone layer was printed with a different orientation, and the line pacing was varied along the sample (Figure 5.9). The sample was divided into 6 regions with different line spacings. The line spacing was increased from 200 µm to 450 µm in 50 µm increments. The drop spacing was fixed at 50 µm. The 1 Pass sample was printed in a single pass. The 2 pass sample was printed in two passes without curing in between the printed layers.

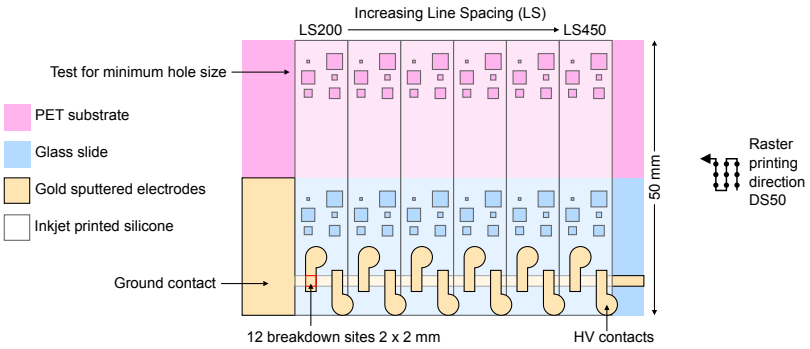

Figure 5.9 – Breakdown samples on glass slide with gold sputtered electrodes. Silicone is printed directly on glass slide at right angles to test different printing parameters. The line spacing was increased from 200 µm to 450 µm in 50 µm increments

The thickness of the printed samples is shown in Figure 5.10. Since the printed membranes had a corrugated profile the minimum thickness of the dielectric layer was measured as close to the breakdown site as possible. The 1 Pass dielectric layers had a mean thickness of 3 µm. The 2 Pass dielectric layers had a mean thickness of 6 µm. This is in contrast to the 5 Pass dielectric layers in the previous section which had a mean thickness of 31 µm.

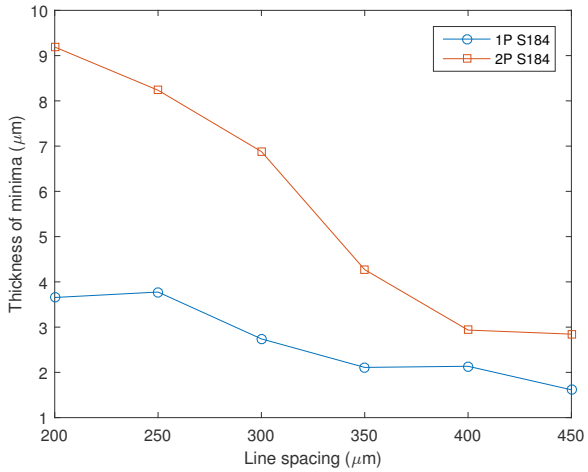

Figure 5.10 – Thickness of 1 pass (1P) and 2 pass (2P) inkjet printed dielectric layers.

The 1 pass and 2 pass samples are plotted alongside the 5 Pass samples in Figure 5.11. The single pass dielectric was calculated to have a characteristic breakdown strength of 134 V/µm and a Weibull slope of 2.6 (shape parameter, beta). The 2 pass dielectric sample was calculated to have a characteristic breakdown strength of 72 V/µm and a Weibull slope of 4.0.

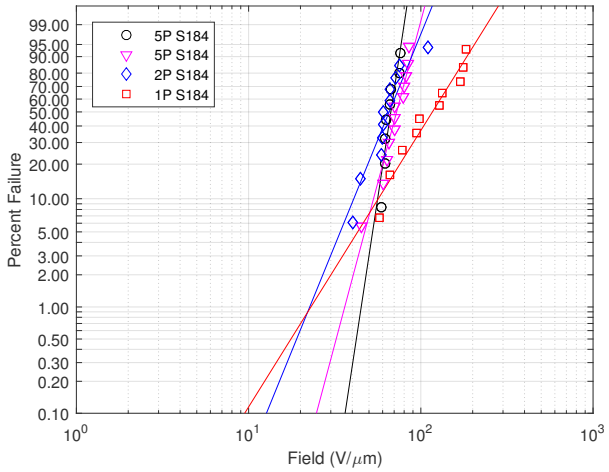

Figure 5.11 – Probability of failure of membranes printed in 5 passes (5P), 2 passes (2P) and 1 pass (1P).

Figure 5.11 shows that the slope increases as the number of passes increases. The increasing slope shows that the spread of the data reduces as the number of layers and thickness of the printed dielectric increase. This suggests that more passes are better because the breakdown strength for low percentage failures is higher and less variable.

5.8.3 Impact of printing on breakdown strength

In this section the impact of different fabrication techniques on the dielectric breakdown strength is investigated. Ink-jet printing is a digital fabrication process where films are assembled drop by drop. It was hypothesised that this would lead to non-uniform and low quality membranes. In contrast, casting produces membranes in a more continuous manner. A doctor blade moves along a flat surface at constant velocity to produce flat and uniform membranes. Here the breakdown strength of a UV cure silicone, Momentive M225-1, is compared when thin films are produced either by casting or by ink-jet printing.

The dielectric films were prepared on a low roughness polyester foil (Melinex ST-506, DuPont Teijin Films). The polyester film was coated with a soluble release layer to aid removal of the thin and fragile dielectric films. A film applicator (Zehntner ZAA 2300, Zehntner GmbH) with a threaded rod (Zehntner ACC378.022, Zehntner GmbH) was

used to cast the soluble release layer at a speed of 8 mm/s. For the cast membranes a 20 wt% mixture of PAA (PolyAcrylicAcid 25% soln. in water MW 50,000, Chemie Brunschwig) in isopropanol was used. For the printed membranes a 6 wt% mixture of PVP (PolyVinylPyrrolidone K90, Fluka) in isopropanol was used.

The silicone was prepared, cast and printed as follows. The silicone was measured out in a base to initiator ratio of 4 g:2 g and combined in a planetary mixer (Thinky ARE 250, Thinky U.S.A. Inc.). Half of this mixture (3 g) was diluted with 16 g of OS-2 (Silicone cleaner and surface prep solvent from Dow) in a conical test tube. The mixture was poured on to the PET substrate and a universal applicator (Zua 2000.220, Zehntner GmbH) with a gap height of 50 µm at 2 mm/s was used to cast a thin film. The printed films were prepared by decanting the mixture and transferring it with a syringe to a printer vial. No filters were used. The films were printed on a Jetlab4 XL printer (MicroFab Technologies, Inc.) with a 80 µm piezo-electric nozzle. The film was printed at room temperature with a droplet and line spacing of 150 µm. The cast and the printed samples were cured for 12 min in a 60 W, 365 nm peak-wavelength Pro-Ma UV Exposure Unit.

Unlike in the previous sections, the membranes here were pre-stretched. To pre-stretch the films the membranes were trimmed using scissors into an octagon shape. Cutting the membranes gives a clean edge which is less likely to tear during stretching. The process to pre-stretch the membranes was already covered in Section 2.1.3 and Figure 2.3. An adhesive frame is attached to the silicone membrane and placed in a vat of boiling water to remove the polyester substrate. The membranes were pre-stretched by a factor of 1.44 on an equi-biaxial stretch rig. Once pre-stretched a permanent frame is attached to hold on to the membrane. The average thickness of the cast membranes and the printed membranes was 1.9 µm and 1.2 µm, respectively.

Breakdown samples with gold electrodes were prepared according to the following protocol. Scotch tape was used to mask a glass slide. A razor blade was used to remove a 1 mm wide strip down the centre of the glass slide. A 1 cm wide strip was also removed on one end of the glass slide for making an electrical connection. The masked glass slide was coated with 30 nm of gold with a gold sputtering machine. Removing the tape leaves a thin well defined gold electrode. The frame holding the pre-stretched silicone frame was placed on to the glass slide. By pressing firmly on one end of the frame the silicone makes contact with the glass slide and wicks on to the surface. Two masks were produced for the second gold sputtering step. The first mask covers the outside of the sample. The second mask is placed directly on the pre-stretched silicone to pattern the high voltage electrodes. The sample is placed into the gold sputtering machine a second time to deposit a 30 nm thick layer of gold. The end result is a breakdown sample with 6 breakdown sites with a 1 mm^2 breakdown region.

The breakdown event may either be detected when the supply voltage drops or when

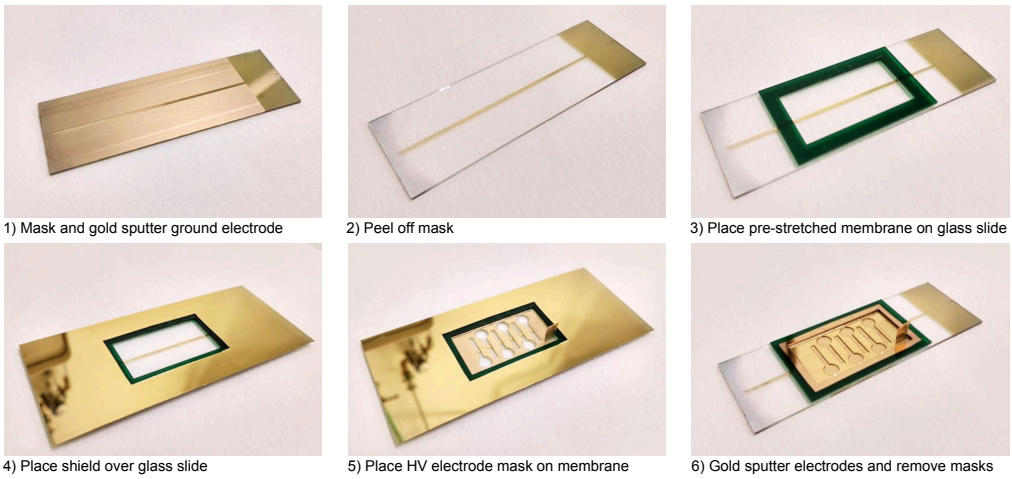

Figure 5.12 – Fabrication process of breakdown samples for pre-stretched membranes

a current spike is detected. For these experiments the later approach was used. The sample is placed in series with a 1 ohm resistor and attached to a high voltage power supply. Since the membranes in this experiment were thin (<2 µm), the voltage to achieve breakdown is below 250 V. A programmable 250 V high voltage power supply (See petapicovoltron.com or Schlatter et al. (2018)) was used to apply a stepped voltage ramp and the voltages were measured with an oscilloscope (1 GHz Mixed Signal Oscilloscope MSO9104A, Keysight Technologies). A positive edge trigger of 50 mV was used to capture the breakdown event when the current through the capacitor exceeded 50 mA. The voltage across the sample and the current through the sample were measured simultaneously. A typical breakdown event is shown in Figure 5.13. The breakdown event is very short and hence an oscilloscope with high rise time is required.

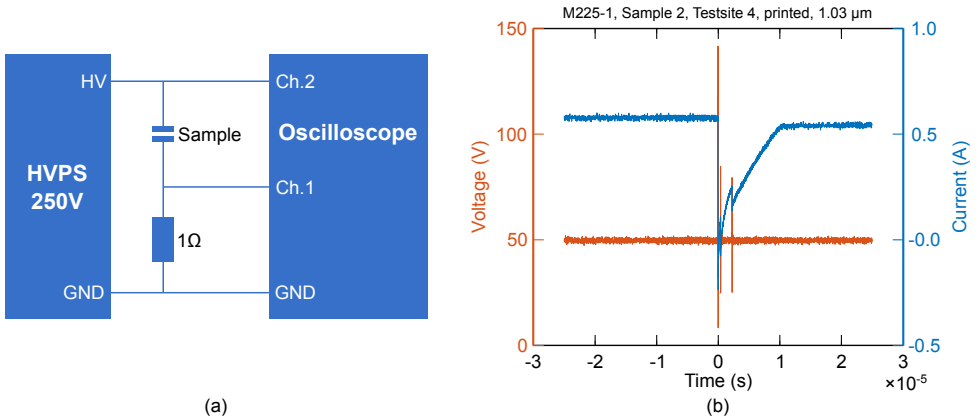

Figure 5.13 – (a) Set-up used to measure fast breakdown events. (b) Voltage and current during a typical breakdown event.

The thickness of the samples was measured with an optical profiler. The thickness was measured by creating a step (Figure 5.14). First the membrane was cut on the inside

perimeter of the frame to remove it. A piece of scotch was then applied on top of the membrane. The scotch was placed as close as possible to the breakdown sites. With a scalpel the membrane was cut using the edge of the scotch tape as a guide. The scotch tape was then peeled off to remove part of the membrane. The thickness was measured with an optical profiler (Wyko NT1100, Veeco Instruments Inc.) in three locations in between the test-sites. The pre-stretched membranes are very uniform hence it is sufficient to measure in only three locations.

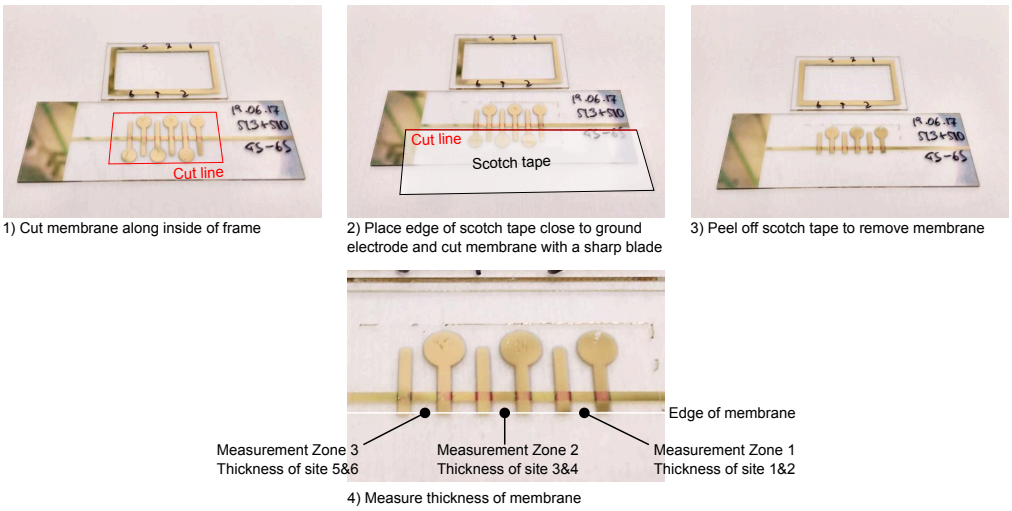

Figure 5.14 – Procedure to measure thickness of pre-stretched membranes on breakdown samples

In total 29 measurements were obtained for cast membranes and 30 measurements were obtained for printed membranes. The results have been plotted in Figure 5.15 with a notched box plot. The red line represents the median. The bottom and the top of the box represent the 25th and 75th percentile respectively. The whiskers represent the minimum and maximum values. The notches represent a 95% confidence interval of the median.

The same data is also presented in Figure 5.16 on a Weibull plot. The cast membranes have calculated characteristic breakdown strength of 107 V/µm and a Weibull slope of 5.9. The printed membranes have a calculated characteristic breakdown strength of 144 V/µm and a Weibull slope of 9.1.

Both plots suggest that the fabrication process has an impact on dielectric strength. The notches on the box plot (95% confidence) do not overlap which suggests that there is a significant difference between the median breakdown strength of cast and printed dielectric layers. The Weibull plot also suggests this. The Weibull plots have similar slopes suggesting that the materials have a similar failure rate. However, the characteristic breakdown strength of printed membranes is 37 V/µm higher than the breakdown strength of cast membranes. This suggests that printing may produce higher quality membranes than casting. To confirm this result and draw conclusions for other silicones additional experiments are required.

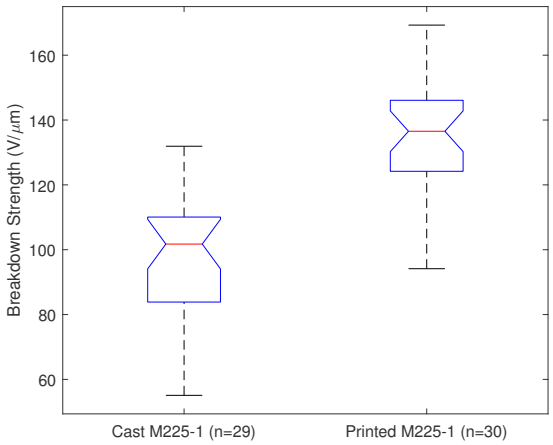

Figure 5.15 – Breakdown strength of pre-stretched membranes fabricated by ink-jet printing and casting. Note the use of a different silicone, M225-1.

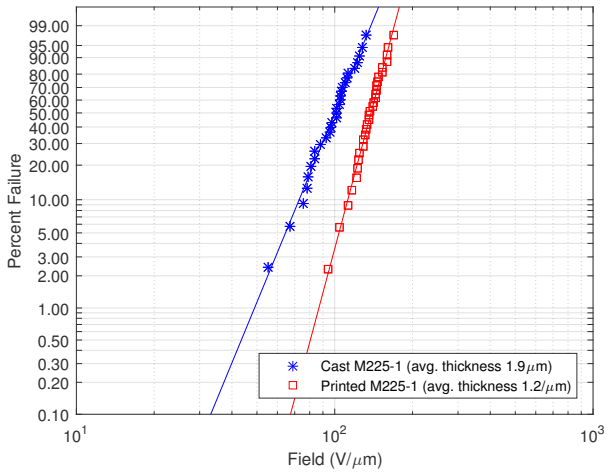

Figure 5.16 – Probability of failure of cast and printed membranes.

5.9 Conclusion

In this chapter a process to print thin and uniform dielectric membranes was presented. A two part silicone mixture was prepared by pre-mixing Sylgard 184 and adding a siloxane solvent to reduce the viscosity. A 5-Pass printing method was developed to print uniform layers of on top electrodes and sacrificial materials. The method produces 30 µm thick printed membranes. When printed on electrode materials the profile of the printed layers was shown to have a height variation of less than 5%. The electrical breakdown strength of the printed dielectric was also measured. Showing that the printed membranes have a breakdown strength of approximately 70 V/µm. The processes developed here may be used pattern thin silicone layers on electrode and dielectric materials. In addition it was shown that ink-jet printing may be used to print holes. Holes enable electrical and fluid vias making it possible to print multi layer soft machines.

Part II

Printed soft machines to demonstrate benefits of printing

6 Ink-jet printed soft peristaltic pump

6.1 Summary

Lab-on-a-chip devices are portable automated systems to perform analyses more easily and more cheaply. The flow of liquids in Lab-on-a-chip devices is typically controlled with external pumps. External pumps are bulky and increase the amount of regents and sample volumes required for an analysis. Integrating soft actuators into a fluidic chip eliminates the need of a permanently attached external pump. A peristaltic pumping method using integrated HASEL actuators is presented in this chapter. The peristaltic pump uses ink-jet printing to fabricate a multi-layer, multi-transducer structure consisting of channels and integrated HASEL actuators. The design enables pumping of aqueous liquids including electrolytes. The flow-rate of the pump was measured to validate the pumping mechanism. The maximum flow-rate of the pump was 0.15 µL/s at 1 Hz operating frequency. The process presented here may be used to create more complex fluidic systems with many integrated pumps and valves.

6.2 Introduction

Manipulating small quantities of fluids is very important in Lab on a chip devices. The concept behind lab on a chip devices is to take the processes normally conducted in a laboratory and perform them on a small chip, typically in the centimetre scale. Shrinking down the size of the equipment makes the lab portable so that an analysis conducted anywhere. Reducing the size of the laboratory also reduces the amount of reagents and sample volumes which are required. For example a pin prick to draw a droplet of blood may be sufficient instead of requiring a nurse to draw millilitres of blood from a patient. Reactions also occur more rapidly at the micro-scale because the diffusion distances are smaller, a higher surface to volume ratio increases reaction times, and the small fluid volumes reduces heating times. The faster reaction times can reduce the time required to get a result. Automation also helps to accelerate the time required to get a result.

Lab-on-a-chip devices are self contained devices where the sample volume is injected and the system does the rest. The ultimate goal of lab on a chip devices is to be able to do an analysis anywhere and by anyone.

Unfortunately after many years of research and development lab-on-a-chip devices are not in widespread use because there isn't a convenient way to fabricate them. Originally the processes developed for the semiconductor industry were used to create fluidic chips. Clean room processes like photo-lithography enable high resolution devices with integrated transducers. The main drawback of clean room processes is the long development times and the cost of manufacturing small production runs. In addition wafer space is expensive, thus making the cost of large area devices exorbitantly high. Alternative fabrication processes have been explored including lamination, moulding, and 3D printing. However most of the effort have been on producing small fluidic chips and the integration of the fluid control and sensing is often neglected. Consequently lab on-a-chip devices still require many external pieces of lab equipment. A number of publications have shown how conventional components can be combined with a soft fluidic chip. However, the miniaturisation of these components is limited and remains bulky when many transducers are required. At present there is no widely accepted fabrication technique which allows for the rapid development of lab-on-a-chip devices with integrated transducers.

Presently the most common way to control the flow of liquids is with an external flow controllers. These are used to pump liquids through the device and to control the flow with pneumatic valves. Pressure sources like this a bulky, expensive and also increase the amount of liquid required for analyses - due to the tubing between the chip and the external equipment. There are alternative ways to pump liquids in lab-on-a-chip devices including electric field driven pumping, hand powered, elastic potential energy, capillary flows, gravity fed, surface tension driven, and osmotic pressure. Electric field driven pumps are an elegant way to move liquid however the electrodes are in direct contact with the fluid. Danger of cell lysis and electrolysis may create create problems (Byun 2014). Hand powered devices are a simple low cost way to provide pressure but may produce false results if the test is not conducted properly. The remaining technologies are all passive and the cannot easily be controlled.

Based on the work in this field it is clear that a better solution is required to bring us one step closer to a compact and portable lab-on-a-chip. The fabrication techniques used today focus either on the fabrication of high resolution channels or on the miniaturisation of standard equipment. Developing the fluidic chip and the transducers seperately results in a system which is simply a scaled down version of laboratory equipment and is clearly limited with how small it can become. A better approach would be to develop a fabrication process capable of printing the fluidic network and integrating transducers directly into the same structure i.e. everything must be silicone based.

Here these problems are addressed by using an integrated approach. Ink-jet printing is used to print both the fluidic system and the HASEL transducers on the same machine. Ink-jet printing is suitable for printing lab-on-a-chip devices because it is significantly cheaper than clean room based processes, can be automated and used by low skilled workers, is suitable for low production runs, and the resolution can produce large area devices with a resolution much greater than most conventional 3D printers. HASEL transducers are well suited for lab-on-a-chip devices because they work directly with fluids, are scalable, can be fabricated from silicone, and can function as actuators and sensors. The integrated approach enables lab-on-a-chip devices with more densely and neatly integrated transducers

In this chapter a peristaltic pump is fabricated to demonstrate the potential of the integrated printing approach. The pump consists of a multilayer structure with two overlapping channels. The channel on top contains a dielectric fluid which is pressurised using three HASEL actuators. The channel on the bottom can contain any aqueous liquid. When the top channel is pressurised using the HASEL actuators the bottom channel can be compressed. By actuating the HASEL actuators in a peristaltic fashion the aqueous liquid in the bottom channel can be pumped around a fluidic circuit. The pump shows that it is possible to control the flow of liquids in a soft fluidic chip. The same idea could be used to make valves to form a more complex device where liquids are stored, pumped, and mixed in sequence to perform an analysis. The solution presented here is compact, fully integrated, silent in operation, electrically powered, and scalable.

6.3 Peristaltic pumping

Peristalsis is defined as the wave of muscle contraction that is used by the body to propel liquids and food down the oesophagus or along the intestine. In the lab a similar technique is used to pump liquids inside of tubes. A peristaltic pump, or roller pump, is shown in figure 6.1. Liquid is moved by pushing rollers along a tube

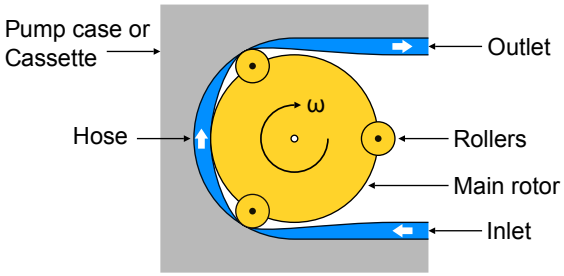

Figure 6.1 – Peristaltic pumping principle. The main rotor with three rollers rotates at a constant speet. The tube carrying the liquid passes through a cassette which holds the tube in a circular track. The rollers compress the tube against the track and force the fluid along the tube.

Peristaltic pumps are used in the laboratory for chemical and medical experiments

because they have some unique properties. In peristaltic pumps the fluid is confined to the tubing and is not exposed to the pump components. Depending on the liquids the pumping components may corrode, contain lubricants with undesirable chemicals, create metal filings due to wear, or may be soiled by residue from other fluids. Peristaltic pumps are sterile and are well suited for medical applications. In addition peristaltic pumps are more gentle than dynamic pumps. Peristaltic pumps subject the fluid to much lower shear forces than other, high speed, pumping mechanisms. The reduced shear forces make these type of pumps ideal for working with cells which are highly sensitive to shear forces. Furthermore peristaltic pumps are bidirectional and prevent back flow. This makes peristaltic pumping useful in dosing applications. The number of rotations of the main rotor directly determine the quantity of liquid which has been pumped.

There are also some disadvantages to peristaltic pumping. The flow is pulsed. Peristaltic pumping are not suitable for applications where constant flow is required. Another disadvantage of peristaltic pumps is that they require long tubes. These tubes must be filled with liquid which may be problematic when only small sample volumes are available.

To overcome the issue of having long external pipes, peristaltic pumps have been implemented in fluidic chips using a coupling fluid (Wu 2008 and Unger 2000). The concept is illustrated in figure 6.2. The pump consists of four channels. The channel underneath contains the medium which is to be pumped around the chip. This channel is relatively short and is confined to the fluidic ship. The three channels which cross over the top contain the coupling fluid. The lower and upper channels are separated by a thin deformable membrane which separates the channels. When the pressure in the top channels is increased it compresses the channel underneath. By pressurising the three channels on top in sequence it is possible to propel the liquid in the channel underneath. The flow of this kind of pump is still pulsed, but the tube containing the medium is now considerably shorter.

A coupling fluid based peristaltic pump moves liquids in a six step sequence. The sequence is illustrated in figure 6.3. The sequence begins with the intake stroke where channel B is pressured followed closely by channel C. This part of the sequence is referred to as the intake stroke because the space under channel A is filled with the medium. During the hold stroke, channel B is de-pressurised followed closely by the pressurisation of channel A. In the final part of the sequence channel C is de-pressurised followed closely by the pressurisation of channel B. During the final part of the sequence the medium is expelled from the pump and the cycle begins again. During each step of the sequence one of the channels remains pressurised so that the liquid cannot flow backwards. During each cycle the amount of liquid contained underneath one of the coupling channels is expelled from the pump. The flow-rate can therefore be estimated if the approximate shape of the channel is known.

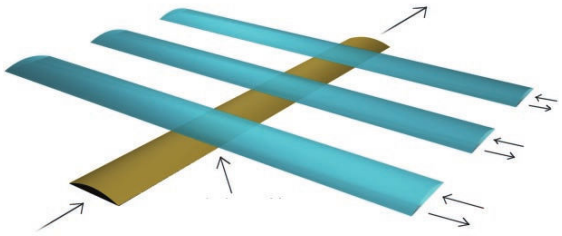

Figure 6.2 – An elastomeric peristaltic pump for (Unger 2000). The main channel (in brown) contains the liquid to be pumped and the three channels (in blue) contain air. The channels are separated by a thin membrane which deflects when the pressure in the air channels is increased. When the pressure in the air channels is higher than the main channel the membrane deflects closing the main channel. Each overlapping channel acts like a valve, but together the valves can pump fluid. By pressurising the three channels with the sequence 101, 100, 110, 010, 011, 001 it is possible to pump the liquid in the main channel. 0 and 1 indicate "valve open" and "valve closed".

The peristaltic pump with a coupling fluid addresses the problem of having to have long external pipes, but it does not reduce the equipment needed to operate the device. A pressure source is with at least three programmable channels is required. It should be noted that this is the requirement for a single pump. When a complex fluidic chip, consisting of multiple pumps and many valves, the number of channels and the number of fluid connections grows rapidly. A better solution would be to integrate the pressure directly into the fluidic chip.

6.4 ink-jet printed peristaltic pump

6.4.1 Design of ink-jet printed peristaltic pump

In this section the design of an integrated peristaltic pump is discussed. The pumping principle is very similar to the pumps presented by (Unger et al., 2000) and (Wu et al., 2008). The integrated pump also uses overlapping channels to pump fluids. However, on-board HASEL actuators are used to pressurise the coupling fluid. This approach reduces the length of the medium channel and thus reduces the amount of reagents required. Another benefit of using a coupling fluid is that the HASEL actuators can be can be distanced from the medium channel. It is not possible to directly pump the medium fluid with HASEL actuators. Aqueous liquids containing salts weaken the silicone based dielectric layers. The weakened dielectric layers lead to rapid breakdown. In addition the fluid of a HASEL actuator must be a dielectric liquid. By using a coupling fluid it is possible to separate the actuator from the medium channel. The pump is therefore able to pump any liquid which can be contained within the silicone channels. Furthermore, by distancing the actuators and using a transparent coupling fluids the aqueous channel remains completely transparent.

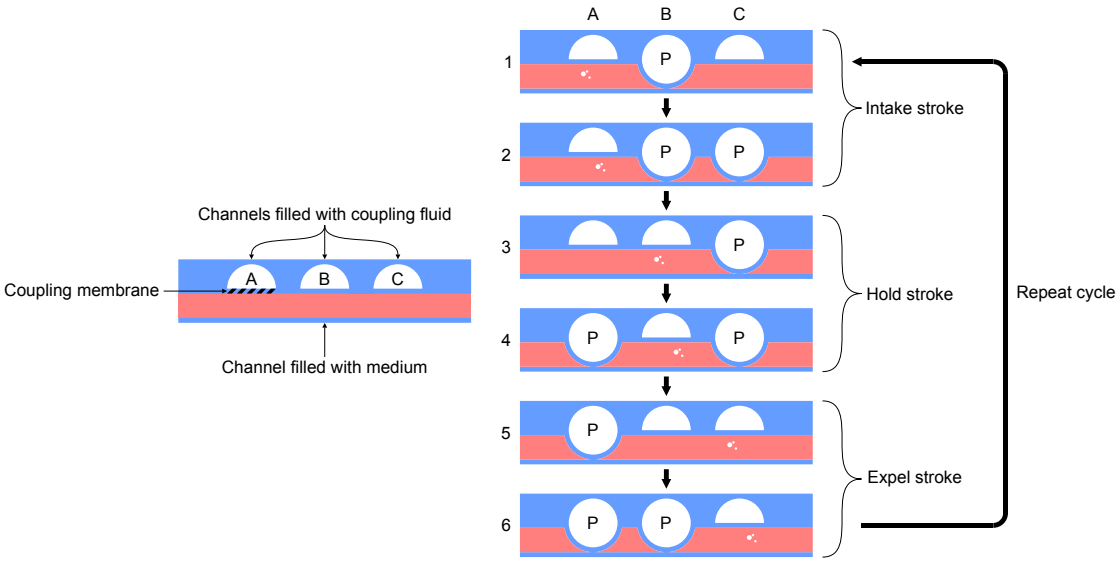

Figure 6.3 – A diagram to show how lquids can be pumped with a coupling fluid and overlapping channels (a) A minimum of three air channels are required to pump liquids. The medium channel and the air channels are separated by a thin membrane which is deflects when the air channels are pressurised (b) A six step sequence to pump fluid.

The design of the ink-jet printed peristaltic pump is shown in Figure 6.4. The peristaltic pump is fabricated by printing a total of seven layers on to a thick silicone base (Figure 6.4c) . The square silicone base is 50 mm wide and is large enough to pattern two peristaltic pumps side by side (Figure 6.41). After fabricating the pump it is divided into two by cutting along the line of symmetry in the middle of the pump (Figure 6.4a). The exploded view of the printed pump is shown in Figure 6.4b. The light blue layers represent printed silicone. The method to print the silicone layers using thermally cured Sylgard 184 (S184) was discussed in chapter 5. The black layers represent printed carbon black (CB) based electrodes. The method to print the electrodes was discussed in chapter 3. And the coloured layers (in pink and yellow) represent printed sacrificial layers consisting primarily of Ethyl Cellulose (EC). The method to print the sacrificial channels was discussed in chapter 4. More details regarding the design decisions of the the thick silicone base, the printed sacrificial channels, and the electrodes are discussed in the following three paragraphs.

A thick base layer is used to provide a firm surface for the channels to push against. It is possible to also print this base layer, but a fully printed structure either takes a significant amount of time to print or is extremely thin. Early versions of the ink-jet printed pump were constructed by printing a 30 µm base layer. However a thin pump is significantly more complicated by design. When a thin base layer is used it is not possible to compress a channel with two crossing over channels. The whole structure is compliant simply deforms. The only way to compress a channel is to make the coupling channel fully envelope the medium channel. These enveloped channels, cuffs, can be

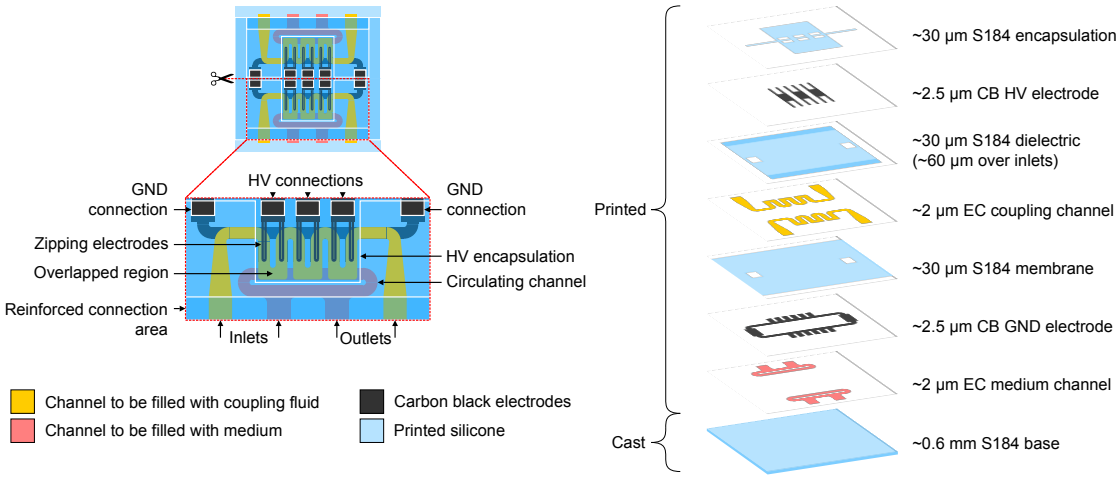

Figure 6.4 – Design of an ink-jet printed peristaltic pump with integrated HASEL actuators (a) Two pumps are printed simultaneously on 50 mm × 50 mm silicone base. A enlarged view shows a single pump with various elements highlighted. The pump has two channels: a circular channel in pink which may be filled with medium or any other aqueous solution, and a winding channel in yellow which is filled dielectric fluid. The channel with the dielectric liquid is printed on top of the channel containing the medium. This arrangement allows the zipping electrodes to force dielectric liquid into the overlapped channel and compress the medium channel (b) An exploded view of the pump with a description of each layer. Seven out of the eight layers are ink-jet printed.

constructed by printing a nine layer structure with fluid vias (Figure 6.5). This approach was abandoned because the nine layer device is more complicated, takes longer to print, and is more prone to channel rupture. In addition the device was extremely thin and requires a rigid frame to be handled. A device with a rigid frame can hardly be defined as being soft and stretchable, for this reason a thick substrate was used instead. The thick substrate is flatter and has better optical transparency, which is important for lab-on-a-chip devices.

The ink-jet printed pump has two channels (Figure 6.4. The medium channel which is filled with an aqueous fluid after fabrication (pink) and the coupling channel which is filled with a dielectric fluid after fabrication (yellow). The medium channel is printed first, followed by the coupling channel. The channels are printed in this order so that the coupling channel is on top of the medium channel. On the overlapped regions the medium channel and the coupling channel are separated by a thin 30 µm dielectric membrane. When the coupling channel is pressurised it causes the membrane to deflect. If the pressure is sufficient it can can completely constrict the medium channel.

The coupling channel is a continuous serpentine channel which overlaps with the medium channel in three locations. The pump was designed with a single continuous channel so that fewer fluid connections have to be made. In addition having a single channel means that the dielectric fluid of all the HASEL actuators are at the same

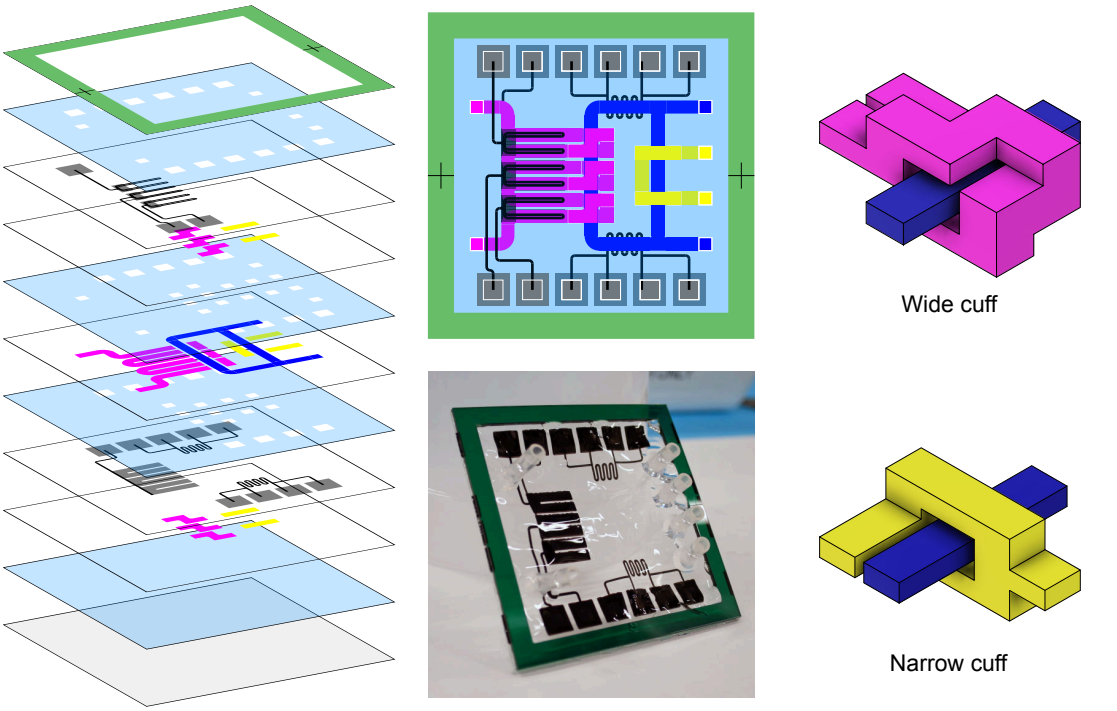

Figure 6.5 – An earlier design of the pump without a thick silicone substrate (a) A eploded view showing 9 printed layers, a grey PET substrate, and a 1 mm thick PMMA frame (b) A diagram and a photograph of the printed pump. The diagram shows the layout of the printed electrodes and the channels. The pink channel is filled with dielectric fluid and the blue channel is filled with an aqueous liquid. The yellow channel is can be filled with air to clamp the aqueous channel. The photo shows how the pump is wrinkled when the PET substrate is removed. The wrinkles are due to residual stresses in the printed structure (c) The cuffs used to clamp the aqueous channel. The wide cuff can displace more fluid when compressed than the narrow cuff.

pressure. This is important if the actuators are to generated the same pressure at a given voltage.

The medium channel was designed as a circulating loop. A circulating loop was incorporated into the pump so that it can be filled with the medium and then closed off. The medium can then be circulated around the chip indefinitely. The loop also makes it possible to characterise the flow-rate of the pump internally with minimum channel impedance. Although it is possible to block a small segment of the loop and force the medium through an external circuit. This was eventually used to measure the flow-rate of the pump with an external flow sensor.

Both of the channels have a width of 2 mm when printed. The width increases to 4 mm towards the edge of the pump. The increase in width is to accommodate the silicone tubing used to make fluid connections (more information on making fluid connections can be found in section 4.7). The area where the connections are made are also reinforced with an additional layer of printed silicone to reduce the chance of it tearing when the tubing is inserted.

The pump has two printed electrode layers. The ground electrode and the HV zipping electrodes. The ground electrode is a 2 mm wide raster printed electrode which follows the underside of the coupling channel. The HV zipping electrodes are slender vector printed electrodes. A close up of one of the actuators is shown in Figure 6.6b. The actuator consist of two HV electrodes which zip simultaneously forcing the coupling fluid into the overlapped region. The coupling fluid becomes pressurised thus pushing on the medium channel. The electrodes and the channel were designed so that the volume of liquid triples within the area of the overlap when the actuators are completely zipped.

The HV zipping electrodes are vector printed to ensure a smooth edge and precise placement above the centre of the channel(Figure 6.6a). The HV electrodes are narrower than the ground electrode to prevent zipping from all sides and trapping fluid. Section 2 (Figure 6.6c) shows how the electrodes overlap. When the coupling channel is filled, the HV electrodes are close to the ground electrode only at the edge of the channel. Here the electric field and generated Maxwell pressure are at their highest. The HV electrode begin zipping from this point and progresses along the channel.

The high voltage electrodes are encapsulated with a layer of printed silicone. The encapsulation layer protects the electrodes from wear and prevents electrical breakdown between the closely spaced zipping electrodes. Connections are made to the two electrodes at the top edge of the pump. The connections are intentionally separated from the liquid connections (bottom edge of the pump) so that the inlets/outlets can be submerged in a solvent without damaging the fragile connection areas.

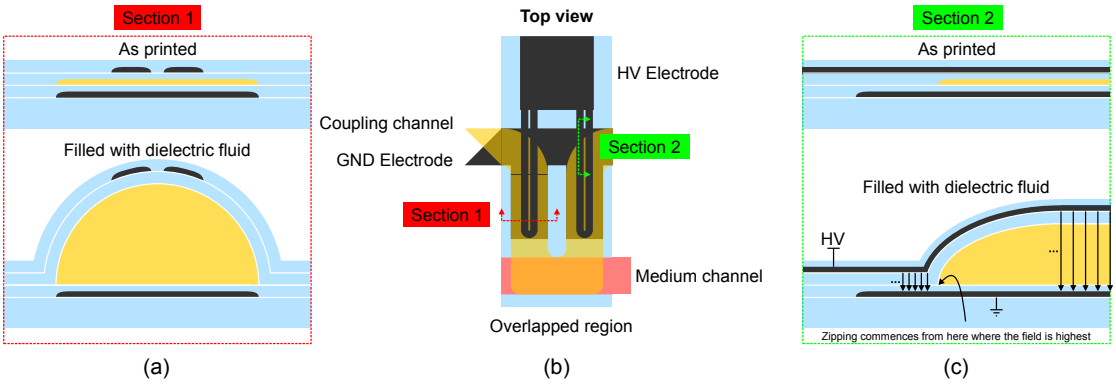

Figure 6.6 – (b) A close up view of one of the HASEL actuators (a) Section 1 shows the placement of the electrodes relative to the dielectric liquid channel. The electrodes are narrower than the channel to prevent zipping form the edges of the channel (c) Section 2 is inline with one of the vector printed zipping electrodes. When a voltage is applied the field is highest where the zipping electrode steps up onto the channel. Zipping therefore occurs from this end of the channel - closest to the HV electrode contact pad.

6.4.2 Fabrication of ink-jet printed peristaltic pump

The majority of the pump is ink-jet printed apart from the thick base layer. The base layer has a thickness of approximately 0.6 mm which would require 20 printed layers to produce. If the 5-pass method were used this would require 20 hours of printing. Therefore in the interest of saving time the base layer was fabricated using a film applicator. In addition the base layer is not patterned and therefore does not need to be ink-jet printed.

The process to make a flat base layer on a portable glass substrate is as follows. A clean glass plate is coated with a water soluble release layer using a threded rod. The release layer consists of 1 g of PVP (Polyvinylpyrrolidone K90 M_r, Fluka) dissolved in 32 g of isopropanol. The silicone (Sylgard 184, Dow) was prepared in a planetary mixer (Thinky ARE 250, Thinky U.S.A. Inc.) with a 10:1 base to catalyst ratio. The silicone was then poured on to the glass plate and cast into a thin film using a universal applicator (Zua 2000.220, Zehntner GmbH). The film was cast with an applicator height of 1 mm and a speed of 5 mm/s. The silicone was then cured at 150° C for 15 mins. Once cured the film was peeled of with the help of deionised water. The film was dried and then cut into 50 mm squares using a razor blade. The squares were then placed in the centre of a glass wafer (0.5 mm thick, 100 mm diameter, float glass wafer) with laser engraved alignment marks. The wafers were placed into a vacuum chamber to remove any trapped air between the wafer and the silicone. The vacuum step ensures that the silicone base layer is completely flat and firmly attached to the glass wafer. This steps helps the base layer withstand processing temperatures up to 100° C.

The processes to make the printed layers was already outlined in part 1 of this thesis.

However certain layers are printed differently depending on the requirements of the printed layer. For this reason a short summary is given below noting how each layer was printed, including the materials used, printing plate/head temperature, printing parameters, post processing (if any), and the time taken to print each layer.

The medium channel is a sacrificial layer consisting of ethyl cellulose. The preparation of the printable mixture is described in section 4.4. The sacrificial layer was raster printed uni-directionally, in two passes (parallel), with a droplet and line spacing of 100 µm, at a print-on-the-fly speed of 50 mm/s, and a printing plate temperature of 40° C. The two pass sacrificial layer took 20 mins to print.

The ground electrode is a carbon black based stretchable electrode. The preparation of the printable electrode mixture is described in section 3.4. The ground electrode was raster printed bi-directionally, in a single pass, with a droplet and line spacing of 100 µm, at a print-on-the-fly speed of 50 mm/s, and a printing plate temperature of 80° C. The ground electrode took 7 mins to print.

The first dielectric layer is made from silicone. The preparation of the printable dielectric mixture is described in section 5.4.The dielectric layer was raster printed bi-directionally, in 5 passes, with a droplet spacing of 50 µm and a line spacing of 500 µm - 62.5 µm (decreasing with every pass), at a print-on-the-fly speed of 25 mm/s, and a printing plate temperature of 80° C. The first dielectric layer took 65 mins to print. The first dielectric layer was cured in an oven at 100° C for 35 mins.

The coupling channel is a sacrificial layer consisting of ethyl cellulose. The preparation of the printable mixture is described in section 4.4. The sacrificial layer was raster printed uni-directionally, in two passes (parallel), with a droplet and line spacing of 100 µm, at a print-on-the-fly speed of 50 mm/s, and a printing plate temperature of 40 °C. The two pass sacrificial layer took 35 mins to print.

The Second dielectric layer is made of silicone. The preparation of the printable dielectric mixture is described in section 5.4.The dielectric layer was raster printed bi-directionally, in 5 passes, with a droplet spacing of 50 µm and a line spacing of 500 µm - 62.5 µm (decreasing with every pass), at a print-on-the-fly speed of 25 mm/s, and a printing plate temperature of 80° C. The second dielectric layer took 65 mins to print. The dielectric layer was cured in an oven at 100° C for 35 mins.

The high voltage zipping electrodes are made from carbon black based stretchable electrode. The preparation of the printable electrode mixture is described in section 3.4. The high voltage zipping electrode consists of a vector printed electrode and a raster printed connection points. The vector printed electrodes were printed in a single pass, with a droplet spacing of 50 µm, at a print-on-the-fly speed of 5 mm/s and a printing plate temperature of 40° C. The raster printed connection points were printed in a single pass, with a droplet and line spacing of 100 µm,

at a print-on-the-fly speed of 50 mm/s and a printing plate temperature of 40° C. The vector and raster printed zipping electrodes took 4 mins to print.

The encapsulation layer is made of silicone. The preparation of the printable dielectric mixture is described in section 5.4.The dielectric layer was raster printed bi-directionally, in 5 passes, with a droplet spacing of 50 µm and a line spacing of 500 µm - 62.5 µm (decreasing with every pass), at a print-on-the-fly speed of 25 mm/s, and a printing plate temperature of 80° C. The encapsulation layer took 38 mins to print. The dielectric layer was cured in an oven at 100° C for 35 mins.

The pumps were separated by cutting along the line of symmetry with a sharp razor blade. The edge with the inlets and outlets was trimmed by 1 mm to to produce a clean edge. Creating a clean edge reduces the chance of the silicone tearing when the tubes are inserted.

The method to make fluid connections was briefly covered in section 4.7. The pump uses a thick silicone base and hence inline fluid connections were made. Four pieces of silicone tubing with an inner diameter of 0.5 mm and an outer diameter of 1.3 mm (310 0504, Deutsch and Neumann GmbH) were cut to a length of 20 mm. One end of each tube was trimmed at 45°. The tapered ends make it easier to insert the tubes into the small channels. The edge of the pump is submerged in a bath of ethanol and using a microscope the tubes are gently inserted into the channels on the edge of the pump. The tubes are inserted to a depth of 4 mm and are rotated so that the flat face is perpendicular to the plane of the pump (Figure 6.7a). Following insertion, the pump was placed into a 80° C oven to evaporate the ethanol. Once dry a fast curing RTV silicone (Dowsil 734, Dow) was applied around the inlets and outlets to create a seal and secure the tubing. Dowsil 734 has a low viscosity and seeps part way into the channel creating a strong bond to the base of the pump. A small amount of RTV silicone is also placed on the thin printed membrane above the taper of the tubes. This is to strengthen the thin printed membrane and reduce the possibility of rubture. A completeld pump is shown in Figure 6.7b.

6.4.3 Flowrate of inkjet printed peristaltic pump

The flowrate of the pump was measured using an external flow sensor. A diagram showing the setup used to make flow measurements is shown in figure 6.8. Syringes are used to fill the peristaltic pump. The serpentine channel was filled with a low viscosity dielectric liquid (Fluorinert electronic liquid FC-40, 3M), and the circulating channel was filled with deionised water. The pressure of these two channels was regulated with a Fluigent pressure controller (MFCS-8C). The high voltge actuation waveform was generated with a 4 channel high voltage power supply (See multi-channel page at https://petapicovoltron.com). The electrical connections to the pump were made with

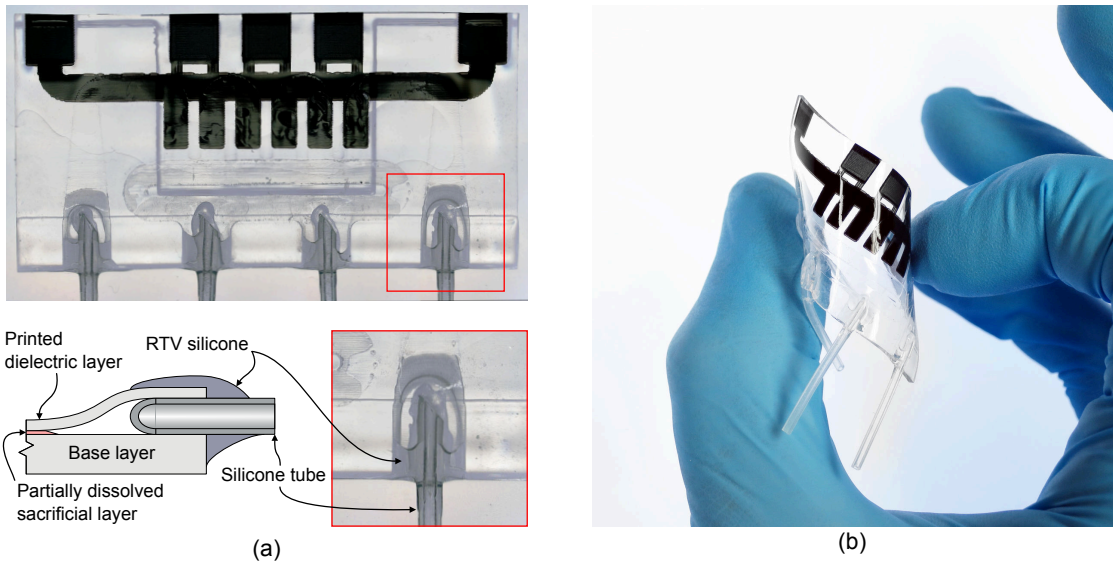

Figure 6.7 – Soft inkjet printed peristaltic pump with fluid connections (a) A photograph showing completed pump with four fluid connections. The channels are easily visible due residue left in the channels after the liquids had evaporated. An enlarged view of a fluid connection is also shown. The diagram next to it shows how the silicone tubes are permanently glued into place using moisture cure silicone (b) A photgraph isllustrating the softness of the pump.

a spring loaded mechanical connector as shown in Figure 6.9.

To test the pump the voltage waveform and the pressure of the channels must be set. The breakdown strength of the printed silicone is about 70 V/µm. The pump has approximately 60 µm of silicone between the electrodes. The absolute maximum voltage for the pump is therefore 4.2 kV. To prevent potential breakdown of the pump it was operated at 3.8 kV (63 V/µm). The pump was tested at multiple frequencies. From 0.2 Hz to 1 Hz in 0.2 Hz increments. The phase shift between the channels was set to 33% (Ch1 0%, Ch2 33%,Ch3 66%). The pressure of the channels were set to be equal. The pressure was increased until the HASEL actuators were no longer able to zip, approximately 30 mbar. The pressure was reduced slightly to 25 mbar. At this pressure the HASEL actuators were reliably zipping and thus pumping fluid.

The results of the flow rate measurements are shown in Figure 6.10. The plot of volume pumped versus time is shown in Figure 6.10a. The ripple in the plots shows that low frequency pumping produces the highest pulsing flows. The gradient of the curves increases when the the pump is operating at 0.2 Hz to 0.8 Hz, with the exception of 0.6 Hz. Finally when the pump was operating at 1 Hz the volume does not increase linearly with time. At 1 Hz the pump increases in volume rapidly up to 20 s after which the volume increases more slowly. The flow-rate was calculated for the pumps between 0.2 Hz to 1.0 Hz in the first 20 s (Figure 6.10b). The bar plot shows there is a general increase in flow from 0.1 µL/s at 0.2 Hz to 0.23 µL/s at 1 Hz.

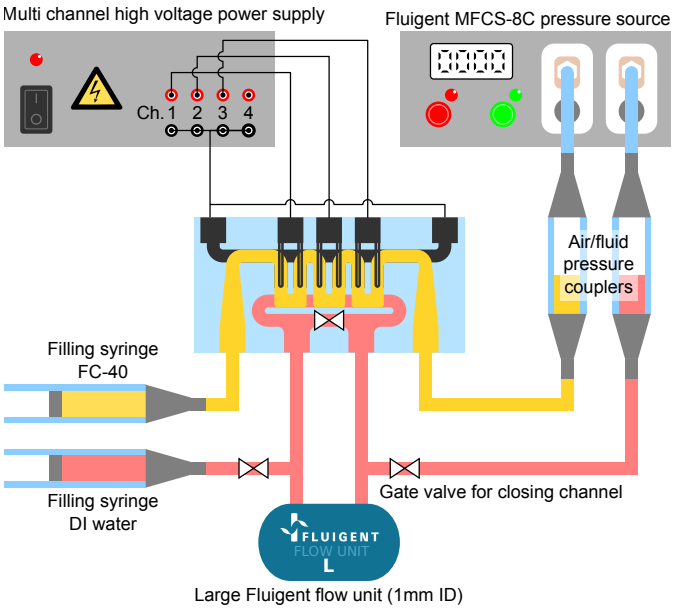

Figure 6.8 – The setup used to measure the flow-rate of the peristaltic pump. Fluid is injected into the channels using syringes. The pressure source is protected with a set of fluid couplers. The fluid couplers have a large volume to prevent the fluids from entering the pressure source. The vertical height of the pressure couplers were setup to be level with the pump before attaching to the pressure source. Three valves were used to completely fill the medium channel without any trapped air. The valves are also used to disconnect the syringes and pressure source during measurements. The pump was powered with a multi channel high voltage power supply. A large Fluigent flow unit was used to measure the flow rate of the pump.

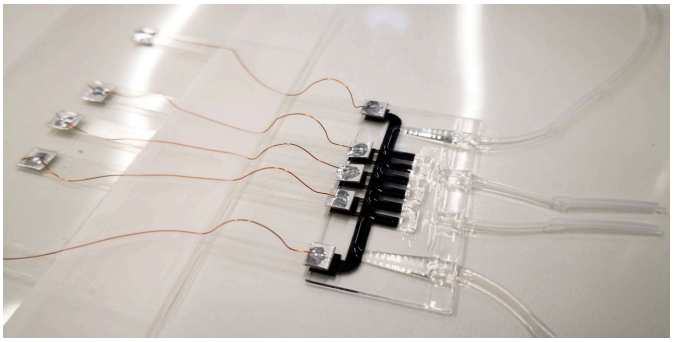

Figure 6.9 – A photo showing how the electrical connections were made to the pump. A small sheet of PET was laser cut to make low stiffness cantilevers. A small piece of metallic tape was wrapped over the end of the cantilevers to make electrical contacts. Flexible winding wire was used to make an electrical connection between the ends of the cantilevers.

6.5 Conclusion

In this chapter an ink-jet printed pump with densely integrated HASEL transducers was presented. The pump consisted of a 2 mm wide channel (when printed) which

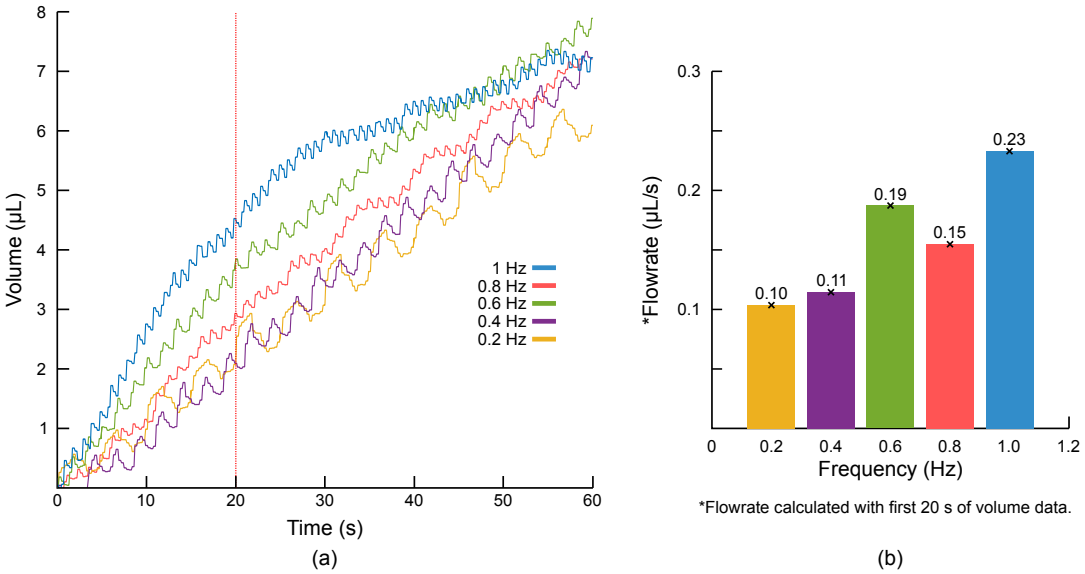

Figure 6.10 – Flowrate of inkjet printed peristaltic pump (a) The volume pumped in the first 60 seconds of pumping at different actuation frequencies (b) The flow rate of the peristaltic pump at different operating frequencies.

was able to circulate fluids through an external circuit. The present design was able to pump liquids up to frequencies of 0.8 Hz giving a maximum flow-rate of 0.15 µL/s. By improving the design and preventing the dielectric fluid from shifting it may be possible to achieve higher flow rates. The pump requires an external pressure source to set the channel pressure and a multi channel high voltage power supply to control the actuators. The pressure source may be removed once the pressure has been set. The 7 layer pump was fabricated primarily by ink-jet printing. Printing enables multi-layer structures consisting of channels and integrated transducers. Printing multiple layers enables the fabrication of overlapping channels to make fluidic systems which can manipulate the flow of aqueous liquids. In addition printing enables more dense integration. The ability to print high resolution features and print silicone encapsulation layers makes it possible to have high voltage transducers in close proximity. The pump was fabricated on a soft silicone base layer which produces a fluidic system which is soft and transparent. Making this fabrication approach suitable for lab on a chip devices where the processes occurring in the chip must be visible at all times. Using soft materials and ink-jet printing enables rapid, and low cost fabrication of fluidic systems with neat and dense integration of transducers.

7 Ink-jet printed soft slug-drive

7.1 Summary

Soft animals have interesting forms of locomotion which enable them to move over many different types of materials and terrains. Of particular interest is the motion of soft bodied animals, gastropods, which move using small repetitive muscle contractions. In this chapter a concept called the slug-drive is introduced. The slug-drive takes inspiration from the motion of gastropods and uses this to displace objects. First a pneumatically actuated slug-drive is fabricated and tested to validate the concept. Following this an integrated slug-drive is fabricated by ink-jet printing. The integrated slug-drive uses 28 integrated HASEL actuators to create a travelling wave of deformation. The device has not yet been tested but is documented here to demonstrate the advantages of printing. Similar approaches may be used in the future to create untethered soft robots with more complex forms of locomotion.

7.2 Introduction

Locomotion is important for animals and robots alike. Animals have developed the means to move in every environment. Animals have the ability to move underwater, on land, and in the air. Humans have also developed machines to navigate in these different mediums, and most of the time we have looked to nature for inspiration. This is particularly true for flight machines which have been heavily inspired by birds and bats (Anders, 2000). On land most machines move using wheels. Wheels are extremely efficient for traversing structured environments but are less suited to natural environments (Armour et al., 2007). To build robots which can navigate natural environments we must look to nature for inspiration.

One animal which is particularly interesting is the slug. The slug is a completely soft, invertebrate, animal which can move on virtually any surface . Slugs can traverse

natural marine, terrestrial, and fossorial (underground) environments (Boxerbaum et al., 2012). Slugs also have the ability to traverse indoor environments and have the ability to crawl up walls and ceilings (Shirtcliffe et al., 2012). slugs are able to navigate more challenging environments,including glass, polytetrafluoroethylene (PTFE, Teflon), metal surfaces, sand, and razor blades (Rogóż et al., 2019). Only man made hydrophobic surfaces present an obstacle to slugs and snails (Shirtcliffe et al., 2012). It is due to these remarkable abilities that engineers have tried to replicate the motion of invertebrate animals such as slugs and snails.

Replicating slug motion is challenging because the motion is difficult to reproduce with conventional materials. Chan et al. (2005) explored two different types of motion by creating two robo snails. One of the robo snails was designed to move using retrograde waves and the other direct waves. The retrograde robot (Figure 7.1a.i) consisted of a helical rotor and many parallel plates which would be raised and lowered as the rotor turned. The principle is similar to a cam shaft. The second robo snail (Figure 7.1a.ii) consisted of sliding pads which were controlled by shape memory alloy wires. This robot moves by displacing one pad at a time. These solutions are great for exploring the different form of motion, however the robots are large, rigid and heavy.

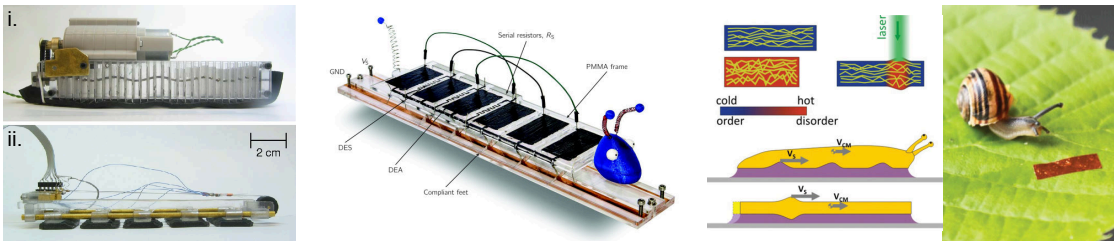

(a) (b) (c)

Figure 7.1 – Robots based on the locomotion of gastropods (a)(i) Robosnail 1. The robot slides on a layer of mucus and uses a form of propulsion similar to peristaltic pumping (ii) Robosnail 2. The robot distributes its weight across all pads and moves one pad at a time Chan et al. (2005) (b) Trevor, a robot inspired by the motion of a caterpillar. Trevor uses an onboard oscillator based on DE switches to control the DE actuators. The robot only needs to be supplied with a DC voltage to crawl forwards. (Henke et al., 2017)(c) Light-induced travelling waves in a liquid crystal elastomer (LCE) generates pedal waves in a millimeter-scale soft robot. (Rogóż et al., 2019)

Another approach explored the use of DE transducers to replicate the motion of a caterpillar (Henke et al., 2017). Caterpillars do not move on a layer of slime, they move by stepping. However the example is still relevant because the caterpillars move by creating a travelling wave of deformation. The caterpillar-like robot Trevor is shown in figure 7.1b. The robot consists of a planar layer of DE actuators which expand in sequence. The expansion of the DE actuators is converted to circular like motion of the feet which move the robot forwards. Trevor uses a set of DE switches to automatically create the travelling wave of deformation. The example shows quite nicely how smart transducers can be utilised to simplify the control of a soft robot. however Trevor is

quite large and uses many rigid components. In addition fabricating a device like this to work reliably is difficult. The switches must be fabricated to have the same response to strain. Printing would be an excellent method to create more reliable and easy to pattern DE switches.

The final example is an extremely small and thin crawling robot (Rogóż et al., 2019). The robot consists of a sheet of liquid crystal elastomer which contracts when it is heated (Figure 7.1). By using a laser a travelling wave of contraction could be induced from a distance to propel the robot forwards.

The robots produced to date are very distant from their biological counterparts. Firstly most robots trying to mimic the motion of gastropods are made from rigid components. The robots described above were fabricated from plastic and metals which are not at all soft. To explore the benefits of soft systems we have to create robots which are truly soft and are made from materials with a stiffness comparable to the animals we are trying to mimic.

In this work a new method of motion is introduced for completely soft robots. The method of motion is loosely based on the motion of gastropods. A travelling wave of deformation is produced by pressurising and de-pressurising a surface of closely spaced inflatable channels. The parallel channels are pressurised using many integrated HASEL actuators which push fluid from the ends of the channels into the middle. Since the fluid is constrained from either end the channel it becomes pressurised and changes shape. By changing the shape of these channels in a particular sequence a travelling wave of deformation can be produced to produce motion.

The remainder of this chapter is divided into 6 sections. The first section explains the principle of motion in more detail. Following this a proof of concept device, the pneumatic slug-drive, is fabricated and tested. The pneumatic slug-drive is a proof of concept to validate the method of motion. Finally a process to ink-jet print a slug drive is presented. The integrated slug-drive demonstrates how ink-jet printing may be used to neatly and densely integrate actuators into a soft robot to produce motion.

7.3 Principle of motion

The slug-drive uses the inflation and deflation of parallel channels to create motion. To understand what parallel channels are, consider an inflatable pool mattress (Figure 7.2a). An inflatable mattress consists of two flat sheets of plastic which have been laminated together to create a channel like structure. When the mattress is inflated it leads to deformations in both x and y directions. The mattress contracts in the x direction and the mattress expands in the y direction. When the channels are are inflated simultaneously the mattress exapands and contracts on the sport. However if the channels can be

induvidually controlled it is possible to make the mattress swim, or to make a slug-drive move.

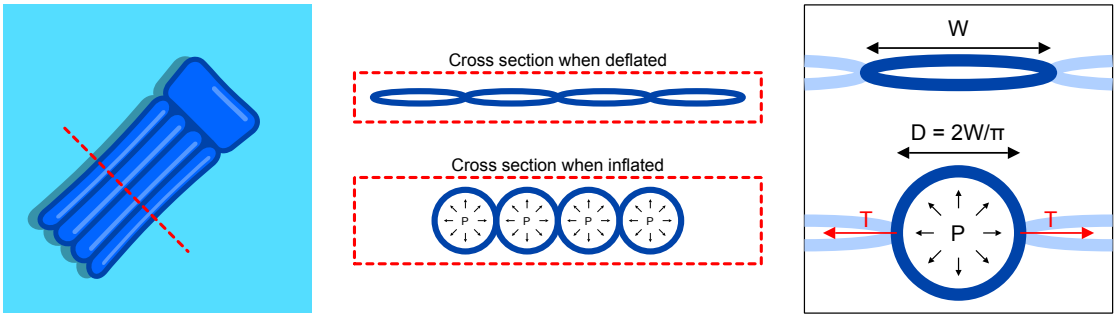

Figure 7.2 – Deformation of parallel channels (a) A pool mattress is a good analogy for the deformation of channels (b) When the mattress is inflated it contracts in the x-direction and expands in the y-direction. These deformations are exploited by the slug drive to create a wave of contraction (c) When individual channels are inflated they become narrower and exert forces on neighbouring channels

A short slug-drive consisting of 6 parrallel channels, or toes, is depicted in Figure 7.3. The sequence begins with the state −−○. In the first step the middle channel is inflated, giving −○○. THis puts the deflated channel under tension. The right channel is then deflated giving the state −○−. This releases some of the tension in the structure. The unbalanced tension force then causes the body to move forwards. The remainder of the sequence involves two more tensioning steps and two more release steps, after which the cycle repeats. The full cycle or sequence is completed in 6 steps and displaces the slug by the width of one inflated channel.

7.4 Pneumatic slug-drive

Before building a fully integrated slug-drive with HASEL transducers a pneumatic proof of concept was fabricated. The proof of concept is a slug-drive which uses external pneumatic flow controller to deform the channels of the slug-drive.

7.4.1 Fabrication of pneumatic slug-drive

The pneumatic slug-drive was fabricated using a mixture of conventional fabrication techniques and printing. The fabrication of the pneumatic slug-drive is depicted in Figure 7.4. The pneumatic slug-drive was fabricated using a pre-cast membrane (Elastosil film 2030 250/20, Wacker Chemie AG), 2 mm wide ink-jet printed sacrificial channels (See chapter 4), and cast layer of UV curable silicone (Silopren UV. Electro 225-1,Momentive Performance Materials Inc.). The gap height was set to 30 µm (relative to the top surface of the Elastosil membrane) and cast at 2 mm/s. The top and bottom layer

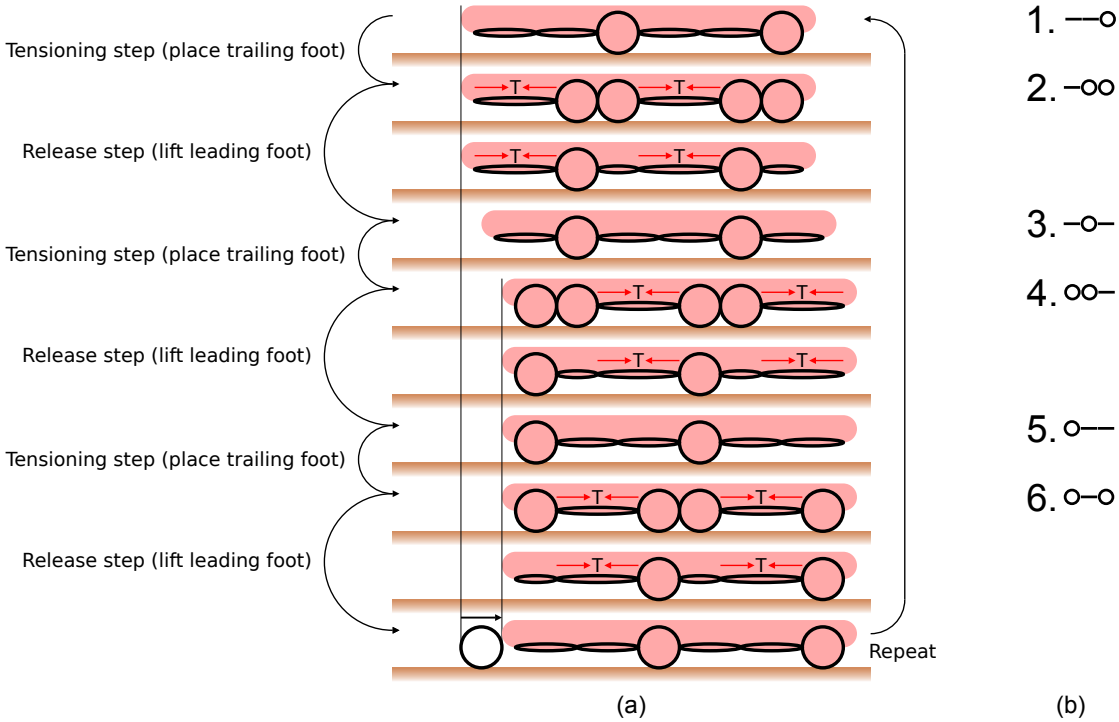

Figure 7.3 – Principle of motion of a slug-drive (a) the sequence consists of 6 steps. When a channel, or a toe, is inflated it puts surrounding channels under tension. This is called the tensioning step. When a toe is lifted the tension is released by shifting the body of the slug. The process is repeated six times after which the cycle repeats. Note that additional steps have been added to show how the tension is released. Theoretically a slug-drive using this form of locomotion can displace itself by the width of one inflated channel when completing a cycle (b) The notation used to the describe the 6 sequence cycle.

therefore have a similar thickness of approximately 20 µm. In step two of fabrication a temporary frame was added so that the substrate can be removed. Perpendicular fluid connections were made to either end of the serpentine channel using the process described in section 4.7. In the third step of fabrication the channels were opened and inflated with air. While the channel was inflated a thick silicone frame was glued onto the top and bottom surfaces using UV cure silicone. The frame was added while the channels are inflated so that the channels are kept open on the edges of the frame. Finally the edges of the thick silicone frame are trimmed to access the channels from the edge.

7.4.2 Speed of pneumatic slug-drive

To test the slug-drive a programmable pressure source (MFCS-8C, Fluigent) was used. Fluid connections were made by inserting small plastic tubes into the side of the slug-drive. Since the holes were not perfectly circular the edge of the slug-drive was sealed using some additional UV cure silicone (Figure 7.5a). Every third channel of the slug-

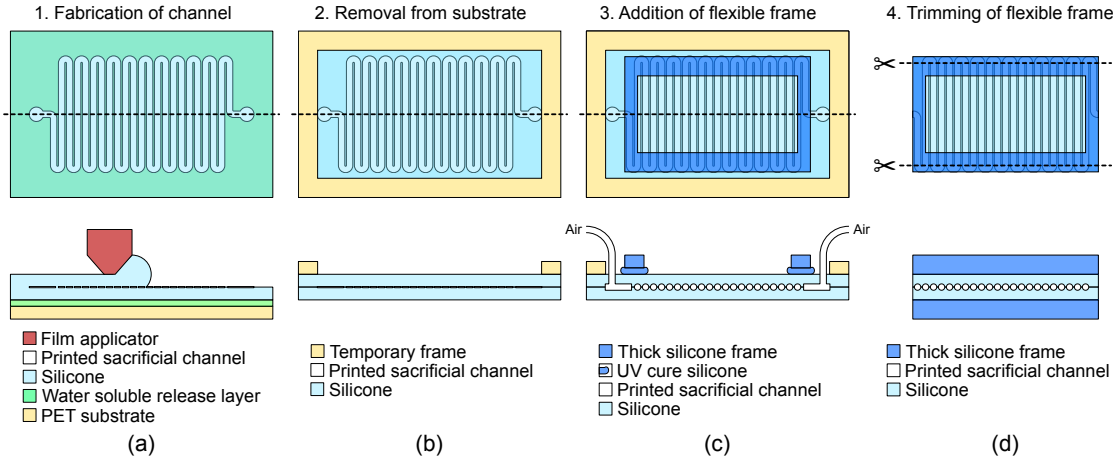

Figure 7.4 – Fabrication process of pneumatic slug drive (a) Parallel channels are formed by casting silicone over a printed sacrificial channel (b) A frame is added to remove the structure from the substrate (c) Fluid connections are added to dissolve the sacrificial material and inflate the channel. A silicone frame is added with UV silicone to preserve the shape of the channels in the silicone frame (d) The temporary frame is removed and the edges of the soft channel are trimmed to access each parallel channel independently.

drive was interconnected so that the the slug-drive can be controlled with only three pressure channels. To generate the pressure profile described in section 7.3 a script was used. The script cycles through the six step sequence with 0.2 s between each step. This was the maximum frequency which produced a square pressure profile at a pressure of 35 mbar. A pressure of 35 mbar inflated the channels to an almost circular profile without over inflating the channels. To determine the speed of the slug-drive a small plastic block was placed on top of the channels (Figure 7.5b). The plastic block measured 15 mm × 5 mm × 4 mm with a weight of 0.5 g. The block was shown to move at approximately 50 µm/s (Figure 7.5c).

The speed of 50 µm/s is much slower than predicted by the sequence diagram in section 7.3. Given a channel width of 2 mm the sequence diagram predicts a speed of approximately 1 mm/s. The predicted speed is 20 times higher than the actual speed. In part this is because the sequence diagram is a great over simplification of the actual situation. Firstly the slug-drive does not transition from perfectly flat to completely round channels. In addition the actual slug-drive has very wide seams between the channels which reduce the efficiency of the slug-drive. In addition the diagram assumes that the parallel channels are infinitely long and are completely free to move. However in reality the channels have a finite length and are constrained on the edges. By reducing the length of the channels the maximum displacement is greatly reduced. The model also does not take into account the traction between the two surfaces. A strip of carbon black material was printed on the surface of the slug-drive to measure the shape of the channels. The printed electrode creates a dry contact which reduces the traction

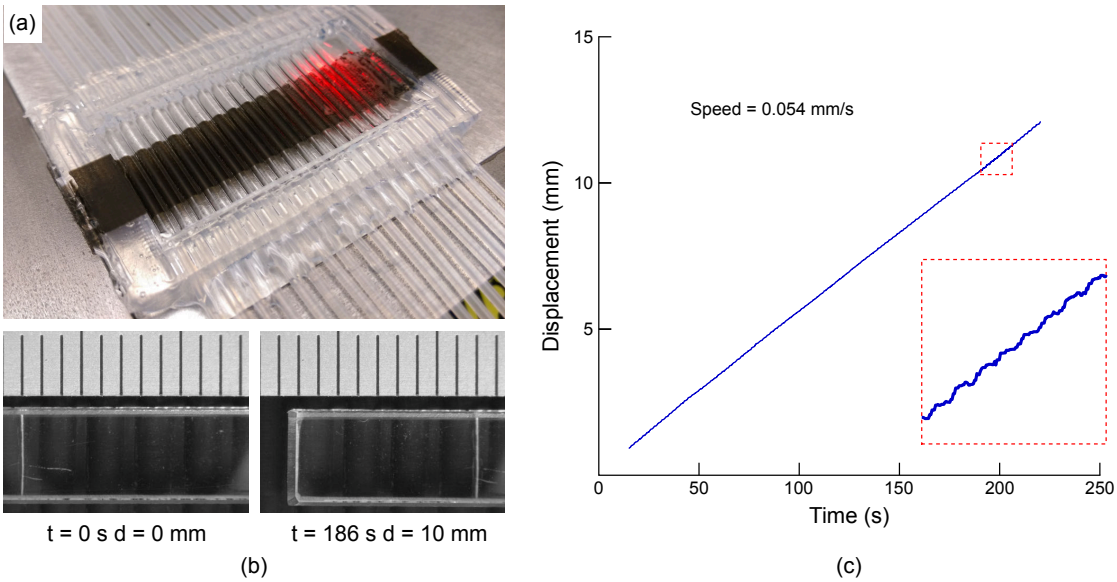

Figure 7.5 – Speed of pneumatic slug drive (a) a photograph of the pneumatic slug drive. A strip of electrode has been printed on the top surface for surface profile measurements (b) A picture of a plastic block placed on the pneumatic slug drive at time 0 s and at time 186 s after which it has been displaced 10 mm (c) The displacement versus time of the plastic block at a frequency of actuation of 0.83 Hz. The inset shows the ripple produced by this type of drive.

between the drive and the block. It is not clear if these differences alone explain the discrepancy between the predicted and measured speeds. However the purpose of the pneumatic slug-drive was to determine if the proposed sequence produces motion. And the pneumatic slug-drive clearly shows that a travelling wave of expansion can be used to produce motion.

7.5 Integrated slug-drive

In this section the design of an integrated slug-drive is discussed. The integrated slug-drive is very similar to the pneumatic slug-drive. However, instead of expanding the channels with a external pressure source, the edge of the channels is lined with HASEL actuators which push dielectric liquid into the channels to make them expand.

7.5.1 Design of integrated slug-drive

The design of an ink-jet printed slug-drive with integrated HASEL actuators is illustrated in Figure 7.6a. The integrated slug-drive has a single slug foot which is 14 mm wide and 30 mm long. The slug foot consists of 14 toes (channels). On the north and on the south side of the device are a total of 28 HASEL actuators which push dielectric liquid from the sides into the centre. These actuators are powered by the power buses

running along the northern and southern sides of the slug-drive. One of the power buses connects to the ground electrode of the HASEL actuators. The remaining three buses are the high voltage connections. These connections correspond to the three phases of the basic sequence diagram. In theory it would be possible to control the device with only four external electrical connections. However the design was made symmetrical to ensure that all the HASEL actuators have a similar response time (similar length = similar resistance). Finally the slug-drive was fabricated on thick silicone base layer just like the pump. Using a base layer means that no frame is required to support the slug-drive. Since the substrate is quite firm an additional sacrificial channel was printed to produce an air cushion. The air cushion lifts the channels off the surface of the base layer allowing them to move freely.

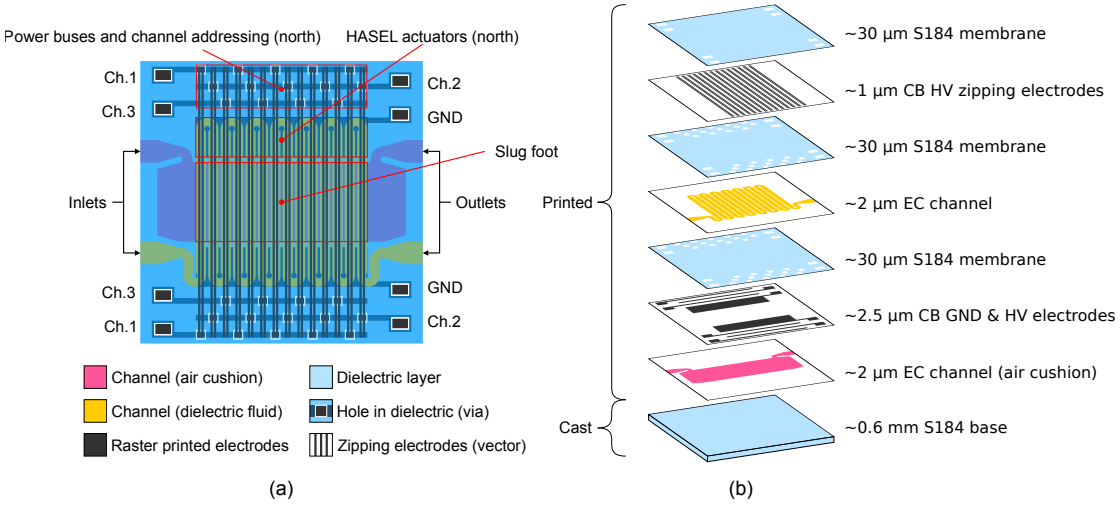

Figure 7.6 – Design of integrated slug-drive (a) The top view showing parts of interest. The slug foot is in the middle of the device. The slug foot uses travelling waves of contraction to displace objects. HASEL actuators on the north and south sides of the slug foot push dielectric fluid into the middle, creating the contractions. The power buses address the actuators so that every third actuator is interconnected (b) An exploded view of the integrated slug-drive. The slug-drive consists of a thick base layer (cast) and 7 printed layers. The approximate thickness of the layers is indicated, along with the materials (Sylgard 184, Ethyl Cellulose, Carbon Black), and a description.

A cross section of the slug drive is shown in Figure 7.7 to better explain the HASEL actuators. The cross section shows the slug-drive *as printed* and *when filled* with fluid. The filled cross section shows how the air-cushion lifts the channels off the thick silicone substrate. Note that the diagram is exaggerated and the air cushion will not be pressurised to this extent. Only a small amount of air is injected so that the channels hover above the base layer.

The diagram (Figure 7.7) also indicates the layout of the electrodes. The ground electrode is patterned underneath the channel carrying the dielectric fluid. The high voltage electrode runs from the edges of the slug-drive over the top of the whole structure.

When a high voltage is applied the field is greatest where the electrodes are in closest proximity. The point is indicated on the diagram and shows where the zipping originates. The volume of liquid in between the two electrodes is then pushed into the central part of the channel. The ratio of HASEL actuator to channel was designed so that the volume of the liquid doubles when the electrodes are fully zipped.

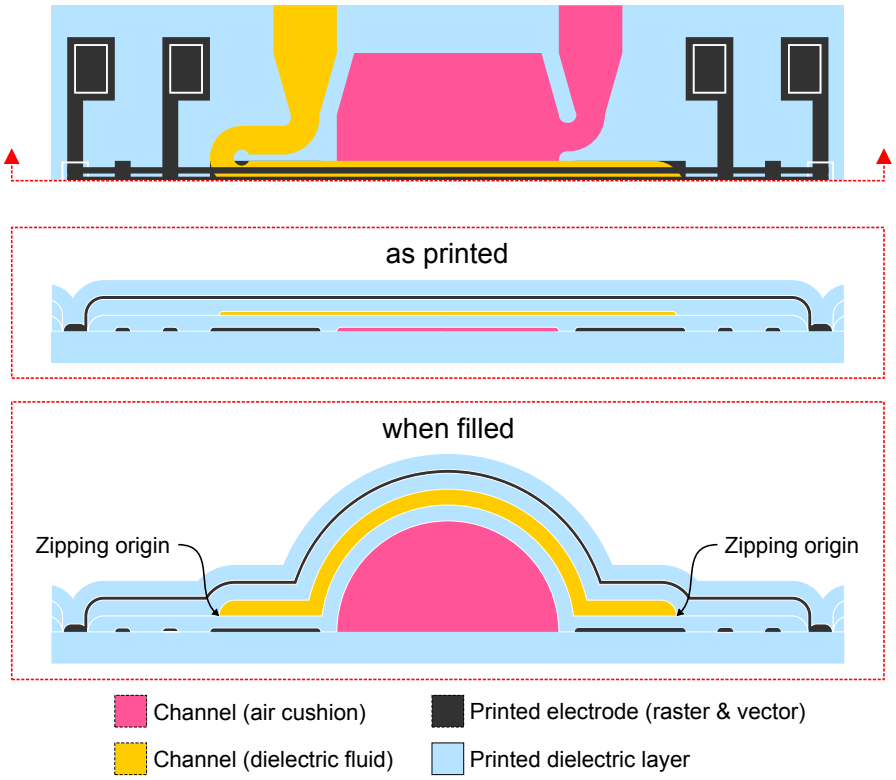

Figure 7.7 – Cross section of integrated slug drive as printed and when filled. The filled cross sections shows where the zipping of the HASEL actuators originates. Note that the drawing is exaggerated and not to scale.

The slug-drive consists of two printed sacrificial channel layers. The bottom channel indicated in magenta functions as an air cushion. The air cushion is slightly longer than the slug foot. The added length gives the channels on the end more freedom to move. The top channel in yellow is the dielectric fluid channel. A serpentine channel was used so that the pressure of the dielectric fluid can be set with a single pressure source. The serpentine channel is 1.8 mm wide and the seams (spacing between adjacent channels) are 0.4 mm wide. The inside turn radius of the serpentine channel was increased from 0.2 mm to 0.5 mm. Increasing the turn radius reduces the probability of the channel bursting when the channels are pressurised.

The slug-drive has two printed electrode layers. The bottom electrode layer holds the ground electrodes and the bus bars. The ground electrode is 30 mm long and 7 mm wide. The bus bars have a width of 1 mm and are separated by 2 mm. The large

spacing of 2 mm is necessary because the printed holes in the dielectric layer result in uneven dielectric layers (see section 5.7). If the bus bars were closer together dielectric breakdown is more likely to happen between a bus bar and the zipping electrodes which are at different potentials. Both the ground electrodes and the bus bars are raster printed. The top electrode layer contains the zipping electrodes. The zipping electrodes are vector printed lines which have an approximate width of 0.4 mm. The zipping electrodes span the full width of the slug-drive an make contact to the bus bars wherever there is a hole in the dielectric layers.

The dielectric layers were printed with the 5 pass method (See chapter 5). The dielectric layers are approximately 30µm thick. Electrical vias or holes are patterned in the first two dielectric layers. These are arranged so that the zipping electrodes are connected to the underlying channels in the order Ch.1 Ch.2 Ch.3 repeating. A suitable size for the electrical vias was determined experimentally. A 1 mm wide electrode was printed on to a thick substrate and a dielectric layer with five different hole sizes (1.8 mm to 1 mm) was printed on top of the electrode. A photograph of this test print is shown in Figure 7.8. A hole size of 1.6 mm was chosen because this results in a hole of approximately 1 mm - the same as the width of the bus bar underneath. The top dielectric layer only has holes to connect to the bus bars and the ground electrodes. This layer was printed to prevent arcing between the high voltage electrodes.

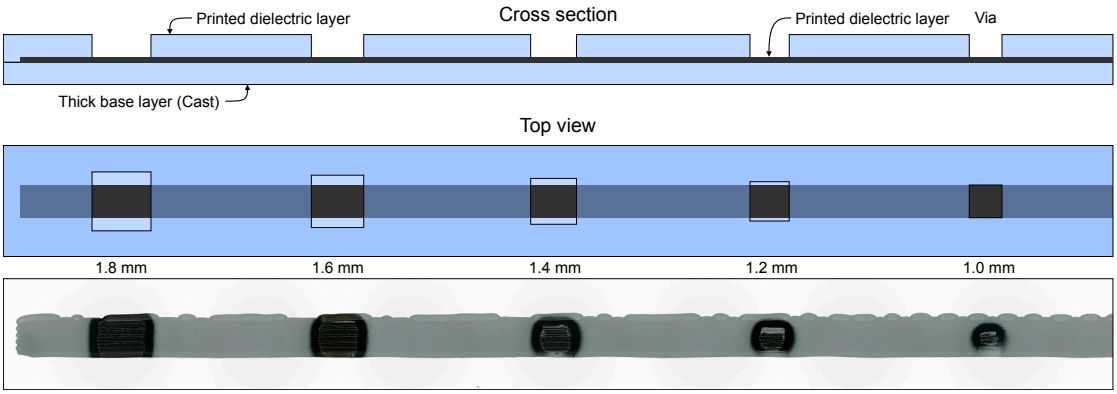

Figure 7.8 – The optimal size of electrical vias was determined experimentally. The diagram shows the size of the holes as designed. The photograph shows the holes on a experimental sample as printed.

7.5.2 Fabrication of integrated slug-drive

The integrated slug drive is fabricated primarily by ink-jet printing. The only part of the slug-drive which is not printed is the base layer. The base layer was fabricated using a film applicator and manually cut into a 50 mm squares. The process to make a 0.6 mm base layer was already described in the fabrication section for the pump (section 6.4.2). The remainder of the slug drive is completely printed.

The processes to make the printed layers was already outlined in part 1 of this thesis. However certain layers are printed differently depending on the requirements of the printed layer. For this reason a short summary is given below noting how each layer was printed, including the materials used, printing plate/head temperature, printing parameters, post processing (if any), and the time taken to print each layer.

The air cushion was formed by printing a sacrificial layer of ethyl cellulose. The preparation of the printable mixture is described in section 4.4. The sacrificial layer was raster printed, uni-directionally, in two passes (parallel), with a droplet and line spacing of 100 µm, at a print-on-the-fly speed of 50 mm/s and a printing plate temperature of 40 °C. The two pass sacrificial layer took 18 mins to print.

Ground electrode and power buses are made from carbon black based stretchable electrode. The preparation of the printable electrode mixture is described in section 3.4. The electrode was raster printed bi-directionally, in a single pass, with a droplet and line spacing of 100 µm, at a print-on-the-fly speed of 50 mm/s and a printing plate temperature of 80° C. Elevated temperatures were used to reduce the flow of the electrode mixture and improve its resolution. The ground electrode and power buses took 8 mins to print.

The 1st dielectric layer is made from silicone (Sylgard 184, Dow). The preparation of the printable dielectric mixture is described in section 5.4.The dielectric layer was raster printed, bi-directionally, in 5 passes, with a droplet spacing of 50 µm and a line spacing of 500 µm - 62.5 µm (decreasing with every pass), at a print-on-the-fly speed of 25 mm/s, and a printing plate temperature of 80° C. The first dielectric layer took 64 mins to print. The dielectric layer was cured in an oven at 100° C for 35 mins.

The serpentine channel is a sacrificial layer consisting of primarily of ethyl cellulose. The preparation of the printable mixture is described in section 4.4. The sacrificial layer was raster printed, uni-directionally, in two passes (parallel), with a droplet and line spacing of 100 µm, at a print-on-the-fly speed of 50 mm/s, and a printing plate temperature of 40 °C. The two pass sacrificial layer took 50 mins to print.

The 2nd dielectric layer is exactly the same as the 1st dielectric layer. The 2nd dielectric layer also took 64 mins to print.

The zipping electrodes are made from carbon black based stretchable electrode. The preparation of the printable electrode mixture is described in section 3.4. The high voltage zipping electrode consists of a vector printed electrode. The vector printed electrodes were printed in a single pass, with a droplet spacing of 50 µm, at a print-on-the-fly speed of 5 mm/s, and a printing plate temperature of 40° C. The vector printed zipping electrodes took 5 mins to print.

The encapsulation layer is made from silicone (Sylgard 184, Dow). The preparation of the printable dielectric mixture is described in section 5.4. The dielectric layer was raster printed, bi-directionally, in 5 passes, with a droplet spacing of 50 µm and a line spacing of 500 µm - 62.5 µm (decreasing with every pass), at a print-on-the-fly speed of 25 mm/s, and a printing plate temperature of 80° C. The encapsulation layer took 64 mins to print and was cured in an oven at 100° C for 35 mins.

The slug-drive as printed is shown in Figure 7.9. The stitched microscope image was taken with a combination of direct and indirect illumination (midway between light and dark field) to capture details of opaque and transparent materials. The choice of lighting highlights the surface profile. The slug-drive in the photo has some additional printed dielectric layers to reduce the chance of breakdown around the vias. The dark circles around the vias represent depressions in the top surface. At the deepest point this depression is approximately 60 µm deep. The the holes in the dielectric layers also have an effect on the vector printed high voltage electrodes. The printed lines become narrower as they approach the power buses. It is not clear if this has a large effect on the resistance of the printed tracks. Some dust particles can also be seen on the microscope image. Dust particles can be damaging to the device if they cross multiple layers. Luckily these dust particles did not fall in between the electrode layers and thus are unlikely to cause any problems.

The steps to finish the slug drive are shown in Figure 7.10. To make the fluid connections the edges of the slug-drive with inlets and outlets were trimmed with a razor blade. A clean cut edge reduces the chance of tearing when the silicone tubes are inserted. The slug-drive is then placed in a Petri dish with ethanol. The ethanol dissolves the sacrificial channels making easier to insert the tubes. Once the tubes are inserted, the device was placed in an oven at 80° C for 15 mins to accelerate the evaporation of the ethanol. An insert in Figure 7.10a shows what an inserted tube looks like. The tubes are permanently secured by adding some moisture cure RTV around the tube. Once the tubes are in place the sacrificial channels can be opened and dissolved. Figure 7.10b shows how a syringe is used to inject ethanol into the channels. The electrical connections were made using magnets (Figure 7.10c). A Plexiglas plate was cut to hold eight cylindrical magnets with the same layout as the electrode contacts on the slug-drive. The slug drive is placed on top of this platform. Eight ball magnets magnets put pressure on the con electrical contacts to secure the slug drive. Connections to the ball magnets were made with ferromagnetic washers and single core wire.

Two slug-drives have been fabricated. The first was shown to actuate. However poor design of the slug-drive led to electrical breakdown. The breakdown occurred between the zipping electrodes and the power buses. When this occurs the power buses become electrically shorted and the channels can no longer be individually controlled. To solve this issue a second version was designed. The spacing between the power buses was increased to reduce the chance of breakdown. An additional layer of silicone was also

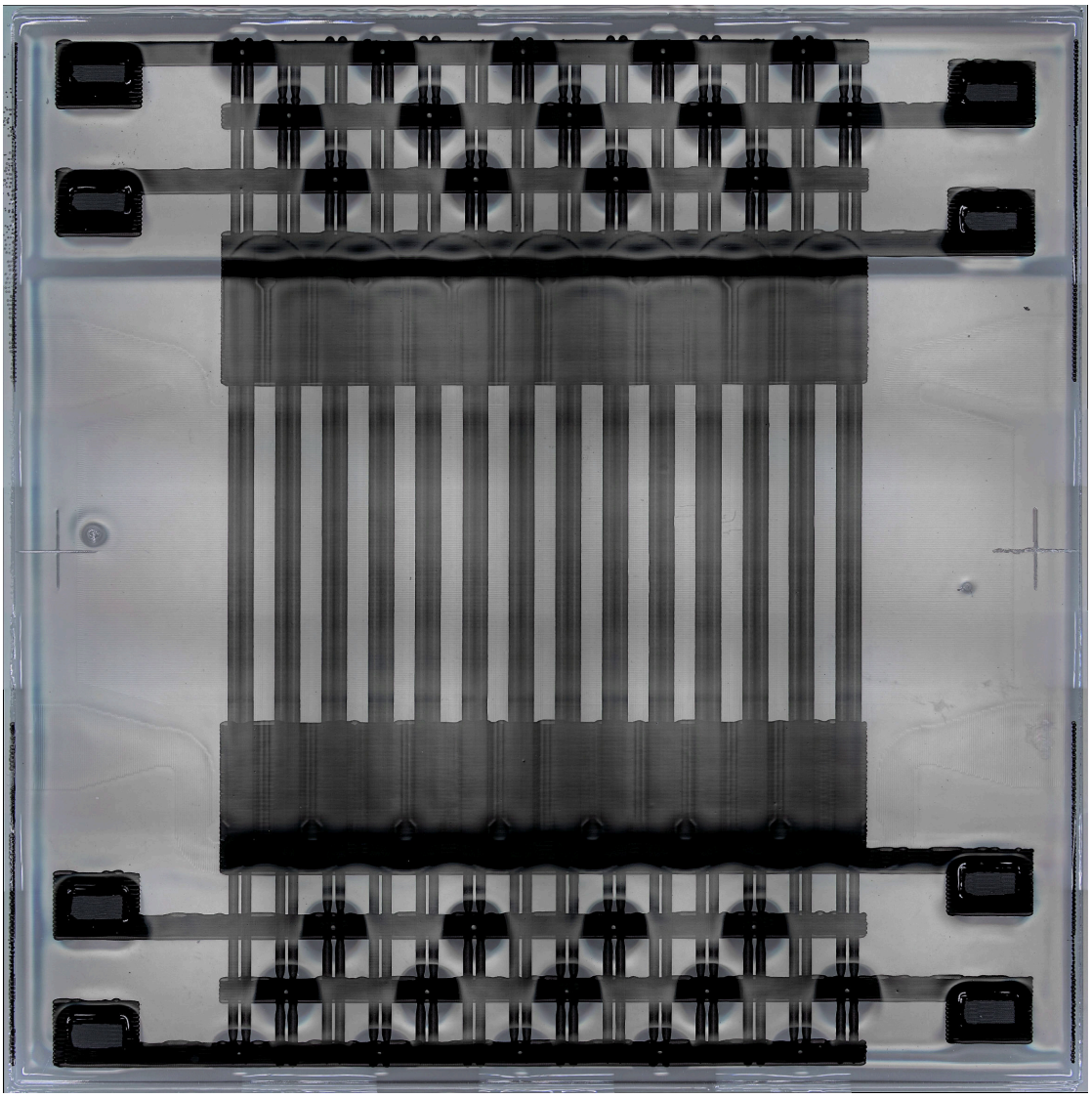

Figure 7.9 – A stitched microscope image of the integrated slug-drive as printed. Special lighting was used to show the sacrificial layers, electrodes, and an indication of surface profile.

printed over the power buses to reduce the probability of failure. The second version has yet to be tested.

7.6 Conclusion

In this chapter the concept of a slug drive was validated with a pneumatic proof of concept. The pneumatic proof of concept showed that producing a wave of deformation can be used to create motion. The pneumatic slug drive was shown to move a small plastic object with a weight of 0.5 g at 50 µm/s. Following the pneumatic proof of

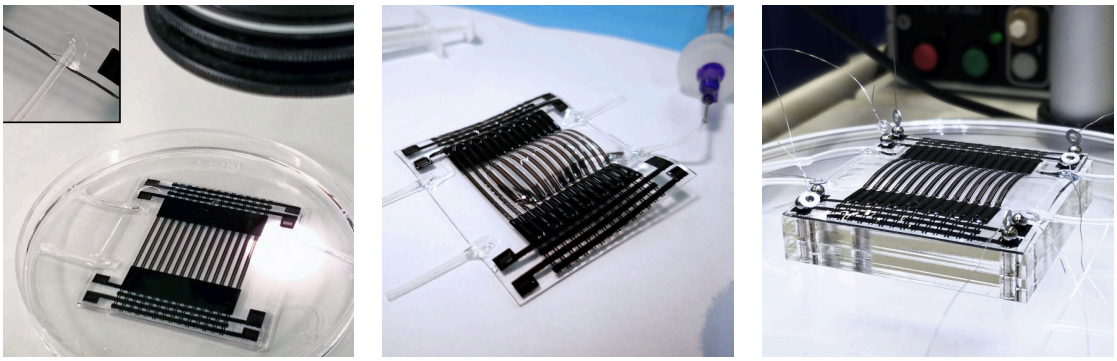

Figure 7.10 – Finishing of the integrated slug-drive (a) The slug drive is immersed in ethanol and tubes are inserted into the inlets and outlets. The inset shows an inserted tube after the ethanol has evaporated (b) The channels are opened by injecting ethanol (c) A magnetic base is used to hold the slug drive and to make electrical connections.

concept a fully integrated slug-drive was introduced. The integrated slug-drive has not been tested but was included in this thesis to highlight some of the benefits of ink-jet printing. The proposed design shows how multiple HASEL actuators can be neatly integrated into a soft structure. Here ink-jet printing has been used to pattern 28 HASEL actuators within an area of 25 mm^2. Integrating both the actuators and the electrical connections greatly reduces the number of external connections required. The proposed slug-drive only has 4 fluid connections compared to pneumatic slug drive which has 14. Furthermore, these fluid connections are only necessary to fill the slug-drive after which they can be disconnected. The slug drive also has less electrical connections. The slug drive would require 24 electrical connections if the addressing were not done on board. Overall ink-jet printing enables us to integrate more transducers into a smaller space. Increasing the number of actuators produces soft robots with more complex forms of locomotion. Soft robots which may be able to imitate the successful forms of locomotion found in nature.

8 Conclusion and future Work

8.1 Conclusion

In this thesis the materials were developed for ink-jet printing soft machines. The electrode material is based on carbon black. The electrode mixture is printable on silicone without the need of surface treatment. With the electrode material high resolution traces and electrodes may be patterned. The electrode is thin, compliant, and sufficiently conductive for electrostatic transducers such as DE and HASEL actuators.

A novel way to create channels was also presented, using a thin printable sacrificial material. The material can be directly printed on silicone. The material is very thin, making it easier to create multi-layer structures without the need of any levelling procedures. Furthermore the channels can be rapidly opened. The ability to print channels in thin and soft structures makes it possible to integrate high performance HASEL actuators into soft machines.

A process to pattern uniform dielectric membranes was also presented. Printing silicone is challenging because of its low viscosity and interaction with substrate materials. A special 5-Pass printing method was introduced to print uniform membranes on different materials, including electrodes and sacrificial channels. The ability to pattern the dielectric layers enables devices with a third dimension. Printing holes in the dielectric layer makes it possible to print electrical and fluid vias. Vias enable complex networks of conductors and fluids to more neatly integrated transducers along with the electrical connections

Two demonstrators were developed to show how these materials can be combined into multi-layer and multi-material structures. The ink-jet printed peristaltic pump is the first of its kind. Showing how ink-jet printing can be used to densely integrate HASEL transducers. Multiple transducers are integrated to create a peristaltic wave of pressure. Overlapping channels are used to couple the pressure to other channels.

Using overlapping channels produces a pump which is able to pump aqueous fluids. This makes the technology highly attractive for lab-on-a-chip applications where the flow of electrolytes must be controlled.

Finally a soft robotic actuator called the slug drive was introduced. The slug drive shows how many HASEL transducers may be integrated and interconnected to create a travelling wave of deformation. The travelling wave of deformation is inspired the locomotion of invertebrate animals. This form of locomotion may in the future enable soft robots to move large distances with small repetitive deformations.

In conclusion the materials and methods presented in this thesis enable complex multi-layer soft machines with neatly and densely integrated transducers.

8.2 Future work

Future work may be focused on material development, improved printing strategies, or the soft machines fabricated with the new printing processes. Below is a list of improvements which may improve the overall performance of the printing process or the printed devices. It should be noted that any changes in one area will have implications on another. It is therefore important to consider all three areas when making changes to the materials, printing strategies, or end application.

The electrode degrades rapidly at high strains and is extremely weak on the contact areas. These problems should be addressed to make more reliable printed devices. The electrode was shown to degrade rapidly at high strains (>5%). The degradation was due to cracking and ablation of the electrode. Cracking of the electrode may be prevented by using liquid dispersants, adding an elastomer, or using an elastomeric dispersant. However, all of these options have undesirable side effects or are not readily available. Liquid dispersants are problematic because they may diffuse out of the electrode and weaken the dielectric layers; Adding an elastomer reduces the conductivity of the electrode and increases its thickness; and elastomeric dispersants are not commercially available. Perhaps the degradation of the printed electrode may be inhibited by encapsulating the printed electrode. However, further experiments are required to determine the efficacy of encapsulation layers. Another problem with the printed electrode is that it is extremely fragile on the contact areas. In this work magnets were used to make a reliable connection. However the thin electrode is easily worn off when the magnets move. It would be beneficial to develop an ink-jet printable electrode material which is more robust, specifically for the contact areas.

The breakdown strength of ink-jet printed Sylgard 184 is sufficient for fluidic systems but is insufficient for soft robotic applications where high pressures and large deformations are required. However, finding an alternative silicone with a higher breakdown strength

which may be ink-jet printed is difficult. Many of the silicones we normally use for DE actuators which have higher breakdown strength have a high viscosity. Using another printing technique with a higher viscosity range may address this problem. In particular direct ink write printers are being developed with nozzle sizes below 50 µm (Sun et al., 2013). With direct ink writing it may be possible to print a larger range of silicones while achieving the same film thickness. Furthermore, the ability to print silicones with less solvent reduces the problem of swelling and reduces printing time.

The sacrificial material may also be improved. The current mixture and printing conditions produce sacrificial channels with relatively high surface roughness. The high surface roughness makes opening the channels more difficult and refracts transmitted light. For the soft machines developed in the thesis the optical properties of the channels do not matter. However, for lab-on-a-chip devices it may be important to have an optically transparent channel without any aberrations. For this reason it would be interesting to develop a sacrificial material with a flatter profile. This may be achieved by adding rheology modifiers to the sacrificial mixture which change the way the sacrificial material dries on silicone. An alternative, possibly simpler, option may be to print a secondary sacrificial material which has better levelling properties. Ethyl cellulose is insoluble in water. By printing a secondary sacrificial material dispersed in water it may be possible to print a secondary sacrificial layer which dries more slowly and creates a flatter profile. For example PAA or PVP dissolved in water. Using a secondary sacrificial material is potentially easier than developing a perfect sacrificial material because the secondary sacrificial material does not need to wet silicone.

The printing strategies in this thesis were developed to address the primary printing challenges and are far from optimised. For the electrodes the primary focus was to print continuous large area electrodes. The parameters given in section 3.6 produce continuous electrodes but the edge quality could be improved. The electrodes were printed bi-directionally with a droplet and line spacing of 100 µm. Printing electrodes bi-directionally is faster but produces electrodes with jagged edges. The edge quality may be improved by printing uni-directionally to better align the printed lines. Another issue with the printing parameters is the overflow created on the final line. When printing with a spacing of 100 µm the final printed line creates a wavy edge. The wavy edge is due to the line spacing. When the electrode mixture is printed with a line spacing of 100 µm the droplets are jetted close to the edge of the previous line. Sometimes the droplets land on the electrode and sometimes the droplets land on the silicone layer. The liquid tends to flow on the surface it is jetted on, leading to a wavy edge rather than a straight edge. This problem may be eliminated by increasing the line spacing.

The strategy for printing dielectric layers can also be improved. Dielectric layers printed with the 5-Pass method have a poor edge resolution. The second pass of the 5-Pass method has an offset of 500 µm. The edge of the dielectric therefore extends more than 500 µm beyond the edges of the design. This is a problem when printing small holes. In

addition the dielectric layers have a different edge profile on the leading and trailing edges (See Figure 5.5). Due to the asymmetry of printed holes, the design tolerances are very complicated and should take into account the direction of printing. To eliminate these problems a more sophisticated multi-pass printing method should be developed. Firstly the layers must be offset compensated. The edges should be trimmed so that offset layers do not cover holes and reduce printing resolution. Secondly, the passes should be printed with alternating directions i.e. the first layer is printed bottom to top, the second layer is printed top to bottom etc. This should improve the symmetry of printed edges.

The strategy for printing sacrificial channels may also be improved. The sacrificial channels are printed in two passes. This approach produces continuous sacrificial layer without holes, but does little to improve the flatness of sacrificial layers. It was already mentioned earlier that printing a secondary sacrificial material may create a smoother sacrificial channel. Alternatively it may be possible to improve the flatness of the sacrificial layers by adjusting the printing parameters. An offset may be used to fill the valleys of the first pass thus improving the flatness drastically.

The peristaltic pump was printed to demonstrate the advantages integrating actuators into a fluidic system. However, the peristaltic pump is not a complete fluidic system. To develop a complex fluidic system the pump must be miniaturised and additional components must be developed. To miniaturise the pump it is necessary to reduce the size of the channels. Doing so presents a new set of challenges. Firstly narrow channels, such as those in Figure 4.2, have not been fabricated and it is unclear if these channels can be opened with the method reported in this thesis. Secondly, the zipping electrodes must be scaled to match the size of the channels. Vector printed electrodes are wider than vector printed channels. For this reason new actuation mechanisms may need to be developed. Besides pumping, complex fluidic systems also require valves, mixers, and sensors. An important next step is therefore to design valves for blocking the flow of liquids and to develop sensor for measuring pressure and flow rate.

Further work on the slug-drive is also required. The antagonistic actuators do not close as predicted when operating at high pressures. As a consequence liquid is transferred between the channels leading to an imperfect wave of deformation. To make a working slug drive a redesign of the actuation mechanism is required. The serpentine channel should be replaced by parallel channels which are closed on one end. This prevents the dielectric liquid from moving between channels and eliminates the problem of competing actuators.

In this thesis the material and processes required to ink-jet print soft machines have been demonstrated. However two critical ingredients for automated soft machines have not been covered in this thesis, namely integrated sensors and integrated logic. Integrated sensors are required to provide feedback for soft actuators. This may include sensors

to measure pressure, flow, and permittivity in fluidic systems. For soft robots this may include pressure sensors to imitate touch and position sensors for proprioception. A slightly more ambitious goal would be to also integrate logic into a soft machine. Integrating sensors and logic into soft machines would greatly reduce the dependence of soft machines on external equipment.

A Appendix

A.1 SU-8 master fabrication

The master mould was fabricated with SU-8 3035, a photo resist ideal for high aspect ratio structures. The recommended process was followed to produce the master mould with a small number of modifications (Figure A.1). A silicon wafer was cleaned using a Piranha wet etch for 5 min at 85° C and rinsed with de-ionised water. The wafer was coated with SU-8 3035 with a spin speed of 500 RPM for 10 s and 2000 RPM for 45 s with an acceleration of 150 RPM/s. The wafer was then soft baked for 30 min at 100° C. The wafer was exposed for 100 s with conventional UV (350-400 nm) radiation. The post exposure bake was first conducted on a hot plate for 1 min at 65° C followed by 5 min in a 100° C oven. The wafer was then developed in a sonic bath with Mr DEV 600 for 1 min. The wafer was then moved to a bath containing fresh developer and sonicated for a further minute. Sonicating the wafer was necessary for removing the un-cured resin from deep and narrow grooves. The structure was then rinsed dry using isopropanol and deionised water.

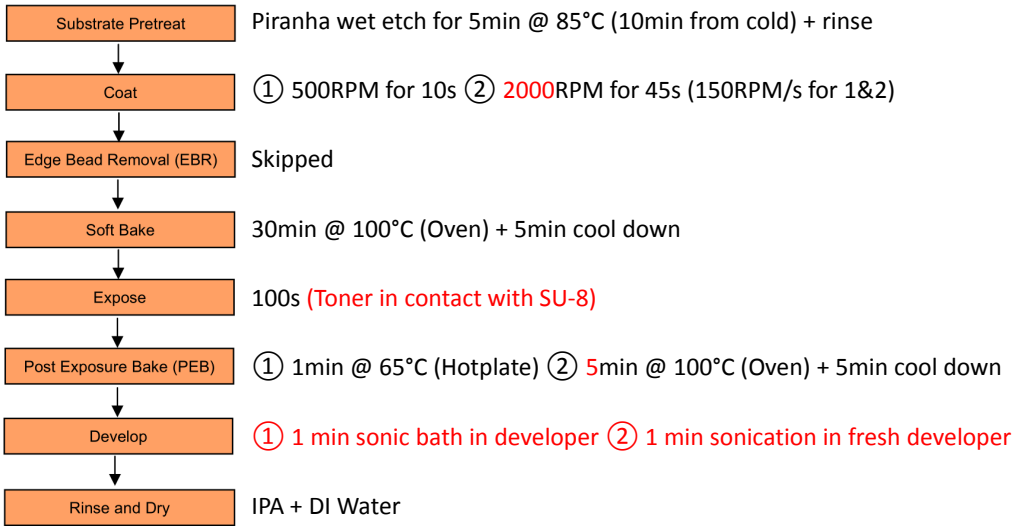

Figure A.1 – Fabrication of SU-8 3035 master mould

Bibliography

Acome, E., Mitchell, S. K., Morrissey, T. G., Emmett, M. B., Benjamin, C., King, M., Radakovitz, M., and Keplinger, C. (2018a). Hydraulically amplified self-healing electrostatic actuators with muscle-like performance. *Science*, 359(6371):61–65.

Acome, E., Mitchell, S. K., Morrissey, T. G., Emmett, M. B., Benjamin, C., King, M., Radakovitz, M., and Keplinger, C. (2018b). Hydraulically amplified self-healing electrostatic actuators with muscle-like performance. Technical Report 6371.

Akbari, S., Rosset, S., and Shea, H. R. (2013). Improved electromechanical behavior in castable dielectric elastomer actuators. *Applied Physics Letters*, 102(7).

Anders, J. B. (2000). AIAA-2000-2543 Biomimetic Flow Control BIOMIMETIC FLOW CONTROL. (June 2000):28.

Araromi, O. A., Rosset, S., and Shea, H. R. (2015). High-Resolution, Large-Area Fabrication of Compliant Electrodes via Laser Ablation for Robust, Stretchable Dielectric Elastomer Actuators and Sensors. *ACS Applied Materials and Interfaces*, 7(32):18046–18053.

Armour, R., Paskins, K., Bowyer, A., Vincent, J., and Megill, W. (2007). Jumping robots: A biomimetic solution to locomotion across rough terrain. *Bioinspiration and Biomimetics*, 2(3).

Atalay, O. (2018). Textile-based, interdigital, capacitive, soft-strain sensor for wearable applications. *Materials*, 11(5).

Baechler, C., Gardin, S., Abuhimd, H., and Kovacs, G. (2016). Inkjet printed multiwall carbon nanotube electrodes for dielectric elastomer actuators. *Smart Materials and Structures*, 25(5).

Bessonov, A., Kirikova, M., Haque, S., Gartseev, I., and Bailey, M. J. (2014). Highly reproducible printable graphite strain gauges for flexible devices. *Sensors and Actuators, A: Physical*, 206:75–80.

Bikas, H., Lianos, A. K., and Stavropoulos, P. (2019). A design framework for additive manufacturing. *International Journal of Advanced Manufacturing Technology*, pages 3769–3783.

Boxerbaum, A. S., Shaw, K. M., Chiel, H. J., and Quinn, R. D. (2012). Continuous wave peristaltic motion in a robot. *International Journal of Robotics Research*, 31(3):302–318.

Carpi, F., De Rossi, D., Kornbluh, R., Pelrine, R., and Sommer-Larsen, P. (2008). *Dielectric elastomers as electromechanical transducers: Fundamentals, Materials, Devices, Models and Applications of an Emerging Electroactive Polymer Technology*.

Chan, B., Balmforth, N. J., and Hosoi, A. E. (2005). Building a better snail: Lubrication and adhesive locomotion. *Physics of Fluids*, 17(11):1–10.

Chen, B., Lu, J. J., Yang, C. H., Yang, J. H., Zhou, J., Chen, Y. M., and Suo, Z. (2014). Highly stretchable and transparent ionogels as nonvolatile conductors for dielectric elastomer transducers. *ACS Applied Materials and Interfaces*, 6(10):7840–7845.

Christianson, C., Goldberg, N. N., Deheyn, D. D., Cai, S., and Tolley, M. T. (2018). Translucent soft robots driven by frameless fluid electrode dielectric elastomer actuators. *Science Robotics*, 3(17):eaat1893.

Cochrane, C. (2007). Design and Development of a Flexible Strain Sensor. *Sensors*, 7:473–492.

De Saint-Aubin, C. A., Rosset, S., Schlatter, S., and Shea, H. (2018). High-cycle electromechanical aging of dielectric elastomer actuators with carbon-based electrodes. *Smart Materials and Structures*, 27(7).

Derakhshanfar, S., Mbeleck, R., Xu, K., Zhang, X., Zhong, W., and Xing, M. (2018). 3D bioprinting for biomedical devices and tissue engineering: A review of recent trends and advances. *Bioactive Materials*, 3(2):144–156.

Derby, B. (2010). Inkjet Printing of Functional and Structural Materials: Fluid Property Requirements, Feature Stability, and Resolution. *Annual Review of Materials Research*, 40(1):395–414.

Dubais, P. and Alexandre, M. (2006). Performant clay/carbon nanotube polymer nanocomposites. In *Advanced Engineering Materials*, volume 8, pages 147–154.

Duduta, M., Wood, R. J., and Clarke, D. R. (2016). Multilayer Dielectric Elastomers for Fast, Programmable Actuation without Prestretch. *Advanced Materials*, 28(36):8058–8063.

Fasolt, B., Hodgins, M., and Seelecke, S. (2016). Characterization of screen-printed electrodes for dielectric elastomer (DE) membranes: influence of screen dimensions and electrode thickness on actuator performance. In *Electroactive Polymer Actuators and Devices (EAPAD) 2016*, volume 9798, page 97983E. SPIE.

Frediani, G., Mazzei, D., De Rossi, D. E., and Carpi, F. (2014). Wearable wireless tactile display for virtual interactions with soft bodies. *Frontiers in Bioengineering and Biotechnology*, 2(SEP).

Frutiger, A., Muth, J. T., Vogt, D. M., Mengüç, Y., Campo, A., Valentine, A. D., Walsh, C. J., and Lewis, J. A. (2015). Capacitive soft strain sensors via multicore-shell fiber printing. *Advanced Materials*, 27(15):2440–2446.

Gan, H. Y., Shan, X., Eriksson, T., Lok, B. K., and Lam, Y. C. (2009). Reduction of droplet volume by controlling actuating waveforms in inkjet printing for micro-pattern formation. *Journal of Micromechanics and Microengineering*, 19(5).

Gonzalez, D., Garcia, J., and Newell, B. (2019). Electromechanical characterization of a 3D printed dielectric material for dielectric electroactive polymer actuators. *Sensors and Actuators A: Physical*, 297:111565.

Hamad, E. M., Bilatto, S. E., Adly, N. Y., Correa, D. S., Wolfrum, B., Schöning, M. J., Offenhäusser, A., and Yakushenko, A. (2016). Inkjet printing of UV-curable adhesive and dielectric inks for microfluidic devices. *Lab on a Chip*, 16(1):70–74.

Henke, E.-F. F., Schlatter, S., and Anderson, I. A. (2017). Soft Dielectric Elastomer Oscillators Driving Bioinspired Robots. *Soft Robotics*, 4(4):353–366.

Huang, J., Li, T., Chiang Foo, C., Zhu, J., Clarke, D. R., and Suo, Z. (2012). Giant, voltage-actuated deformation of a dielectric elastomer under dead load. *Applied Physics Letters*, 100(4).

Huang, J. C. (2002). Carbon black filled conducting polymers and polymer blends. *Advances in Polymer Technology*, 21(4):299–313.

Jones, R. W., Wang, P., Lassen, B., and Sarban, R. (2010). Dielectric elastomers and compliant metal electrode technology. *Proceedings of the Mediterranean Electrotechnical Conference - MELECON*, pages 368–373.

Jung, K., Koo, J. C., Nam, J. D., Lee, Y. K., and Choi, H. R. (2007). Artificial annelid robot driven by soft actuators. *Bioinspiration and Biomimetics*, 2(2).

Kellaris, N., Venkata, V. G., Rothemund, P., and Keplinger, C. (2019). An analytical model for the design of Peano-HASEL actuators with drastically improved performance. *Extreme Mechanics Letters*, 29:100449.

Kellaris, N., Venkata, V. G., Smith, G. M., Mitchell, S. K., and Keplinger, C. (2018). Peano-HASEL actuators: Muscle-mimetic, electrohydraulic transducers that linearly contract on activation. Technical Report 14.

Keplinger, C., Kaltenbrunner, M., Arnold, N., and Bauer, S. (2010). Röntgen's electrode-free elastomer actuators without electromechanical pull-in instability. *Proceedings of the National Academy of Sciences of the United States of America*, 107(10):4505–4510.

Keplinger, C., Sun, J. Y., Foo, C. C., Rothemund, P., Whitesides, G. M., and Suo, Z. (2013). Stretchable, transparent, ionic conductors. *Science*, 341(6149):984–987.

Kim, T. A., Kim, H. S., Lee, S. S., and Park, M. (2012). Single-walled carbon nanotube/silicone rubber composites for compliant electrodes. *Carbon*, 50(2):444–449.

Kovacs, G., Düring, L., Michel, S., and Terrasi, G. (2009). Stacked dielectric elastomer actuator for tensile force transmission. *Sensors and Actuators, A: Physical*, 155(2):299–307.

Litteken, D. A. (2017). Evaluation of strain measurement devices for inflatable structures. *58th AIAA/ASCE/AHS/ASC Structures, Structural Dynamics, and Materials Conference, 2017*, (January):1–17.

Liu, Y. F., Pai, Y. F., Tsai, M. H., and Hwang, W. S. (2012). Investigation of driving waveform and resonance pressure in piezoelectric inkjet printing. *Applied Physics A: Materials Science and Processing*, 109(2):323–329.

Lotz, P., Matysek, M., and Schlaak, H. F. (2011). Fabrication and application of miniaturized dielectric elastomer stack actuators. *IEEE/ASME Transactions on Mechatronics*, 16(1):58–66.

Low, S. H. and Lau, G. K. (2014). Bi-axially crumpled silver thin-film electrodes for dielectric elastomer actuators. *Smart Materials and Structures*, 23(12).

Maffli, L., Rosset, S., Ghilardi, M., Carpi, F., and Shea, H. (2015). Ultrafast all-polymer electrically tunable silicone lenses. *Advanced Functional Materials*, 25(11):1656–1665.

Majidi, C. (2014). Soft Robotics: A Perspective - Current Trends and Prospects for the Future. *Soft Robotics*, 1(1):5–11.

Manion, C. A., Fuge, M., and Bergbrieter, S. (2018). Modeling and Evaluation of Additive Manufactured HASEL Actuators *. *International Conference on Intelligent Robots and Systems (IEEE/RSJ)*.

McCoul, D., Rosset, S., Schlatter, S., and Shea, H. (2017). Inkjet 3D printing of UV and thermal cure silicone elastomers for dielectric elastomer actuators. *Smart Materials and Structures*, 26(12).

McKay, T. G., Rosset, S., Anderson, I. A., and Shea, H. (2015). Dielectric elastomer generators that stack up. *Smart Materials and Structures*, 24(1).

McKinley, G. H. and Renardy, M. (2011). Wolfgang von Ohnesorge. *Physics of Fluids*, 23(12):1–17.

Mitchell, S. K., Wang, X., Acome, E., Martin, T., Ly, K., Kellaris, N., Venkata, V. G., and Keplinger, C. (2019). An Easy-to-Implement Toolkit to Create Versatile and High-Performance HASEL Actuators for Untethered Soft Robots. *Advanced Science*, 1900178.

Moretti, G., Papini, G. P. R., Daniele, L., Forehand, D., Ingram, D., Vertechy, R., and Fontana, M. (2019). Modelling and testing of a wave energy converter based on dielectric elastomer generators. *Proceedings of the Royal Society A: Mathematical, Physical and Engineering Sciences*, 475(2222).

Nelson, J. R. and Wissing, W. K. (1986). Morphology of electrically conductive grades of carbon black. *Carbon*, 24(2):115–121.

Ngo, T. D., Kashani, A., Imbalzano, G., Nguyen, K. T., and Hui, D. (2018). Additive manufacturing (3D printing): A review of materials, methods, applications and challenges. *Composites Part B: Engineering*, 143(December 2017):172–196.

O'Brien, B., Thode, J., Anderson, I., Calius, E., Haemmerle, E., and Xie, S. (2007). Integrated extension sensor based on resistance and voltage measurement for a dielectric elastomer. In *Electroactive Polymer Actuators and Devices (EAPAD) 2007*, volume 6524, page 652415. SPIE.

Park, T., Kim, K., Oh, S.-r., and Cha, Y. (2019). Electrohydraulic Actuator for a Soft Gripper. 00(00):1–8.

Pekas, N., Zhang, Q., and Juncker, D. (2012). Electrostatic actuator with liquid metal-elastomer compliant electrodes used for on-chip microvalving. *Journal of Micromechanics and Microengineering*, 22(9).

Pelrine, R. E., Kornbluh, R. D., and Joseph, J. P. (1998). Electrostriction of polymer dielectrics with compliant electrodes as a means of actuation. *Sensors and Actuators, A: Physical*, 64(1):77–85.

Phung, H., Nguyen, C. T., Nguyen, T. D., Lee, C., Kim, U., Lee, D., Nam, J. D., Moon, H., Koo, J. C., and Choi, H. R. (2015). Tactile display with rigid coupling based on soft actuator. *Meccanica*, 50(11):2825–2837.

Poulin, A., Saygili Demir, C., Rosset, S., Petrova, T. V., and Shea, H. (2016). Dielectric elastomer actuator for mechanical loading of 2D cell cultures. *Lab on a Chip*, 16(19):3788–3794.

Raut, N. C. and Al-Shamery, K. (2018). Inkjet printing metals on flexible materials for plastic and paper electronics. *Journal of Materials Chemistry C*, 6(7):1618–1641.

Reitelshöfer, S., Göttler, M., Schmidt, P., Treffer, P., Landgraf, M., and Franke, J. (2016). Aerosol-Jet-Printing silicone layers and electrodes for stacked dielectric elastomer actuators in one processing device. In *Electroactive Polymer Actuators and Devices (EAPAD) 2016*, volume 9798, page 97981Y. SPIE.

Rich, S. I., Wood, R. J., and Majidi, C. (2018). Untethered soft robotics. *Nature Electronics*, 1(2):102–112.

Rizzello, G., Naso, D., York, A., and Seelecke, S. (2016). Closed loop control of dielectric elastomer actuators based on self-sensing displacement feedback. *Smart Materials and Structures*, 25(3).

Rogóż, M., Dradrach, K., Xuan, C., and Wasylczyk, P. (2019). A Millimeter-Scale Snail Robot Based on a Light-Powered Liquid Crystal Elastomer Continuous Actuator. *Macromolecular Rapid Communications*, 1900279:1900279.

Röntgen, W. C. (1880). Ueber die durch Electricität bewirkten Form- und Volumenänderungen von dielectrischen Körpern. *Annalen der Physik*, 247(13):771–786.

Rosset, S., Ararom, O. A., Schlatter, S., and Shea, H. R. (2016). Fabrication process of silicone-based dielectric elastomer actuators. *Journal of Visualized Experiments*, 2016(108).

Rosset, S., De Saint-Aubin, C., Poulin, A., and Shea, H. R. (2017). Assessing the degradation of compliant electrodes for soft actuators. *Review of Scientific Instruments*, 88(10).

Rosset, S., Niklaus, M., Dubois, P., and Shea, H. R. (2008). Mechanical characterization of a dielectric elastomer microactuator with ion-implanted electrodes. *Sensors and Actuators, A: Physical*, 144(1):185–193.

Rosset, S. and Shea, H. R. (2013). Flexible and stretchable electrodes for dielectric elastomer actuators. *Applied Physics A: Materials Science and Processing*, 110(2):281–307.

Rossiter, J., Walters, P., and Stoimenov, B. (2009). Printing 3D dielectric elastomer actuators for soft robotics. In *Electroactive Polymer Actuators and Devices (EAPAD) 2009*, volume 7287, page 72870H. SPIE.

Rus, D. and Tolley, M. T. (2015). Design, fabrication and control of soft robots. *Nature*, 521(7553):467–475.

Rwei, S. P., Ku, F. H., and Cheng, K. C. (2002). Dispersion of carbon black in a continuous phase: Electrical, rheological, and morphological studies. *Colloid and Polymer Science*, 280(12):1110–1115.

Schlaak, H. F., Jungmann, M., Matysek, M., and Lotz, P. (2005). Novel multilayer electrostatic solid state actuators with elastic dielectric (Invited Paper). *Smart Structures and Materials 2005: Electroactive Polymer Actuators and Devices (EAPAD)*, 5759(May 2005):121.

Schlatter, S., Illenberger, P., and Rosset, S. (2018). Peta-pico-Voltron: An open-source high voltage power supply. *HardwareX*, 4:e00039.

Schlatter, S., Rosset, S., and Shea, H. (2017). Inkjet printing of carbon black electrodes for dielectric elastomer actuators. In *Electroactive Polymer Actuators and Devices (EAPAD) 2017*, volume 10163, page 1016311. SPIE.

Shin, D. Y., Yoo, S. S., Song, H. E., Tak, H., and Byun, D. (2015). Electrostatic-force-assisted dispensing printing to construct high-aspect-ratio of 0.79 electrodes on a textured surface with improved adhesion and contact resistivity. *Scientific Reports*, 5.

Shintake, J., Piskarev, E., Jeong, S. H., and Floreano, D. (2018). Ultrastretchable Strain Sensors Using Carbon Black-Filled Elastomer Composites and Comparison of Capacitive Versus Resistive Sensors. *Advanced Materials Technologies*, 3(3):1–8.

Shirtcliffe, N. J., McHale, G., and Newton, M. I. (2012). Wet adhesion and adhesive locomotion of snails on anti-adhesive non-wetting surfaces. *PLoS ONE*, 7(5):5–9.

Sinatra, N. R., Teeple, C. B., Vogt, D. M., Parker, K. K., Gruber, D. F., and Wood, R. J. (2019). Ultragentle manipulation of delicate structures using a soft robotic gripper. *Science Robotics*, 4(33):eaax5425.

Sirbu, I.-D., Moretti, G., Dire, S., Fambri, L., Vertechy, R., Meniglio, D., and Fontana, M. (2019). Electrostatic actuator for tactile display based on hydraulically coupled dielectric fluids and soft structures. (March):68.

Sommer, J. and Sommer, J. (2014). *Troubleshooting Rubber Problems*.

Sun, K., Wei, T. S., Ahn, B. Y., Seo, J. Y., Dillon, S. J., and Lewis, J. A. (2013). 3D printing of interdigitated Li-ion microbattery architectures. *Advanced Materials*, 25(33):4539–4543.

Truby, R. L., Wehner, M., Grosskopf, A. K., Vogt, D. M., Uzel, S. G., Wood, R. J., and Lewis, J. A. (2018). Soft Somatosensitive Actuators via Embedded 3D Printing. *Advanced Materials*, 30(15).

Tsai, M. H. and Hwang, W. S. (2008). Effects of pulse voltage on the droplet formation of alcohol and ethylene glycol in a piezoelectric inkjet printing process with bipolar pulse. *Materials Transactions*, 49(2):331–338.

Unger, M. A., Chou, H. P., Thorsen, T., Scherer, A., and Quake, S. R. (2000). Monolithic microfabricated valves and pumps by multilayer soft lithography. *Science*, 288(5463):113–116.

Voon, S. L., An, J., Wong, G., Zhang, Y., and Chua, C. K. (2019). 3D food printing: a categorised review of inks and their development. *Virtual and Physical Prototyping*, 14(3):203–218.

Waarden, M. V. D. (1950). Stabilization of Carbon-Black Dispersions in Hydrocarbons. *Journal of Colloid Science*, pages 317–325.

Wang, Z., Zhu, M., Kawamura, S., and Hirai, S. (2017). Comparison of different soft grippers for lunch box packaging. *Robotics and Biomimetics*, 4(1):1–9.

Wu, J., Roberts, R. C., Tien, N. C., and Li, D. (2014). Inkjet printed silver patterning on PDMS to fabricate microelectrodes for microfluidic sensing. In *Proceedings of IEEE Sensors*, volume 2014-Decem, pages 1100–1103. Institute of Electrical and Electronics Engineers Inc.

Wu, M. H., Huang, S. B., Cui, Z., Cui, Z., and Lee, G. B. (2008). Development of perfusion-based micro 3-D cell culture platform and its application for high throughput drug testing. *Sensors and Actuators, B: Chemical*, 129(1):231–240.

Xu, D., Tairych, A., and Anderson, I. A. (2015). Stretch not flex: Programmable rubber keyboard. *Smart Materials and Structures*, 25(1).

Yu, K., Zhang, Z., Liu, Y., and Leng, J. (2011). Carbon nanotube chains in a shape memory polymer/carbon black composite: To significantly reduce the electrical resistivity. *Applied Physics Letters*, 98(7).

Yuan, W., Brochu, P., Ha, S. M., and Pei, Q. (2009). Dielectric oil coated single-walled carbon nanotube electrodes for stable, large-strain actuation with dielectric elastomers. *Sensors and Actuators, A: Physical*, 155(2):278–284.

Zhao, X. and Suo, Z. (2010). Theory of dielectric elastomers capable of giant deformation of actuation. *Physical Review Letters*, 104(17).